LUT UNIVERSITY
School of Energy Systems
Energy Technology
BH10A2000 Master's Thesis

Ville Heimonen

CURRENT INDUCTION TO STRUCTURES DUE TO CHANGING MAGNETIC FIELD

Examiners: Associate professor Ahti Jaatinen-Värri
Associate professor Janne Nerg

Supervisors: M.Sc. (Tech.) Matti Hernesniemi

ABSTRACT

LUT University
School of Energy Systems
Master's Degree Programme in Energy Systems

Ville Heimonen

Current induction to structures due to changing magnetic field

Master's Thesis

2019

116 pages, 59 figures, 17 tables and 12 appendices

Examiners: Associate professor Ahti Jaatinen-Värri, Associate professor Janne Nerg

Supervisors: M.Sc. (Tech.) Matti Hernesniemi

Keywords: magnetic field, induction, current, reactor, coil, STATCOM, SVC

This master's thesis has been done for GE Grid Solutions Oy and the aim of the thesis was to analyze magnetic fields created by reactor coils in STATCOM and SVC substations. The focus was especially to study the effects of a changing magnetic field to surrounding structures. The thesis should give better understanding, how close to a reactor coil different conductive structures can exist and determine critical values of the magnetic field regarding to this issue. The induced currents can cause problems such as, generate unnecessary losses and cause heating of the structures.

There are two different instances on how the induction of current can occur and cause problems. The current can induce to a structure that forms a whole loop and large amount of magnetic flux crosses the loop window. Notable eddy currents can form to long ferromagnetic structures that are parallel to the external magnetic field.

Laboratory tests and simulations showed that, the higher the material electrical conductivity, the more induced current and losses would be generated to structures that form whole loops. There are many variables that define whether a loop would become a problem in a substation, such as: loop size, material thickness, material electrical conductivity and angle relative to the magnetic field. For ferromagnetic materials, as carbon steel, the eddy currents proved to be more problematic than the induced circulating current through the loop.

TABLE OF CONTENTS

NOMENCLATURE

General

A	area	[m^2]
D_m	mean diameter	[m]
P	power	[W]
T	temperature	[°C], [K]
T_0	reference temperature	[°C]
ΔT	temperature difference	[°C], [K]
V	volume	[m^3]
f	frequency	[Hz]
g	acceleration of gravity	[m/s^2]
h	height	[m]
l	length	[m]
m	mass	[kg]
t	time	[s]
ρ	density	[kg/m^3]
θ	angle of inclination	[degrees]

Electromagnetics

B	magnetic flux density	[Vs/m^2], [T]
B_r	remanent magnetic flux density	[Vs/m^2], [T]
C	integration path contour	
D	electric flux density	[C/m^2], [As/m^2]
E	electric field intensity	[V/m]
F	Lorentz force	[N]
H	magnetic field intensity	[A/m]
H_c	coercive field intensity	[A/m]
I	current	[A]
J	electric current density	[A/m^2]
L	inductance	[H]
N	winding number of turns	

$\hat{O}$	azimuthal unit vector	
R	resistance	[Ω]
R_{AC}	AC resistance	[Ω]
R_0	resistance at reference temperature	[Ω]
$\hat{R}$	radial unit vector pointing away from the charge	
S	distance between charge and observation point	[m]
U	voltage	[V]
ΔU	voltage difference	[V]
X_L	inductive reactance	[Ω]
Z	impedance	[Ω]
dl	differential vector element of path length	[m]
k_n	hysteresis loss per cycle	[J/m^3]
q	electric charge	[C]
r	radial distance from the current	[m]
v	charge velocity	[m/s]
x	winding cross section width	[m]
α	Steinmetz's constant	
ε	permittivity	[F/m]
ε_r	relative permittivity	
ε_0	permittivity of the vacuum	[8.854·10^{-12} F/m]
μ	permeability	[H/m]
μ_r	relative permeability	
μ_0	permeability of the vacuum	[4π·10^{-7} H/m]
ρ	resistivity	[Ω/m]
ρ_v	electric volume charge density	[C/m^3]
δ	penetration depth	[m]
ϑ	material resistivity temperature coefficient	[1/°C]

Heat transfer

L	characteristic length	[m]
Nu	Nusselt number	
Pr	Prandtl number	

Ra	Rayleigh number	
Ra_c	critical Rayleigh number	
Ra_θ	Rayleigh number for inclined surfaces	
Re	Reynolds number	
a	surface length	[m]
b	surface width	[m]
$f_1(Pr)$	Prandtl number function for vertical surfaces	
$f_2(Pr)$	Prandtl number function for horizontal surfaces	
w	air velocity	[m/s]
α	convection coefficient	[W/(m^{2}K)]
β	isobaric volume expansion coefficient	[1/K]
ε	material degree of emission	
σ	Stefan-Boltzmann constant	[5.6704·10^{-8} W/(m^{2}K^4)]
λ	thermal conductivity	[W/(m·K)]
κ	thermal diffusivity	[m^2/s]
ν	kinematic viscosity	[m^2/s]

Mathematical operators

$\nabla\times$	curl
$\nabla\cdot$	divergence
∂	partial derivative
$\times$	cross product

Subscripts

amb	ambient
C	convection
circ	circulating
forced	forced convection
free	free convection
lam	laminar
h	hysteresis
m	medium

peak	peak value
R	radiation
RMS	root mean square value
surf	surface
total	total
turb	turbulent

Abbreviations

AC	alternating current
B-H	hysteresis curve
C	minimum distance between reactors
DC	direct current
emf	electromotive force
FACTS	flexible alternating current transmission system
FSC	fixed series compensation
MSC	mechanically-switched capacitor
MSR	mechanically-switched reactor
m_x	reactor minimum horizontal clearance
m_y	reactor minimum vertical clearance
RLC	resistor, inductor and capacitor circuit
RMS	root mean square
SC	synchronous condenser
STATCOM	static synchronous compensator
SVC	static var compensator
TC	thermocouple
TCR	thyristor-controlled reactor
TCSC	thyristor-controlled series compensation
TSC	thyristor-switched capacitor
VSC	voltage source converter

1 INTRODUCTION

STATCOM and SVC substations are part of the GE Grid Solutions flexible alternating current transmission system portfolio. They are a crucial part of the todays AC transmission system, when the increase of renewable energy sources has created more uneven generation of power to the grid. (Kurka 2017b, 3-9) The main purposes of the STATCOM and SVC are to stabilize the voltage in the AC transmission system, increase the transient stability, damp system power oscillations, filter harmonics and reduce flicker in the AC network. (Kähkönen 2016a, 22)

Changing magnetic fields created by air core reactor coils in STATCOM or SVC substations can cause significant induction of current to nearby conducting structures. The induced current to structures may cause problems in substations, such as, producing unnecessary losses and the temperature of structures can rise to dangerous levels due to the losses. A major problem can arise if the electrically highly conductive structure forms a whole loop in the presence of a changing magnetic field. The induced circulating current through the loop can generate significant amount of losses and heat.

The object of the thesis was to study magnetic fields created by air core reactor coils. The aim was especially in the effects of a changing magnetic field to conductive structures. Several laboratory tests and simulations were conducted to determine the magnetic field of a reactor coil and to define the induced current, losses and heating for different structures and materials due to the changing magnetic field. The laboratory tests and simulations should give better understanding what materials should be used in structures nearby reactors and how adverse conducting loops can be in STATCOM or SVC substations.

The background information presented in the thesis includes theory about magnetic and electric fields, Maxwell’s equations and processes on how the energy of the electric and magnetic fields can turn into heat.

2 ELECTROMAGNETISM

There are four fundamental forces in the physical universe. These are the nuclear force, the weak-interaction force, the gravitational force and the electromagnetic force. The electromagnetic force exists between all charged particles and in microscopic systems, it is the major force. Although the electromagnetic force functions at an atomic level, effects of the force can be transmitted to the macroscopic world via electromagnetic waves. They can pass through free space and material media. (Ulaby et al. 1997, 12) Electromagnetism covers electricity, magnetism, electric fields, magnetic fields and electromagnetic waves. The focus in circuit theory is on the voltage between two terminals and on the current in a conductor. The emphasis in electromagnetism is however on the space between conductors and on the electromagnetic fields in the space. (Kraus & Carver 1973, 1)

2.1 Electric and magnetic field

In short, an electric field is a vector field around an electric charge. The electric charge applies a force on other charges. The electrical force is comparable to the gravitational force apart from two anomalies. The electric charge is the source of the electric field, not mass as in the gravitational force. Both fields weaken as the square of the distance from their sources, but electric charges can have negative or positive polarity. The electrical force then can be attractive or repulsive. Coulomb's law can be used to explain the electrical forces influence on the electric charge. It states that two charges with same polarity repel each other and charges with opposite polarity attract one another. The electrical force acts on a straight line between the charges. Intensity of the force is proportional to the product of the magnitudes of the charges and inversely proportional to the square of the distance between them. (Ulaby et al. 1997, 13)

The electric field intensity due to any charge, as shown in equation (1), can be derived from the Coulomb's law. The permittivity ε in the equation is obtained by multiplying the dimensionless relative permittivity ε_r of the material by the permittivity of the vacuum ε_0 ($8.854 \cdot 10^{-12}$ F/m). A point of charge *q'* in an electric field (due to other charges) experiences

a force influencing it equal to the *q'* charge, multiplied by the electric field intensity. Electric field *E* due to a charge *q* is presented in figure 1. (Ulaby et al. 1997, 13-14)

$$\boldsymbol{E} = \hat{\boldsymbol{R}} \frac{q}{4\pi\varepsilon S^2} \quad (1)$$

E = electric field intensity [V/m]
$\hat{R}$ = radial unit vector pointing away from the charge
q = charge [C]
ε = permittivity [F/m]
S = distance between the charge and observation point [m]

The electric charge has two major properties. Firstly, the net electric charge cannot be created or destroyed, which is the electric charge conservation law. The second important property is that for a point in space influenced by many point charges, the total vector electric field is equal to the vector sum of the electric fields at that point caused by the individual charges. This is the principle of linear superposition and it allows calculation of the electric field due to complex distributions of charge. There is no need to consider the forces influencing on each individual charge due to the fields by all other charges. (Ulaby et al. 1997, 14)

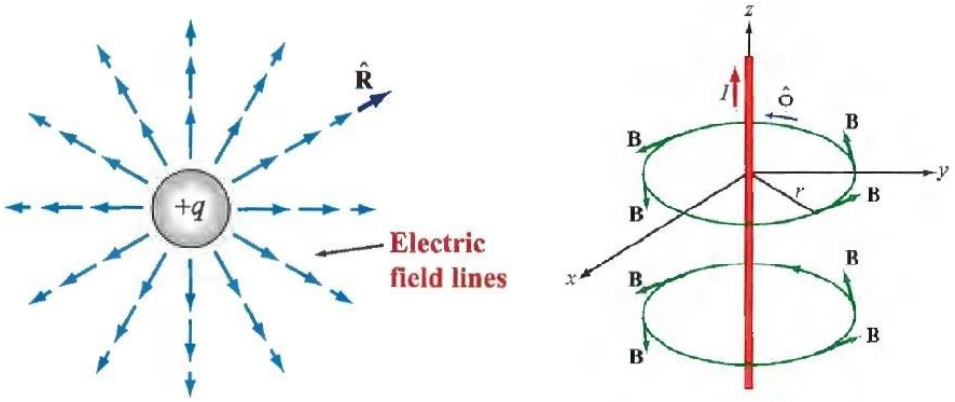

Figure 1. Electric field (left) and magnetic field induced by a current (right) (modified from Ulaby et al. 1997, 14-16)

A magnetic field is a vector field that defines the magnetic effect of magnetized materials and electric currents. Every magnet has a north and south pole that are diametrically opposite

to each other no matter the shape of the magnet. The magnetic force forms a magnetic field around a magnet which pass through the north and south pole. Similar to the electric charge, alike magnetic poles of different magnets repel one another and unlike poles attract each other. However, magnetic poles exist always in pairs and they cannot be separated as electric charges. (Ulaby et al. 1997, 15)

Permanent magnets are not the only source of magnetic fields. Electric current can also form a magnetic field. In a wire with current I flowing through it, a magnetic field is induced around the wire. The field forms closed circular loops around the wire, which is presented in the figure 1. The magnetic field lines surrounding a magnet, or the wire, as in the figure 1, illustrates the magnetic flux density B. The Biot-Savart law links the magnetic flux density at a point in space to the current in a conductor, as in the case of the figure 1. The Biot-Savart law is shown in equation (2). The permeability μ in the equation is obtained by multiplying the relative permeability μ_r of the material by the permeability of the vacuum μ_0 ($4\pi \cdot 10^{-7}$ H/m). Most of the materials have their relative permeabilities close to one, which means that their magnetization properties are the same as for the vacuum. Only ferromagnetic materials have the relative permeability higher than one. (Ulaby et al. 1997, 15)

$$\boldsymbol{B} = \hat{\boldsymbol{O}}\frac{\mu I}{2\pi r} \tag{2}$$

B = magnetic flux density [Vs/m^2], [T]
$\hat{O}$ = azimuthal unit vector
μ = permeability [H/m]
I = current [A]
r = radial distance from the current [m]

In electromagnetics, it is important to know if and how electric and magnetic quantities vary with time. Static quantity does not change with time. DC, direct current, is usually used as synonym for static. DC describes also other electromagnetic quantities than just currents. Dynamic quantity varies with time, but there is no definitive information about the nature of the variation. If the quantity is dynamic, one cannot distinguish any specific patterns in the variation. Waveform indicates to the magnitude profile plot of a quantity as a function of

time. If the waveform of the quantity repeats at a regular interval, the quantity is periodic. Sinusoid and square waves are examples of periodic quantities. Sinusoidal quantity varies sinusoidally or cosinusoidally with time. Current with periodical waveform is called AC, alternating current. There are three branches in electromagnetics: electrostatics, magnetostatics and dynamics (time-varying fields). Associated condition for electrostatics is stationary charges and for magnetostatics it is steady currents (DC). Electrostatics and magnetostatics have their own branches in electromagnetics, because the induced electric and magnetic fields are not connected to one another. Dynamics is more general branch in electromagnetics. It covers time-varying fields induced by time-varying sources, which are currents and associated densities. As an example, a time-varying magnetic field generates a time-varying electric field and the other way around. (Ulaby et al. 1997, 16-17)

2.2 Maxwell's equations

Maxwell's equations are a set of fundamental relations on which the modern understanding of electromagnetism is based on. Maxwell's equations are based on experimental analyses originally made by Coulomb, Gauss, Ampère, Faraday and others. They establish a connection between the electric field and electric charge, and between the magnetic field and electric current. These equations also explain the relation between the electric and magnetic fields and fluxes. (Ulaby et al. 1997, 178) Maxwell's equations consist of four equations: Faraday's law, Ampère's law, Gauss's law and no monopoles equation. (Ida 2015, 572) However, two more independent vector equations are required to solve the electromagnetic problem, which are called the two constitutive relations. In the four Maxwell's equations the number of unknows is 12 and only six scalar equations are available. The Gauss's law and no monopoles equations are not independent in a time-varying application. They can be derived from the other two equations, with help of the continuity equation. Also, the Lorentz force equation should be included in a complete set of equations for solving an electromagnetic field problem. The Lorentz force equation cannot be derived from Maxwell's equations, which is why it should be recognized as a part of the complete set. If the electromagnetic problem is time-dependent, only the Faraday's law and Ampère's law

from Maxwell's equations with the constitutive relations are required for the solution, because they are independent from each other. (Ida 2015, 571-572)

2.2.1 Faraday's law

According to the Faraday's law or the Faraday's induction law, a current is induced to a closed wire loop if a magnetic flux through the loop is changing. The induced current has always a direction in the loop to create flux preventing the change in the magnetic flux density (Lenz's law). Figure 2 shows that when the magnetic flux density *B* is decreasing, the induced current in the loop creates a magnetic field which has the same direction as the magnetic flux density. The induced current has a direction that produces the field around the loop in such a way that it is increasing the magnetic flux density. Thus, when the *B* value is increasing, the direction of the induced current is the opposite. The magnetic field created by the induced current is now opposing the magnetic flux density *B*. (Kraus & Carver 1973, 305-306)

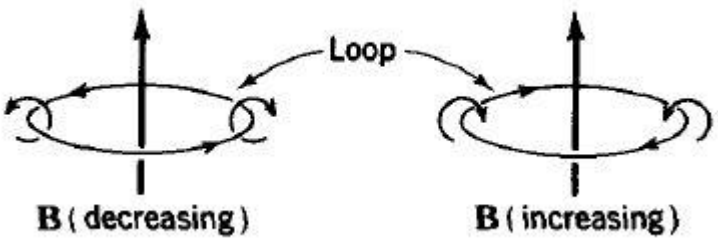

Figure 2. Induced currents for changing magnetic flux density (Kraus & Carver 1973, 306)

The current formed in the loop is due to an induced voltage which is called the electromotive force (emf). (Ida 2015, 516) The electromotive force can be obtained from integrating an electric field around the loop. The electric field in the loop is produced by the changing magnetic field. (Kraus & Carver 1973, 306) There are three cases where the electromotive force can be created in the conducting closed loop. In the first case, there is a stationary loop linked by a time-varying magnetic field. The induced emf here is called the transformer emf. With the second case, in a static magnetic field there is a moving loop with a time-varying

surface area. Now the induced emf is called the motional emf. In the final case, there is a moving loop in a time-varying magnetic field. The total electromotive force is the sum of the transformer and motional emf. (Ulaby et al. 1997, 284)

If the conducting loop has a gap, the electromotive force occurs between the terminals. Figure 3 presents this situation, where numbers 1 and 2 are the terminals and *E* is the electric field. The emf between points one and two depends on the integration path of the electric field *E* from the point one to two. It is assumed that the two points in the figure 3 are infinitely close together. Then the emf between the points acquired by integrating the electric field around the loop from the point one to two is equal to the electric fields line integral around the closed loop. However, the electromotive force becomes negligible if the *E* is integrated straight across the gap from the point one to two. This means no current flows between the points. (Kraus & Carver 1973, 306-307)

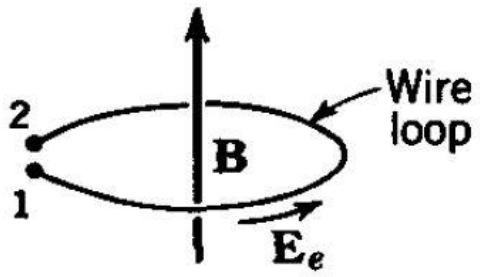

Figure 3. Emf in the open circuit loop (Kraus & Carver 1973, 306)

The differential form of the Faraday's law is shown in equation (3). The connection between electric and magnetic fields can be easily seen from this equation. The electric field intensity curl is not zero thus, the electric field is non-conservative. That is why the electric field intensity cannot be defined as the gradient of a scalar potential. Also, the electrostatic potential cannot be used for calculation. The equation (3) shows that the Faraday's law is general. This means that the induced electromotive force can exist without a loop. The induction of current can also occur in conducting volumes, which is known also as eddy currents. (Ida 2015, 517)

$$\nabla \times \mathbf{E} = -\frac{\partial \boldsymbol{B}}{\partial t} \tag{3}$$

E = electric field intensity [V/m]
B = magnetic flux density [Vs/m^2], [T]
t = time [s]

2.2.2 Ampère's law

The Ampère's law is the only law in the Maxwell's equation set on which Maxwell made modification. He introduced displacement currents to the Ampère's law. (Ida 2015, 566-567) The Ampère's law before Maxwell's modification is shown in integral form in equation (4). It states that magnetic field intensity H circulation around a closed path C is equal to the current enclosed by the path. (Ida 2015, 396) The closed path can be in any shape, but the current must flow through it. There are three cases in figure 4: **a**, **b** and **c**. The line integral of the magnetic field intensity H around contour C, is equal to the current I crossing the surface enclosed by the contour in the cases **a** and **b**, but not in **c**. Contours in the cases **a** and **b** encloses the current, but not in the case **c**. Even if the magnitude of H varies along the path, the line integral of H is equal to the current. If the contour C does not enclose the current, the line integral of H is zero. (Ulaby et al. 1997, 254-255)

$$\oint_C \boldsymbol{H} \cdot d\boldsymbol{l} = I \tag{4}$$

H = magnetic field intensity [A/m]
dl = differential vector element of path length [m]
I = current [A]
C = integration path contour

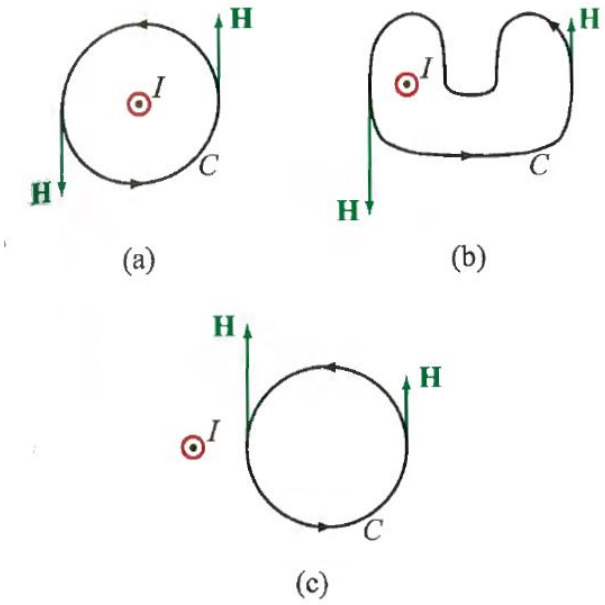

Figure 4. Ampère's law (Ulaby et al. 1997, 255)

The Ampère's law can be derived from the Biot-Savart law, but in some problems the Ampère's law is much easier to apply. For highly symmetric current configurations the Ampère's law is much better choice than the Biot-Savart law. (Ida 2015, 396) For example the Ampère's law is useful for calculating the magnetic field intensity of a long wire, inside a long solenoid or toroidal coil and magnetic field intensity due to an infinite sheet. (Ida 2015, 396-400) These examples allow the choice of suitable Ampèrian contours around the current distributions. (Ulaby et al. 1997, 255) The Ampère's law is universally applicable, but it might not be feasible to be used in more complex applications. (Ida 2015, 396; Ulaby et al. 1997, 255)

The original form of the Ampère's law can be used to solve a magnetic field in a static case. In a time-varying case however, some modification to the original state of the law is required. The addition of the displacement current to the Ampère's law simply states that electric charge is conserved. Propagation of power has a finite speed, which displacement current considers. Equation (5) shows the Ampère's law with Maxwell's modification in differential form. The displacement current is the last term in the right-hand side of the equation. (Ida 2015, 566-572) The displacement current can be explained with a capacitor. In an AC circuit, current flows through the capacitors insulating material. This is the displacement current

between the conducting plates of the capacitor. It acts like a real current and has the same properties, but it does not transfer any free charges. (Ulaby et al. 1997, 299-300)

The total current through a surface is the sum of conducting current and displacement current. The displacement current is zero in a perfect conductor and with DC. On the other hand, the conducting current is zero through the insulating material of the perfect capacitor. In nature however, perfect conductors and capacitors do not exist, thus in an AC circuit the total current through a surface is always a combination of conducting and displacement current. (Ulaby et al. 1997, 299-300) However, for low frequency applications, the quasi-static form of the Ampère's law might be preferable to be used. Then the displacement current term of the equation is neglected, because it would be negligible small with low AC frequencies. (Pyrhönen & Nerg 2004, 7.24)

$$\nabla \times \boldsymbol{H} = \boldsymbol{J} + \frac{\partial \boldsymbol{D}}{\partial t} \tag{5}$$

H = magnetic field intensity [A/m]
J = electric current density [A/m^2]
D = electric flux density [C/m^2], [As/m^2]
t = time [s]

2.2.3 Gauss's law

According to the Gauss's law, the total electric flux through a closed surface is equal to the charge enclosed by this surface. It is important to note that the charge must be on the surface or it does not contribute to the electric flux through the surface. The Gauss's law can be used for calculating some cases in electrostatics. If the charge configuration is known, the electric field intensity or electric flux can be calculated using the Gauss's law. It can be also used for calculating the equivalent charge in a volume. In this case the electric field must be known everywhere in space, but especially where the Gauss's law is applied. The Gauss's law in differential form is presented in equation (6). (Ida 2015, 143-144)

$$\nabla \cdot \boldsymbol{D} = \rho_v \quad (6)$$

D = electric flux density [C/m^2], [As/m^2]
ρ_v = electric volume charge density [C/m^3]

2.2.4 No monopoles or Gauss's law for magnetism

The no monopoles law is the magnetostatic counterpart for the Gauss's law. The no monopoles is also known as the Gauss's law for magnetism. The differential form of the law is presented in equation (7). The right-hand side of the equation (7) is zero. This means that for the electric point of charge, there is no counterpart in magnetism. For the electric point of charge the hypothetical magnetic counterpart is called a magnetic monopole. However, as can be seen from the equation (7), single magnetic poles do not exist in nature. Hence the name, no monopoles. In other words, magnetic field line is always a closed loop. (Ulaby et al. 1997, 249)

$$\nabla \cdot \boldsymbol{B} = 0 \quad (7)$$

B = magnetic flux density [Vs/m^2], [T]

2.2.5 Constitutive relations

The two constitutive relations are required for solving the electromagnetic system. The four Maxwell's equations (equations 3, 5, 6 and 7) do not specify material properties at all. Electromagnetic fields are material dependent, and the constitutive relations indicate this dependency. (Ida 2015, 571)

Equation (8) presents the relation between the magnetic flux density and magnetic field intensity. (Ulaby et al. 1997, 236) The magnetic permeability is material related. It can be

though as the counterpart for conductivity of the material. It is then a measure how easily magnetic field forms in the material. The permeability for most materials is constant, but for ferromagnetic materials (e.g. iron) the relation between magnetic flux density *B* and magnetic field intensity *H* is nonlinear. Also, the permeability for most dielectrics and metals (except ferromagnetic metals) is the same as the permeability of the vacuum. Ferromagnetic materials have permeabilities higher than the vacuum. (Lehner 2010, 304; Ulaby et al. 1997, 236)

$$\boldsymbol{B} = \mu \boldsymbol{H} \tag{8}$$

B = magnetic flux density [Vs/m^2], [T]
μ = magnetic permeability [H/m]
H = magnetic field intensity [A/m]

Equation (9) shows a simple relation between the electric field intensity and electric flux density. This relation is based on the estimation of the permittivity. The permittivity itself is an experimental evaluation. (Ida 2015, 175)

The permittivity is also material dependent. It is a measure of the polarization in the material. The permittivity describes how much electric charge is needed to create one unit of electric flux in a medium. (Ida 2015, 173-175) The electric polarization indicates the density of electric dipole moments in a dielectric material. The polarization can be compared to material magnetization and it illustrates how material changes the applied electric field. It also tells how the material reacts to an applied electric field. (Ulaby et al. 1997, 14-15) Permittivities for different materials are always higher than the permittivity of the vacuum. Permittivities are possible to be measured for different materials. (Ida 2015, 173-175)

$$\boldsymbol{D} = \varepsilon \boldsymbol{E} \tag{9}$$

D = electric flux density [C/m^2], [As/m^2]
ε = permittivity [F/m]
E = electric field intensity [V/m]

The material properties, permittivity and permeability can be linear or nonlinear, isotropic or anisotropic, and homogenous or non-homogenous. Linear material property means that when the field (magnetic or electric) changes, the property does not change. Linear material property is not the same as linear variation. For example, if the permeability of the material varies linearly with the applied field, the material is then nonlinear in permeability. A material whose physical properties are the same in any point of the material is homogenous. If a direction of space does not affect the properties of a material, then the material is isotropic. (Ida 2015, 176)

2.2.6 Lorentz force equation

The Lorentz force equation describes the total electromagnetic force effecting a moving charge, as shown in equation (10). It considers both, electric and magnetic fields. Electric and magnetic forces have few substantial differences. The electric force is always in the direction of the electric field, but the magnetic force is perpendicular to the magnetic field. The electric force acts always on a charged particle, whether it's moving or not, but magnetic force acts on the charged particle only when it's moving. When the electric force is displacing a charged particle, energy is consumed. However, the magnetic force does no work displacing the charged particle. (Ulaby et al. 1997, 237 & 273)

$$\boldsymbol{F} = q(\boldsymbol{E} + \boldsymbol{v} \times \boldsymbol{B}) \tag{10}$$

F = Lorentz force [N]
E = electric field intensity [V/m]
q = electric charge [C]
v = charge velocity [m/s]
B = magnetic flux density [Vs/m^2], [T]

2.3 Heat transfer by electromagnetism

There are several ways on how the energy of electricity and magnetism can turn into heat. These include the resistance of the material and the magnetic hysteresis phenomena. The heat produced by electromagnetism is usually thought as losses of the system. The exception is induction or resistance heating process for materials. (Makarov et al. 2016, 39; Lupi et al. 2015, 1)

2.3.1 Resistance of the material

According to Ohm's law, resistance can be found using equation (11). The resistance is a proportionality constant; thus, the equation is linear. Equation (11) shows that there is a relation between the voltage across the resistance and the current through the resistance. For an ohmic conductor, the resistance can be found differentiating the Ohm's law, presented in the equation (11), under specific conditions. (Makarov et al. 2016, 33 & 36)

$$U = RI \tag{11}$$

U = voltage [V]
R = resistance [Ω]
I = current [A]

The short and open circuit are the two limiting cases of the resistance voltage-current characteristics shown in figure 5. In the figure 5, U is the voltage and I the current. The short circuit happens when the resistance becomes zero. This represents an ideal wire. When the resistance is zero, there is no voltage drop across the wire, but any current can flow through it. Infinite resistance signifies that the resistance becomes an open circuit. Then, at any voltage there is no current flowing through the wire. This represents an ideal vacuum gap. (Makarov et al. 2016, 34)

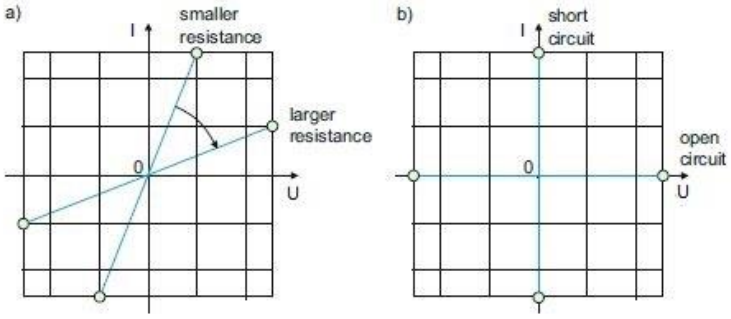

Figure 5. Voltage-current characteristics for resistance (modified from Makarov et al. 2017, 34)

Work in joules required to pass 1 coulomb of charge through the resistance is the voltage across the resistance. The power transferred to the resistance is the product of work per unit charge, because in one second exactly *I* (current) coulombs pass through the resistance. The power also represents the number of charges passing in one second through an element. Figure 6 presents the power rectangles for the voltage-current dependence. The electric power *P* is equal to the to the rectangle areas in the figure. (Makarov et al. 2016, 35)

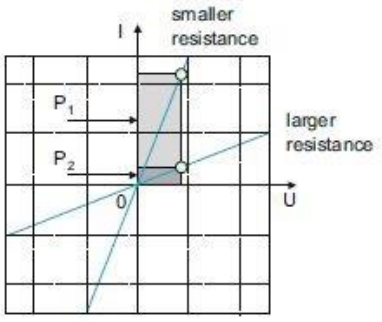

Figure 6. Voltage-current characteristics for resistances and absorbed powers (modified from Makarov et al. 2016, 35)

The resistance absorbs the electric power delivered to the resistance. The electric power absorbed by the resistance of an ohmic conductor transforms into heat. This heat loss is known as the electric power loss. There are three equal interpretations for the absorbed power of the resistance. Equations (12), (13) and (14) show these definitions, which are obtained from the Ohm's law. Equation (12) presents the basic definition, which can be used for any passive circuit element. The power for resistance can be calculated also in terms of voltage with equation (13) and in terms of current with equation (14). (Makarov et al. 2016,

35 & 39) These equations apply also for the AC if there is a pure resistor without any capacitive and inductive properties in the circuit. (Ahoranta 2017, 133)

$$P = UI \tag{12}$$

P = power [W]
U = voltage [V]
I = current [A]

$$P = \frac{U^2}{R} \tag{13}$$

P = power [W]
U = voltage [V]
R = resistance [Ω]

$$P = RI^2 \tag{14}$$

P = power [W]
R = resistance [Ω]
I = current [A]

Temperature of the material influences the resistance. Usually, when the conductor's temperature increases, the resistance of the conductor increases also. For both AC and DC, the increased resistivity of the conductor forms non-uniform distributions of current density which leads to a non-uniform internal heat sources in the material. (Lupi et al. 2015, 3)

The resistance of the same size conductor for alternating current is larger than for direct current due to skin effect and proximity effect. The skin effect arises from the issue that for AC currents, the current is not evenly distributed over the conductor. Due to electromagnetic induction, the current density decreases from the surface towards the center of the conductor.

The current density due to the skin effect in a cylindrical conductor can be seen from figure 7, where J is the current density, B_I is a magnetic flux produced by the current I and B_i is a reaction magnetic field due to eddy current i. The AC magnetic flux induces eddy currents in the conductor. These induced eddy currents increase the value of the current close to the conductor's surface and reduce it in the center. The skin effect gets stronger as the frequency of the AC increases. This phenomenon causes a reduction to usable cross-section area of the conductor, which increases the resistance. (Silva & Bak 2013, 4; Lupi et al. 2015, 8-9)

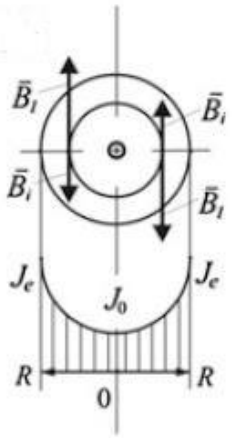

Figure 7. Current density in the conductor due to skin effect (modified from Lupi et al. 2015, 9)

An important parameter of the skin effect is the penetration depth of the electromagnetic wave in the material. Penetration depth describes the degree of attenuation of electromagnetic field in the conductor. This basically means that, with a low penetration depth, the current flows only at close to the surface of the conductor. The penetration depth can be calculated with equation (15). The penetration depth value is the distance from the surface of the conductor at which the current density is decreased to a value $e = 2.718$ times lower than at the surface. From the equation (15), can be noted that the penetration depth depends on the electromagnetic properties of the material and the frequency. Therefore, different materials have different penetration depths at the same frequency. (Lupi et al. 2015, 9-10) Ferromagnetic materials have low penetration depths, which means that their AC-resistance is much greater than their DC-resistance. (Zaidi et al. 2014, 2)

$$\delta = 503\sqrt{\frac{\rho}{\mu_r f}} \quad (15)$$

δ = penetration depth [m]
ρ = resistivity [Ω·m]
μ_r = relative permeability
f = frequency [Hz]

The proximity effect occurs when there are two conductors nearby and AC current is flowing in both conductors to opposite directions. The current distribution in the conductors change because of the AC current. The currents in each conductor strive to arrange themselves so that the energy stored in the magnetic field minimizes. This leads into minimum inductance of the system. (Aebischer & Friedli 2018, 1-4) Eddy currents are induced to the conductors similarly to the skin effect. The induced eddy current in the conductor has direction that the magnetic field created by the eddy current opposes the external magnetic field that has produced it. The proximity effect depends on the AC frequency and the distance between the conductors. The redistribution of current density in the conductors can be similarly explained by the induced eddy currents when the currents in the conductors are in the same direction. Figure 8 presents the proximity effect with two conductors and alternating current *I* flow in both. On the left side of the figure, currents of the conductors are flowing in opposite directions and on the right side in the same direction. *J* is the current density inside the conductors and *B* the magnetic flux. (Silva & Bak 2013, 4; Lupi et al. 2015, 14)

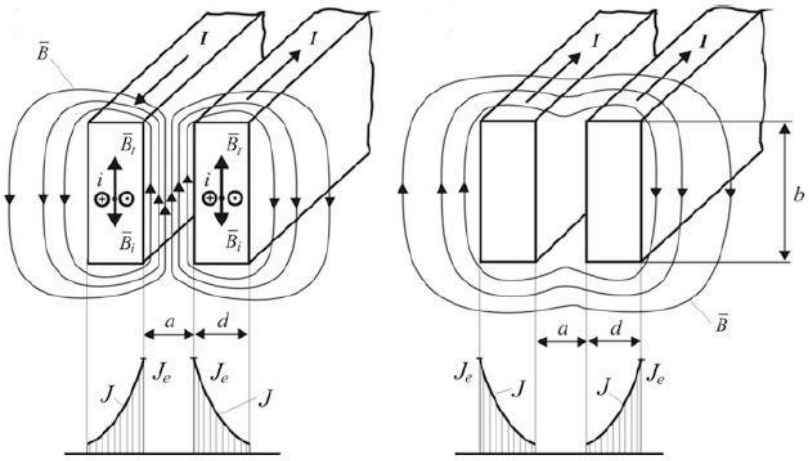

Figure 8. Current density in conductors due to proximity effect (modified from Lupi et al. 2015, 15)

2.3.2 Magnetic hysteresis

Magnetic moments in ferromagnetic materials tend to align in the same direction as an external magnetic field. These materials even stay partially magnetized when the external magnetic field is removed. (Ulaby et al. 1997, 261) Materials which are ferromagnetic have their relative permeabilities higher than one. Relative permeability gives the ratio between permeability of the material and permeability of the vacuum. For example, iron is ferromagnetic material and its relative permeability is about 6000. (Ida 2015, 442-444)

The ferromagnetic properties are easier to understand with the help of magnetized domains within a ferromagnetic material. Magnetized domains are very small, in the magnitude of 10^{-9} mm^3 to 1.0 mm^3 (Ida 2015, 444) regions where the magnetic moments of all atoms are aligned permanently with each other. The alignment of the magnetic moments is due to strong coupling forces between the magnetic dipole moments. When there is no external magnetic field, the magnetic domains are randomly orientated compared to each other. When this unmagnetized ferromagnetic sample is placed in an external magnetic field, the magnetized domains align partially with each other. Figure 9 shows magnetized domains in a ferromagnetic material. In the case **a**, domains are randomly orientated in the material. In the case **b**, magnetized domains start to align with an external magnetic field and the external

field causes domains to grow. Case **c** shows a situation where aligned domains occupy most of the volume in the ferromagnetic material. (Ulaby et al. 1997 261-262; Ida 2015, 445)

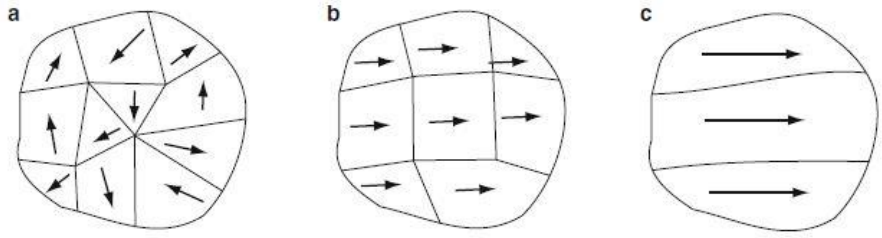

Figure 9. Magnetized domains in a ferromagnetic material (Ida 2015, 445)

The magnetization curve is a good way of explaining the magnetization behavior of a ferromagnetic material. The magnetization curve, or the *B*-*H* curve, is a plot of the ferromagnetic material internal magnetic flux density *B* against an external magnetic field intensity *H*, which is experimentally proven. It is also known as the hysteresis curve. Figure 10 presents a magnetization curve for iron. The point *O* presents the initial condition, on which the material is in non-magnetized state. The magnetic flux density in the material increases along the curve as the external field is increased. When all the magnetized domains in the material are aligned with the external field, magnetization of the material does not increase anymore even though the external field intensity is increased. This is called a saturation point H_S and it's shown in the figure as point M_1. The curve between points *O* and M_1 is called an initial magnetization curve. (Ida 2015, 445)

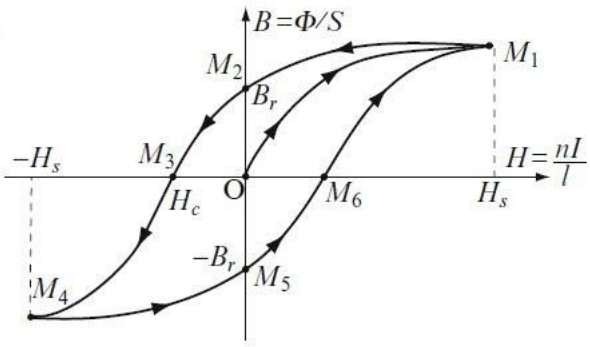

Figure 10. B-H curve for iron (modified from Ida 2015, 445)

When the external field is decreased from the saturation point, the magnetization curve does not follow the initial curve. There is a lag in the realignment of the magnetized domains, which causes the internal magnetic flux to decrease slower. At the point M_2, the external magnetic field intensity is zero, but in the material, there is still remanent magnetic flux density B_r. Now, the material has an internal magnetic field without the external field. Reducing the internal magnetic flux density to zero requires applying an external magnetic field in the opposite direction. At the point M_3, the internal magnetic flux of the material is reduced to zero. The external magnetic field intensity at the point M_3 is called coercive field intensity H_c. The magnetization curve from the point M_4 to M_1 is the same as the curve from the point M_1 to M_4, only in opposite direction. The full loop is now complete. If the cycle is continued by increasing and decreasing the external magnetic field intensity, which happens for example with AC current, the magnetization of the material follows this outer loop in the figure 10. (Ida 2015, 446)

The area inside the magnetization curve loop presents the energy required to move the domain walls and align them. The energy of the magnetization is lost to heat in the process. Each cycle of the AC magnetization field traces the loop one time. Energy is lost during each cycle per unit volume of the material. It is easily understandable that a narrow loop causes less losses than a wide loop. Materials which have narrow magnetization loops are called soft magnetic materials and those with wide loops are hard magnetic materials. It can be also noted that the slope of the magnetization curve at any point gives the permeability of the material at that specific field level. (Ida 2015, 446; Ulaby et al. 1997, 262)

2.3.3 Eddy currents

The previously discussed Faraday's law, as shown in equation (3), is general. For this reason, actual physical loop is not required for the Faraday's law to be applicable. Flux induction, hence, the electromotive force and current, can occur even if the loop is not noticeable. In figure 11, there are three cases; **a**, **b** and **c**, where uniform time-dependent magnetic flux *B* flows through objects. In the case **a**, there is a loop where current *I* is induced to the loop due to changing magnetic flux *B*. In the case **b**, a cylindrical conductor is placed in the *B*-

field and current is also induced inside the conductor, even though there is no loop. The cylinder in the case **b** can be though as been composed of thin short-circuited cylindrical loops, as shown in the case **c**. Every loop in the case **c** has an electromotive force which then produces an induced current in each loop. These currents are called eddy currents and they can occur in any conducting volume. Eddy currents dissipate power in the conductive volume, thus produce heat in the material. (Ida 2015, 542)

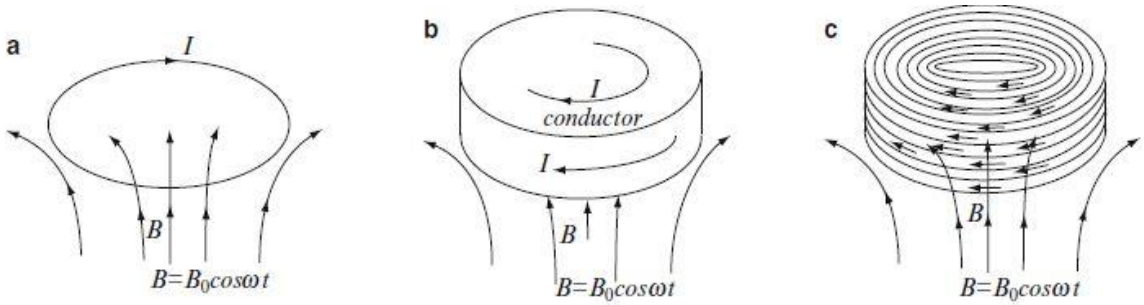

Figure 11. Eddy currents (Ida 2015, 542)

The frequency of the changing magnetic flux effects on the induced eddy currents in a way that, higher frequencies produce more eddy currents and power dissipation in the material. In reality, the magnetic flux density changes in the material due to the skin effect. For this reason, more power is dissipated on the surface of the material than in inner parts. (Ida 2015, 544)

3 STATCOM AND SVC

Static synchronous compensator, STATCOM and static var compensator, SVC, are part of the GE's FACTS; flexible alternating current transmission system. They are power electronic devices which provide reactive power dynamically to an AC network. STATCOM and SVC support the voltage along the transmission line, improving the efficiency and reliability of the AC transmission system. FACTS solutions can be built to support new or existing transmission systems. (Oinonen 2017, 2) Other than STATCOM or SVC, FACTS solutions also include synchronous condenser (SC), fixed series compensation (FSC) and thyristor-controlled series compensation (TCSC). All these systems have their own advantages and disadvantages, which is why all of them are still used in today's AC network systems. (Kähkönen 2016a, 3-4) Figure 12 presents GE's different FACTS solutions. Reactive power compensation systems are connected to the AC network using shunt or series connection. STATCOM, SVC and SC are connected to the network via shunt connection. FSC and TCSC are connected in series with the network. (Oinonen 2017, 2)

The main purposes of STATCOM and SVC are to stabilize the voltage in the AC transmission system, increase the transient stability, damp system power oscillations, filter harmonics and reduce flicker in the system. STATCOM and SVC controls the voltage of the transmission line to compensate for reactive power balance. (Kähkönen 2016a, 22)

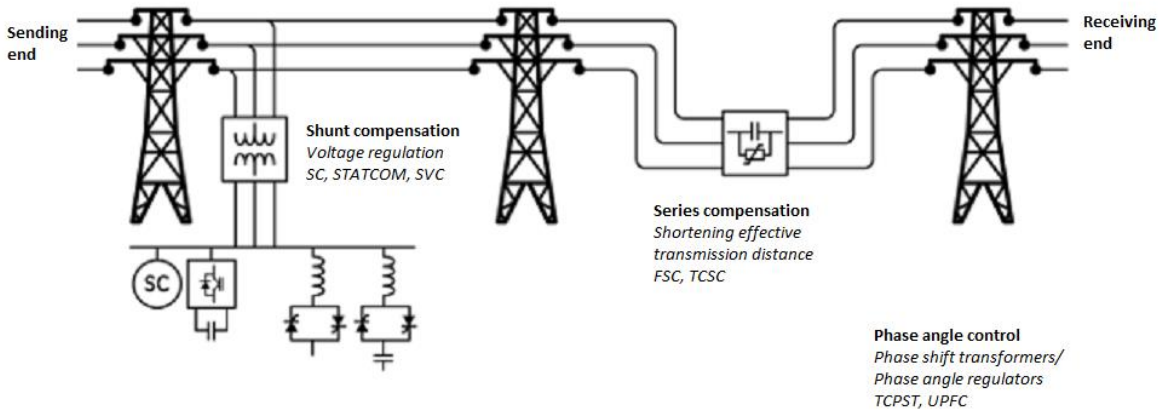

Figure 12. GE FACTS solutions (modified from Oinonen 2017, 2)

3.1 STATCOM

The operation of STATCOM is based on a series of associations between different devices to synthetize a sinusoidal AC waveform. The main components of the STATCOM are voltage source converter (VSC) valves, phase reactors, step-down transformer and control system. (Oinonen 2017, 8) STATCOM produces alternative current with VSC valves. By controlling VSC valves in a specific way, the STATCOM can produce inductive or capacitive current independent of the grid voltage. The output AC waveform of the STATCOM VSC valves is a staircase like. The basic idea of the STATCOM is shown in figure 13. The magnitude of the voltage produced by the STATCOM is adjusted in terms of the system voltage to generate or absorb reactive power. (Kähkönen 2016b, 2-7) VSC valve control does not produce much low order harmonics, which is an advantage compared to the SVC control. (Kurka 2017a, 4)

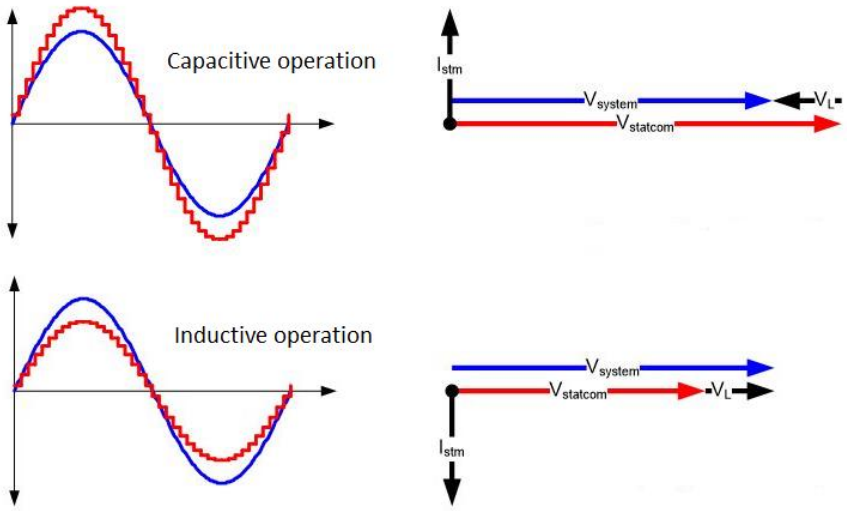

Figure 13. Basic idea of the STATCOM (modified from Kähkönen 2016b, 7)

Figure 14 presents a STATCOM system in a generalized simple diagram. It should be noted that in a real STATCOM there is one VSC valve for each of the three phases and several VSC branches might be connected to the substation's main busbar. One complete valve can have several valve modules depending on the STATCOM requirements and each valve module has eight submodules. (Kähkönen 2016c, 3-13) In the case of unsymmetrical operation range, the operation power range can be extended with thyristor-switched

capacitors, thyristor-controlled reactors or passive shunt connected reactors. In some cases, also a harmonic filter is required. (Kähkönen 2016d, 9)

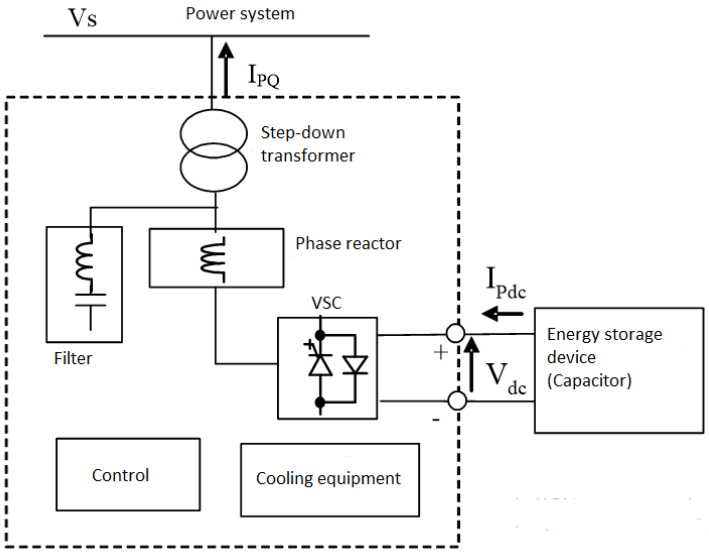

Figure 14. Generalized STATCOM configuration (modified from Kähkönen 2019, 58)

3.2 SVC

SVC absorbs the inductive reactive power when the system voltage is too high, and when the voltage is too low, capacitive reactive power is generated into the transmission line. Its main components are thyristor-switched capacitors (TSC), thyristor-controlled reactors (TCR), thyristor valves, harmonic filters, step-down transformer and control system. There might also be mechanically-switched capacitor (MSC) and mechanically-switched reactor (MSR) branches depending on the need for the reactive power. The required capacitive reactive power by the system is produced with capacitors and the inductive reactive power with reactors. (Kähkönen 2016a, 22-27) Modern SVC's also contains a GE patented main reactor, which increases the performance and makes the SVC more cost-efficient for demanding networks. Figure 15 shows a simplified single line diagram of the SVC with main components. (Kähkönen 2019, 44)

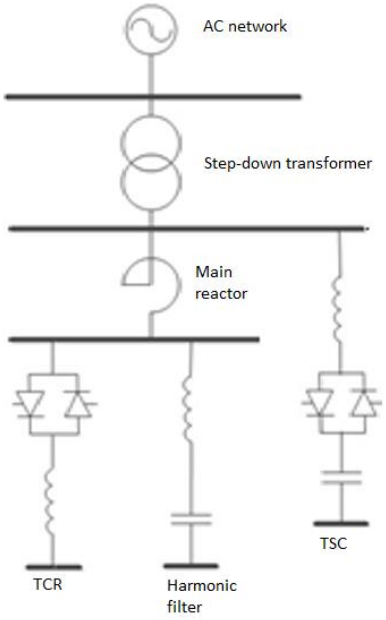

Figure 15. SVC simplified single line diagram (modified from Kähkönen 2019, 44)

Harmonic filters are required in the SVC, because the control of the thyristor valves for the TCR's causes harmonics. In order to control the SVC output continuously, the thyristor valve for the TCR must be able to regulate the current flow through it. This is done by changing the firing angle α of the thyristor valve. Between a fully conducting state (α = 90°) and fully blocking state (α = 180°), the current of the thyristor valve becomes distorted, as shown in figure 16. Harmonics in terms of the firing angle α, that escapes from the TCR branch are presented in figure 17. Harmonic currents which are dividable by three, for example third and ninth harmonic, circulates between the delta connected step-down transformer secondary and they cannot escape to the grid. Harmonic filters are required only for those harmonic currents that escapes from the TCR branch. Each harmonic current requires its own filter if single frequency tuned filters are used. The number of harmonic filters depends on the SVC requirements. Thyristor-switched capacitors are not a source of harmonics, even though the control is done with thyristor valves. This is because TSC's can either be fully on or off. (Kähkönen 2019, 10-17)

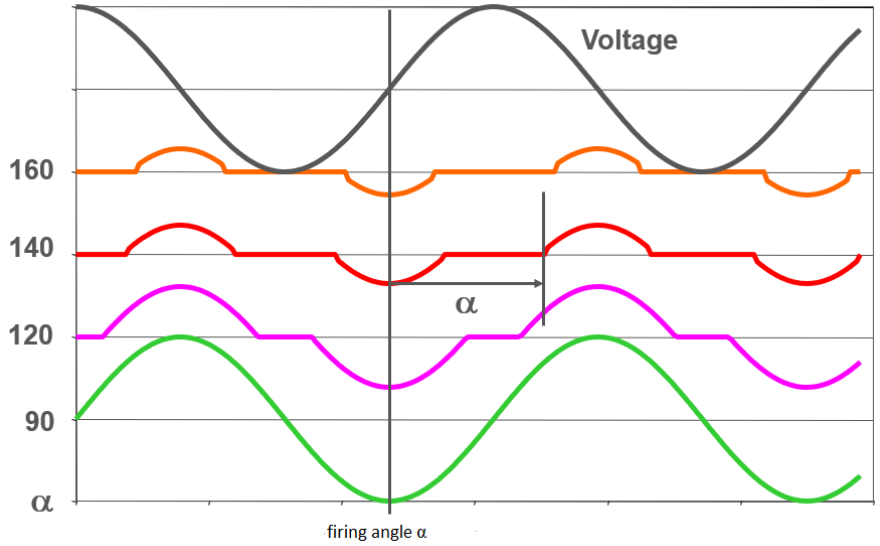

Figure 16. TCR current waveforms (modified from Kähkönen 2019, 15)

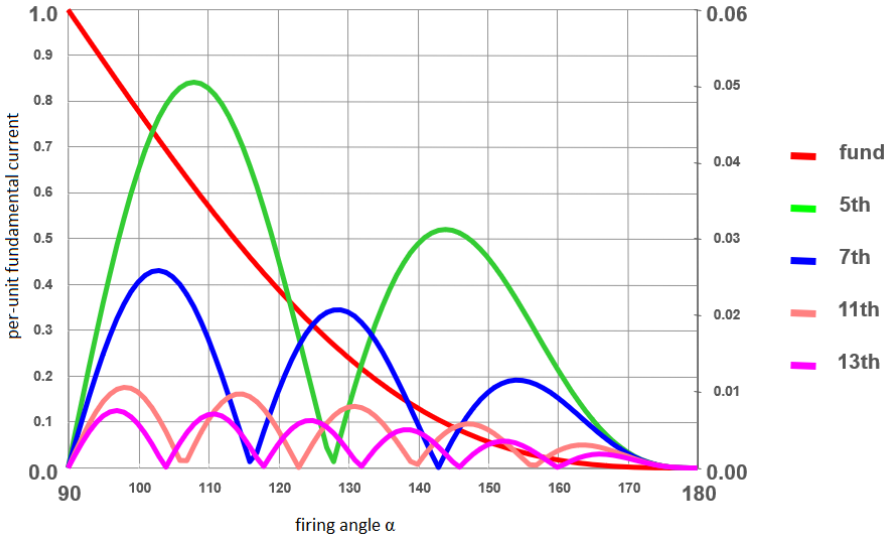

Figure 17. Harmonics produced by the control of the TCR (modified from Kähkönen 2019, 16)

4 DEFINING THE PROBLEM

The main sources of magnetic fields in the STATCOM and SVC substations are the air core reactor coils. The air core reactors are used for example in the STATCOM phase reactors, SVC TCR's, SVC main reactors, MSR's and harmonic filters. Other sources of magnetic fields worth mention are busbars with high current, cabling between components, VSC valves and thyristor valves. However, the magnetic field produced by any individual component other than air core reactors is much smaller than what the reactor coils produce. (Kauppi 2018, 12)

The major problem of the changing magnetic fields produced by air core reactors are the induced currents. Two types of induction can cause problems: eddy currents in nearby metal structures and circulating currents in closed conducting loops at any distance, where the changing magnetic field is significant enough to cause induction. Eddy currents are relatively easy to approximate and clearance distance due to eddy currents can be given quite accurately. The clearance requirement due to induction in conducting loops is very difficult to approximate accurately. There are many variables which effect the influence of the induced current. Affecting variables include the distance from the reactor to the loop, angle of the loop relative to the magnetic field, loop size, loop thickness, loop conductivity and magnetization properties of the loop. Conducting loops where the induction can occur include for example concrete reinforcements, metal fences, structural members of a building and unintentional loops made by substation grounding. Induced currents can cause severe damage to different structures, substation buildings and equipment. The problem can arise if the conductor is entirely or partially thin and induced current flowing in the conductor is high. The resistance of the conductor becomes higher in a section where the conductor cross-section is smaller, which increases losses in that section and causes it to heat. The heat can cause damage to the equipment or even start fires. The induction also generates extra losses for the reactors. The unintentional induced current circulating in the substation grounding can cause interference to current measurements and signaling. (Kauppi 2018, 12-34; Keikko 2018)

4.1 Air core reactors

Generally, air core reactors can be divided into five different groups: damping reactors, harmonic filter reactors, shunt reactors, current limiting reactors and neutral earthing reactors. These reactor types are used in power generation, transmission and distribution networks, industrial sites and electrical test laboratories. Even though air core reactors in the STATCOM and SVC systems might serve a different purpose depending on the application, the construction of the reactors are fundamentally similar. Reactors are basically coils, with aluminium winding encapsulated in fiberglass. The winding consists of many aluminium conductors connected in parallel and insulated with polyester film. Conductors are encapsulated in epoxy impregnated fiberglass filaments, forming cylinders. The total amount of cylinders depends on the reactor rating. Cylinders are connected in parallel through spider-arms, which are located on top and below the coil. Each cylinder has 1-10 layers and each layer has 1-20 aluminium conductors connected in parallel forming an electrical round. The number of conductors in each cylinder is different and it depends on the optimization of the reactor design. Figure 18 shows and example of the reactor design. Single reactor might have two-piece design, when the two halves are stacked on top of each other. This is usually the case for big reactors. (Keikko 2018)

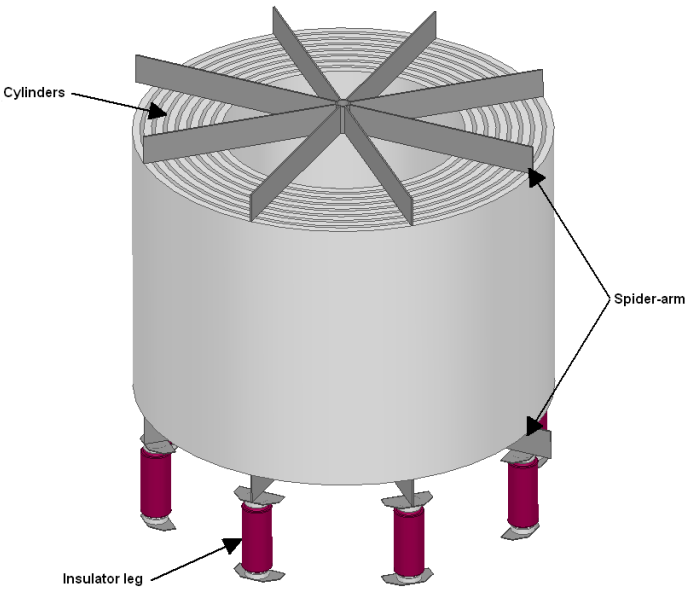

Figure 18. Air core reactor design

There are two types of clearance requirements for air core reactors that needs to be considered. The first one is eddy current clearance which is referred by GE with $\mathbf{m_x}$, $\mathbf{m_y}$ and **C** clearances. The $\mathbf{m_x}$ is a minimum horizontal clearance from the center of the reactor to any metal structure. The $\mathbf{m_y}$ is a minimum vertical clearance from the top or bottom spider-arm to any metal structure. The **C** clearance tells the minimum distance between reactors on other phases from center to center. It should be noted, that the clearances $\mathbf{m_x}$, $\mathbf{m_y}$ and **C** are defined from the reactor point of view. That is, to avoid unnecessary reactor losses and to guarantee the reactor operation at the rated values. The second and more problematic clearance type is for the induced currents in metal structures that form loops, created by the magnetic fields of the reactors. There have not been any real studies to resolve this issue by GE. Thus, there are only estimates on how close conducting loops can exist to reactors. The main object for the thesis is to get better understanding on safe distances for large metal structures and structures forming conducting loops. Definite clearances would help the designing and optimization of STATCOM and SVC substation layouts, as well as give guideline for a structural design in areas with high magnetic field. (Kauppi 2018, 12-26)

4.1.1 Coil inductance, inductive reactance and impedance

Inductance is an important quantity of a reactor. The inductance describes how much energy an inductor (coil) can store in a magnetic field which has been produced by the inductor itself. The inductance of a coil is then a magnetic flux through the coil created by a unit current in the same coil. The bigger the inductance, the greater the magnetic field produced by the coil. The inductance of a coil is dependent on the cross-section area of the coil, number of turns in the winding, height of the coil and the coil core material. For air core reactors, the core material is of course air and it has almost the same permeability as the vacuum. Increasing the cross-section area and the number of turns, increases the inductance for the same height coil. The inductance for a coil with height to radius ratio over one can be calculated using equation (16). (Makarov et al. 2016, 272-274)

$$L = \frac{\mu A N^2}{h} \tag{16}$$

L = inductance [H]
μ = core magnetic permeability [H/m]
A = cross-section area [m^2]
N = number of turns
h = coil height [m]

In an AC circuit the inductance can be explained as coils structure influence on the inductive reactance. The inductive reactance is a property of an inductor in the AC circuit, which opposes the change in the current. Reactance contributes to the total impedance of the AC circuit. The inductive reactance is directly proportional to the coil's inductance and AC frequency according to equation (17). This is also the impedance for a lossless coil. (Ahoranta 2017, 141-143)

$$X_{\mathrm{L}} = 2\pi f L \tag{17}$$

X_{L} = inductive reactance [Ω]
f = AC frequency [Hz]
L = inductance [H]

A real coil also has some resistance in the winding. Thus, the total coil impedance is a combination of inductive reactance and resistance according to equation (18). (Ahoranta 2017, 147)

$$Z = \sqrt{R^2 + X_{\mathrm{L}}^2} \tag{18}$$

Z = impedance [Ω]
R = resistance [Ω]
X_{L} = inductive reactance [Ω]

4.1.2 Reactor magnetic field

The ANSYS model of a magnetic field density produced by a single-cylinder reactor coil is presented in figure 19. The magnetic field outside the air core reactor becomes quite strong. The changing magnetic field can induce currents to conducting loops reasonably far away. The multi-cylinder structure does not have much effect on the produced magnetic field compared to the single-cylinder structure. Spider-arms however do affect the magnetic field at close distances. They deform the magnetic field slightly. Spider-arms are used to distribute alternating current to different cylinders. Thus, it means that high current levels flow through spider-arms, which then produce their own magnetic field. The deformation is limited only to close distances from the reactor and outside the $\mathbf{m_x}$ distance, the magnetic field should be uniform. (Keikko 2018)

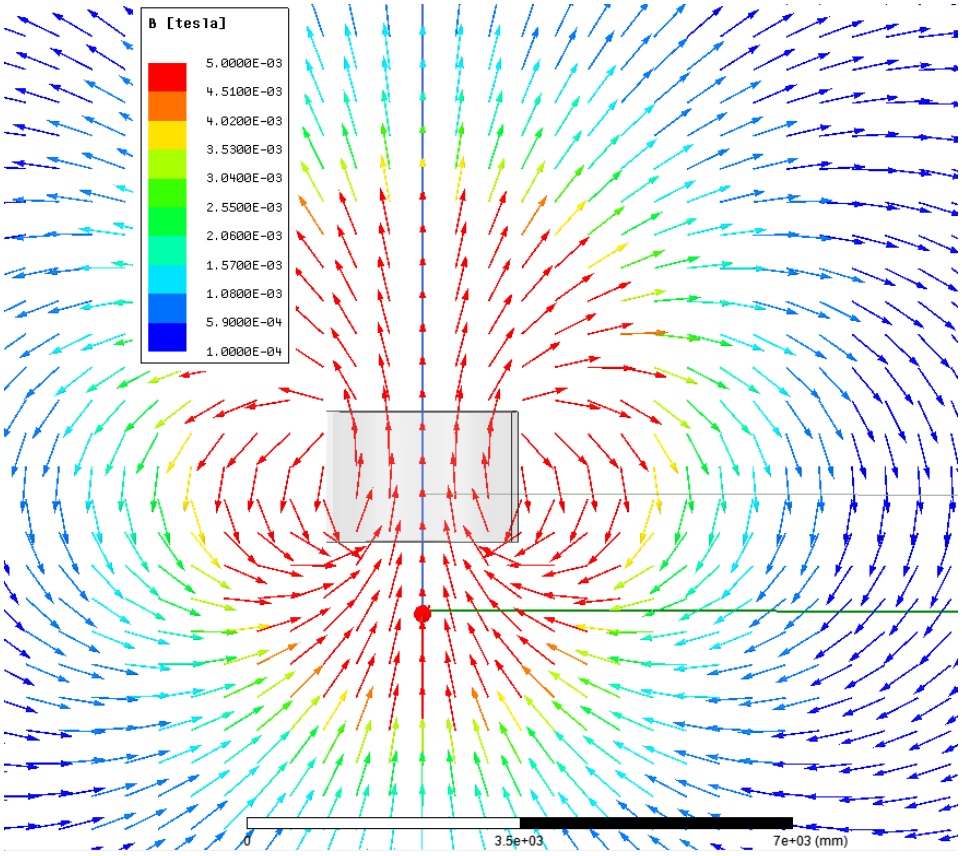

Figure 19. Air core reactor coil magnetic flux density vector field

As mentioned before, TCR's of the SVC generates harmonic currents depending on the firing angle of the thyristor. Harmonics can cause temporary current spikes, that create strong temporary magnetic fields. The frequency of the magnetic field caused by harmonic currents is the same as the frequency of the harmonic current. Harmonic currents are usually smaller than the current of the fundamental frequency, which is why harmonics are not necessary to be studied in the thesis. The strongest RMS (root mean square) magnetic fields are more important in terms of the induction and for TCR's, these occur at full load. (Tornberg 2019)

Even though air core reactors create strong magnetic fields outside the reactor, that can cause problems; the benefit of air core dry-type reactors is that they provide linear response of impedance in terms of the current. That is essential in numerous applications. (Keikko 2018)

5 EXPERIMENTAL PART

For the thesis, series of laboratory tests and simulations were conducted to determine the magnetic field around an air core reactor, induction of current to a loop and how much the loop structure warms due to losses caused by the induced current. These experiments should help to understand what kind of materials should be used in structures close to air core reactors and investigate the effects of the changing magnetic field further away from the reactors. Comparing the results between the lab tests and simulations should verify, whether the ANSYS software is suitable for simulating reactor magnetic fields and the effects of current induction to different structures, when designing STATCOM or SVC substations.

The air core reactor coil used for laboratory tests and simulations was a bottom half of a two-piece thyristor-controlled reactor (TCR) for the SVC. The reactor in question had a rated current of 2577 A RMS and total rated inductance of about 23 mH. The inductance for one half of the reactor was then about 12 mH. Both halves of the reactor had eight cylinders and the average number of turns per cylinder was 79. The average pitch for the aluminium winding was 21 mm. The outer diameter of the reactor was about 2770 mm and bore 2000 mm. The height of the bottom half of the reactor with post insulators was about 2870 mm. The reactor used for testing is presented in figure 20. As simplified, one reactor half can be thought as a cylindrical coil with 79 turns and with 21 mm pitch for the winding. The $\mathbf{m_x}$ clearance for this particular reactor was 3850 mm. The induction tests were planned to be conducted at from very close distance to outside of the $\mathbf{m_x}$ distance. Then it is possible to see the effect of eddy currents in addition to circulating current in the loop.

Figure 20. Air core reactor used in the laboratory tests and as a model for simulations

Loops to test the induction were extracted from capacitor racks. Four different loops were tested: a whole steel loop, a steel loop with a ≈5 mm cut, a whole aluminium loop and an aluminium loop with a ≈5 mm cut. Whole and cut loops for the same material were identical, except for the cut. The idea of the cut loops was to determine whether a small gap in the loop is enough to prevent the current flow due to induction and what are the effects due to eddy currents. Figure 21 shows the steel and aluminium loops. Cuts for both loops are shown in figure 22. The cut for the steel loop was a quite smooth 5 mm cut with a tolerance of 1 mm. The cut for the aluminium loop was more difficult to cut with an angle grinder, thus the cut gap became between three and nine millimeters. The aluminium loop cut was an average of about 5 mm. The steel loop was constructed from L-shaped steel bars with 100 mm profile. The length of the loop was 1388 mm and width 560 mm. The thickness of the steel was 10 mm. The exact material of the steel loop was S355J0 (EN 1.0553) structural steel. The aluminium loop was constructed with two T-shaped aluminium bars and two square tubes. The T-bar had profile of 105x55 mm and thickness of 5 mm. The length of T-bars was 1220 mm. T-bars were connected together from close to the ends by square tubes. Square tubes had a profile of 45x45 mm and material thickness of 4 mm. The length of square tubes was 495 mm. The exact material of the aluminium loop was AlZn5Mg1, and the EN standard equivalent for this material is EN 7020 aluminium. CAD drawings of the capacitor racks from which the loops were extracted are shown in appendix 1.

Figure 21. Loops used in laboratory tests and as models for simulations (aluminium; left and steel; right)

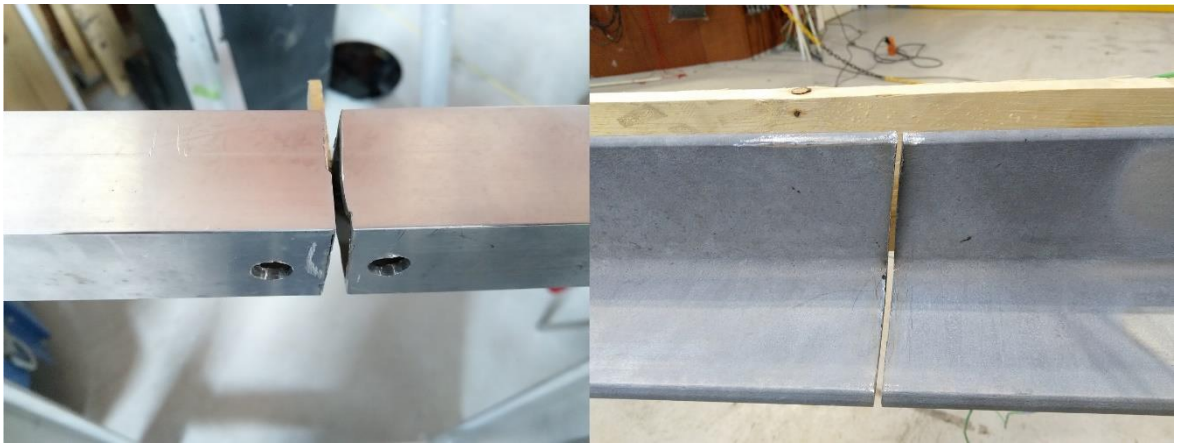

Figure 22. Cuts for the aluminium loop (left) and for the steel loop (right)

5.1 Laboratory tests

In the laboratory, series of tests were conducted with the reactor coil, and steel and aluminium loops. Main goals for the laboratory tests was to collect reliable data of the magnetic field produced by the reactor, how much current was induced to the loops and how much the loops heat due to the induction. This data is then compared to the ANSYS simulations. The laboratory tests should also give a good insight how ferromagnetic material (steel loop) and non-ferromagnetic material (aluminium loop) behaves in a changing magnetic field. The laboratory tests included measuring the steel and aluminium loop DC resistance and AC resistance, measuring magnetic field produced by the reactor coil at different distances, measurements of the induced current in the whole and cut loops at various distances and different angles. Temperature measurements of the loops were taken

in each induction test. The main AC test current for the reactor was decided to be set as 3000 A RMS, just because it was a nice round number. It is slightly larger than the rated current of the reactor, but it should not cause any problems for the reactor.

5.1.1 Test circuit

The circuit driving the reactor coil was a parallel resonant RLC-circuit. The parallel resonant RLC-circuit is a current divider circuit and it can be used to create large currents. Current amplitudes through the inductor and capacitor can be significantly larger than the supply current. The circuit, that was used to supply current for the reactor is presented in figure 23. (Makarov et al. 2016, 493) According to (Makarov et al. 2016, 487) the resonance condition for any AC circuit states that the reactance of the equivalent circuit impedance seen by the power source must be equal to zero. In the case of the test circuit, resonance condition exists if the reactance of the capacitor bank is equal to the inductor reactance. The object of the RLC-circuit was to provide 3000 A of sinusoidal AC current to the reactor. The 3000 A RMS current level was used in all laboratory tests, expect for one reactor coil magnetic field test where 1500 A current level was used.

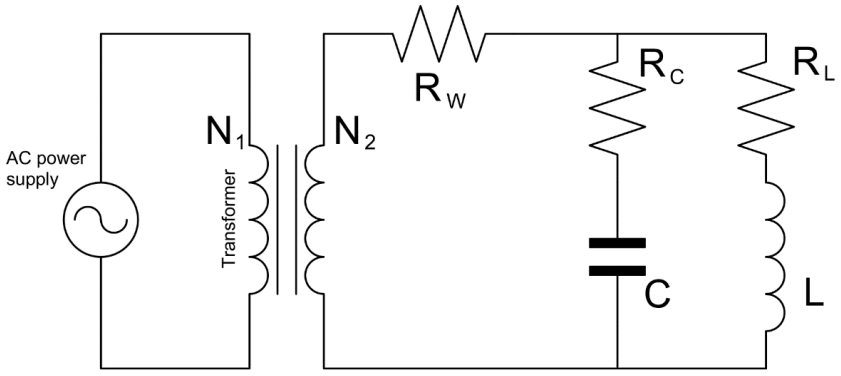

Figure 23. Circuit supplying current for the reactor

The R_W in the figure 23 represents the resistance of wires. Parasitic resistances of the realistic capacitor and inductor are represented as the R_C and R_L in the figure 23. The resonant effect is weakened by the resistance, which results in finite voltages/currents at the resonance. (Makarov et al. 2016, 487) The *C* represents the capacitor bank and the capacitance of the

capacitor bank could be adjusted almost freely. The L is the inductor and, in this case, the reactor coil. The inductance of the reactor was previously mentioned 12 mH. The AC power supply was able to provide a maximum of 200 kVA of power to the circuit and the transformer had a turn ratio N_1/N_2 of 500/12000. The power supply was a ZENONE GV1K 500V-200KVA-1 and the transformer was made by GBE in 2017. The transformer had an efficiency of 94 %. The capacitor bank was tuned as close as possible to achieve a parallel resonance between the capacitor bank and the reactor coil. However, the capacitance of the capacitors was temperature dependent and the capacitor bank was located outdoors. The capacitance did not stay uniform throughout the tests and that is why the reactor current was not exactly 3000 A during tests. Also, the power supply was tuned by hand to achieve the required 3000 A at the reactor, thus exactly 3000 A of current for the reactor would be impossible to achieve. The maximum error in the reactor current during laboratory tests was about 3 %. Figure 24 shows the form of the reactor current and it is very close to a pure sinusoidal AC. Photos of the reactor circuit equipment can be found in appendix 2.

Figure 24. Reactor coil current form

5.1.2 DC and AC resistance measurements

The first test was to measure the DC resistance and the AC resistance for steel and aluminium loops. It was assumed that the inductive and capacitive properties for both loops were insignificantly small, thus the loop impedance would contain only resistive component. The DC resistance measurement result of a loop helps to determine the correct electrical conductivity value to be used in ANSYS simulations, as will be explained later in the report. With the AC resistance measurement value, it is possible to calculate the loss by circulating

current in a loop when the current flow through a loop is known. DC and AC resistance measurements were done using 4-wire Kelvin method as presented in figure 25. The circuit diagram of the measurement is on the left in the figure and on the right, the four terminals connected to the cut steel loop. However, when measuring the AC resistance, separate AC power supply was used, and a ten-ohm resistor needed to be added to one of the main current-carrying wires to increase the circuit resistance for the AC power supply. If the circuit resistance was too low, the power supply would not deliver any power to the circuit. In the circuit diagram, the resistor would be on the wire *C2*.

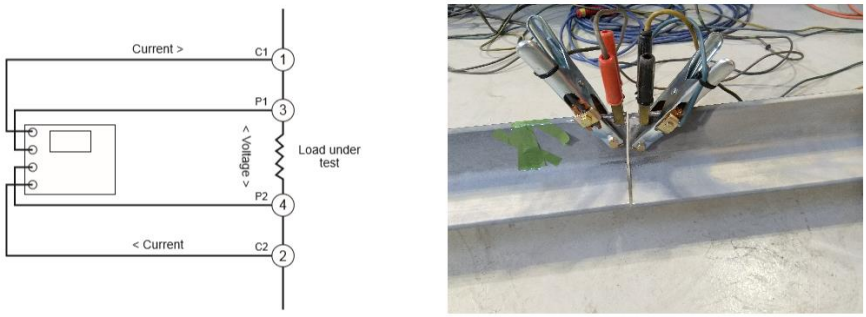

Figure 25. 4-wire resistance measurement (Martin 2014, 1) and four terminals connected to the cut steel loop

The DC resistance measurements were conducted using a Sefelec MGR10 10 A milliohmmeter. The Sefelec MGR10 includes power supply and the current used in the tests was 10 A. Possible error in the resistance measurement with this equipment was about 2 %. The power supply used for AC resistance measurements was an Elgar SW 5250A. The frequency used for testing was 50 Hz. Two RMS current levels were used for AC resistance testing: 10 A and 20 A. For the impedance analysis a YOKOGAWA WT3000 Precision power analyzer was used. Possible error on the AC resistance measurement can be more than in DC measurements due to the 10 Ω resistor. However, the 4-wire resistance measurement method should ensure that only the voltage across the load (loop) is measured. The resistance of the current probes should not affect significantly on the measurement. (Martin 2014, 1) The ambient temperature during both, DC and AC measurements was 20 °C with 2 °C tolerance. Two measurements were conducted per loop in both DC and AC tests and an average from the two measurements was calculated. Measurement results for the DC and AC resistance tests are presented in tables 1 and 2. From the measurement results, it can be clearly seen that the DC and AC resistance of the aluminium loop are considerably lower

than for the steel loop. This was expected, since the resistivity of the aluminium is lower than for the steel. According to ANSYS calculations in the chapter 5.2.4 “Electrical conductivity determination for the loops”, the electrical resistivity of the aluminium loop was $3.95 \cdot 10^{-8}$ Ωm and $2.40 \cdot 10^{-7}$ Ωm for the steel loop. It can be also noted that for both loops, AC resistance values were higher than the DC resistance values. This is due to the skin effect in the material with the AC current. The skin effect was emphasized in the steel loop where the AC resistance value was almost double compared to the DC resistance value. The skin effect could be seen also in ANSYS simulations. More details of the resistance measurements can be found in appendix 2.

Table 1. DC resistance measurement for steel and aluminium loops

Current	10	A
Ambient temperature	20	°C

	DC resistance, measurement 1 [mΩ]	DC resistance, measurement 2 [mΩ]	DC resistance, average [mΩ]
Steel loop	0.420	0.422	0.421
Aluminium loop	0.147	0.150	0.148

Table 2. AC resistance measurement for steel and aluminium loops

Current	10 & 20	A, RMS
AC frequency	50	Hz
Ambient temperature	20	°C

	AC resistance, measurement 1 [mΩ]	AC resistance, measurement 2 [mΩ]	AC resistance, average [mΩ]
Steel loop	0.780	0.815	0.797
Aluminium loop	0.173	0.178	0.176

5.1.3 Reactor coil magnetic field measurement

The magnitude of the magnetic flux density produced by the reactor was measured separately with two different reactor current levels. These measurements were required to ensure, that the simplified ANSYS reactor model produces similar magnetic field in simulations as the

real reactor. The reactor AC current levels used were 1500 A RMS and 3000 A RMS. The AC frequency was 50 Hz and the magnetic flux density measurement height was 1.5 m from the ground. With the 1500 A current level, measurements were conducted from 3.1 m to 11.0 m and with 3000 A from 4.0 m to 11.0 m. Total of 17 measurements were conducted. The tolerance for the measurement height was about 10 mm and for the distance about 20 mm. The distance was measured from the center of the reactor. HIOKI 3470 Magnetic field HiTester with 2 mT sensor was used for measurements. A picture of the magnetic field tester can be found in appendix 2. Results of the magnetic field measurements are presented in table 3. Measured magnetic flux densities are right in the expected range. The actual current flowing through the reactor is not exactly 1500 A or 3000 A, due to the nature of the test circuit. The reactor current was measured with PEM CWT Rogowski Current Waveform Transducer and Hioki MR 8880-20 scope. The current measurement equipment is presented in appendix 2.

Table 3. Measurement of the magnetic flux density magnitude caused by the reactor

Initial values		**Measurements**	
Reactor test current, RMS [A]	Measurement distance [mm]	Reactor current, RMS [A]	Magnetic flux density, RMS [mT]
1500	3100	1530	1.89
1500	4000	1530	0.90
1500	5000	1530	0.45
1500	6000	1530	0.26
1500	7000	1530	0.17
1500	8000	1530	0.11
1500	9000	1530	0.08
1500	10000	1530	0.06
1500	11000	1530	0.04
3000	4000	3040	1.79
3000	5000	3040	0.90
3000	6000	3040	0.53
3000	7000	3040	0.33
3000	8000	3040	0.23
3000	9000	3040	0.16
3000	10000	3040	0.11
3000	11000	3040	0.08

5.1.4 Loop induction tests

The most important tests were the loop induction tests, where was measured how much current would induce to loops with different materials in various distances and positions. To estimate how adverse the induced current might be, temperature measurements from the loops were equally important. The desired reactor current for all induction tests was 3000 A RMS and the AC frequency was 50 Hz. There was a slight variation in the current as explained before. The reactor current measuring equipment was the same as explained in the chapter 5.1.3 “Reactor coil magnetic field measurement”. The PEM CWT Rogowski Current Waveform Transducer probe was also used for measuring the current in loops, but different scope was utilized. The scope for reading the current value from the loop was a YOKOGAWA DL850. The current measuring equipment for loops is presented in appendix 2. In each test, four thermocouples were used to measure the temperature of the loop. Thermocouples were placed in the middle of each side of the loop. The accurate placement of thermocouples is presented in appendix 3. The ambient temperature was measured with two thermocouples fairly close to the loop. Thermocouples were placed in a container filled with water and outer layer insulated to achieve stable measurements. Photos of the ambient temperature measurement setup are shown in appendix 3.

First, currents and temperatures were measured from the uncut steel and aluminium loops in horizontal orientation at different distances relative to the reactor. The measurements were conducted every meter, from 2.0 m to 6.0 m distance from the reactor. The distance was measured from the center point of the reactor to the closest edge of a loop relative to the reactor. The height of the loops was kept at 1.5 m in all tests. The height was measured from the bottom edge of a loop to the ground. The tolerance for the distance measurement was 20 mm and for the height measurement 10 mm. The loop angle could vary from the horizontal position about one degree. The basic setup of the measurements is presented in figure 26, where the TC abbreviation refers to thermocouple. The same setup was used in all tests for both loops in horizontal orientation except for the change in the loop distance. The loop was placed on a wooden structure, which was hanged from an overhead crane. With the crane, the loop position could be changed effortlessly. The measurement results are presented in table 4.

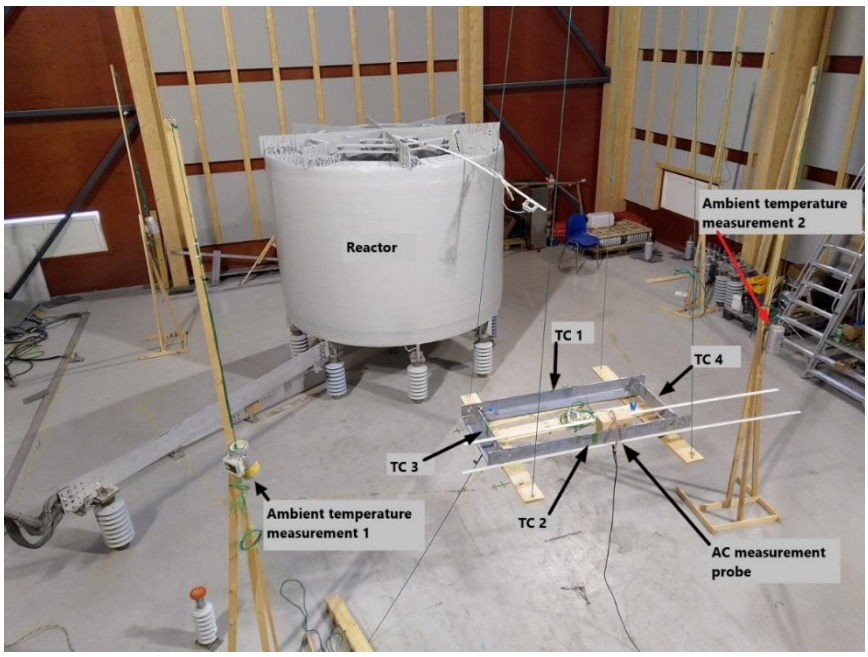

Figure 26. Laboratory test setup for the steel loop in horizontal orientation at 4.0 m distance

Table 4. Uncut steel and aluminium loops in horizontal orientation, laboratory test results

Loop distance [mm]	2000	3000	4000	5000	6000	
Reactor RMS current [A]	3020	3030	3030	3040	3030	Steel
	3060	3010	3020	3020	3020	Aluminium
Loop RMS current [A]	765	263	139	87	73	Steel
	1997	947	461	241	147	Aluminium
Ambient temperature 1 [°C]	22.1	21.9	23.0	21.1	20.5	Steel
	24.7	18.5	18.3	27.3	22.9	Aluminium
Ambient temperature 2 [°C]	22.8	22.4	24.6	22.4	21.9	Steel
	26.2	19.9	19.5	28.6	23.9	Aluminium
Thermocouple 1 [°C]	110.7	37.4	28.1	23.7	22.8	Steel
	131.7	46.4	26.1	29.0	24.1	Aluminium
Thermocouple 2 [°C]	88.5	31.9	25.9	22.3	21.2	Steel
	163.6	47.2	25.7	29.2	24.2	Aluminium
Thermocouple 3 [°C]	103.9	32.8	26.4	22.8	21.9	Steel
	127.8	42.0	23.9	29.2	24.1	Aluminium
Thermocouple 4 [°C]	93.6	33.3	26.3	22.6	21.5	Steel
	144.7	44.7	25.7	29.1	24.3	Aluminium

Next, measurements were conducted to the uncut steel and aluminium loops in different orientations. Two loop angles relative to the horizontal orientation were tested for both

loops: 45 degrees and 90 degrees. The loop distance from the center point of the reactor to the closest edge of the loop relative to the reactor was 3.0 m in all tests. Loops were at 1.5 m height. The height was measured from the bottom edge of a loop to the ground. Tolerances for the distance, height and loop angle are the same as in the tests at horizontal orientation. Figure 27 presents setups for the measurements at 45 and 90 angle orientations. Results of the measurements are shown in table 5.

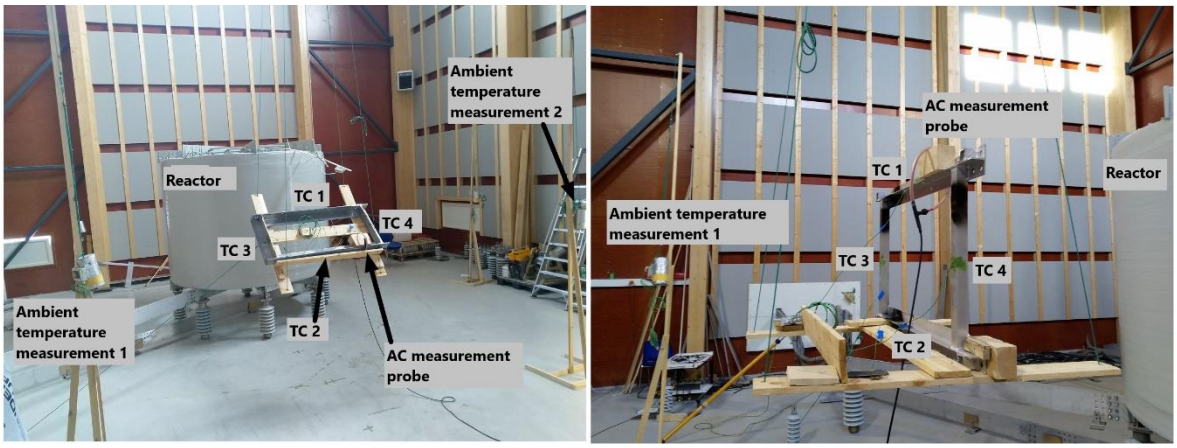

Figure 27. Laboratory test setup for the steel loop at 45-degree angle (left) and for the aluminium loop at 90-degree angle (right)

Table 5. Uncut steel and aluminium loops in different orientations, laboratory test results

Loop angle [degrees]	45	90	
Reactor RMS current [A]	3020	3040	Steel
	3030	3080	Aluminium
Loop RMS current [A]	202	25	Steel
	843	165	Aluminium
Ambient temperature 1 [°C]	26.0	24.2	Steel
	21.7	15.7	Aluminium
Ambient temperature 2 [°C]	27.5	26.7	Steel
	24.4	17.2	Aluminium
Thermocouple 1 [°C]	38.6	34.0	Steel
	48.7	19.2	Aluminium
Thermocouple 2 [°C]	33.8	29.8	Steel
	42.5	18.7	Aluminium
Thermocouple 3 [°C]	55.2	85.9	Steel
	47.2	17.7	Aluminium
Thermocouple 4 [°C]	55.2	86.5	Steel
	46.2	17.4	Aluminium

For the cut loops, measurements were conducted for three loop angles: 0, 45 and 90 degrees. 0 degrees refers to a horizontal orientation and 90 vertical orientation. The loop distance for both, steel and aluminium at all angles was 3.0 m from the center point of the reactor to the closest edge of a loop relative to the reactor. The loop height from the bottom edge of a loop to the ground was 1.5 m in all tests. Tolerances for the distance, height and loop angle were the same as in previous measurements. Measurement setups for cut loops were the same as for whole loops and the thermocouple numbering order was also kept same. Measurement results are presented in table 6.

Table 6. Cut steel and aluminium loops in different orientations, laboratory test results

Loop angle [degrees]	**0**	**45**	**90**	
Reactor RMS current [A]	3080	3060	3050	Steel
	3050	3050	3040	Aluminium
Loop RMS current [A]	12	18	14	Steel
	9	12	15	Aluminium
Ambient temperature 1 [°C]	17.6	20.3	20.0	Steel
	16.4	15.1	14.2	Aluminium
Ambient temperature 2 [°C]	18.8	21.9	21.8	Steel
	17.1	15.3	14.7	Aluminium
Thermocouple 1 [°C]	19.8	27.0	28.0	Steel
	23.0	20.0	18.3	Aluminium
Thermocouple 2 [°C]	18.4	23.2	27.0	Steel
	18.9	17.6	17.0	Aluminium
Thermocouple 3 [°C]	18.7	45.0	81.5	Steel
	18.3	16.9	16.3	Aluminium
Thermocouple 4 [°C]	18.9	48.3	74.3	Steel
	19.3	18.0	16.5	Aluminium

An interesting phenomenon was noticed with the steel loop in vertical orientation and at 45-degree angle, which was not expected. The sides which were upright and relatively parallel to the magnetic field produced by the reactor coil heated significantly. This happened also with the cut loop when it was sure that there would not be any circulating current flowing around the loop. Figure 28 presents a thermal camera image of the steel loop in vertical orientation and at 45-degree angle. The heating of the upright sides of the loop occurs due to the eddy currents. Ferromagnetic steel has the relative permeability much higher than one that intensifies the magnetic flux density inside the steel structure compared to the external field. High magnetic flux density induces high currents circulating inside the structure

according to Faraday's induction law. The aluminium loop did not heat much due to the eddy currents because the relative permeability of the aluminium is very close to one. Simulations showed how the eddy currents are circulating inside the steel loop, which are presented in figure 38, page 86. The magnetic flux density at 3.0 m distance was expected to be low enough to avoid any significant eddy currents, even though it was inside the $\mathbf{m_x}$ distance. According to simulations, the magnetic flux density at 3.0 m from the reactor should be about 5.7 mT.

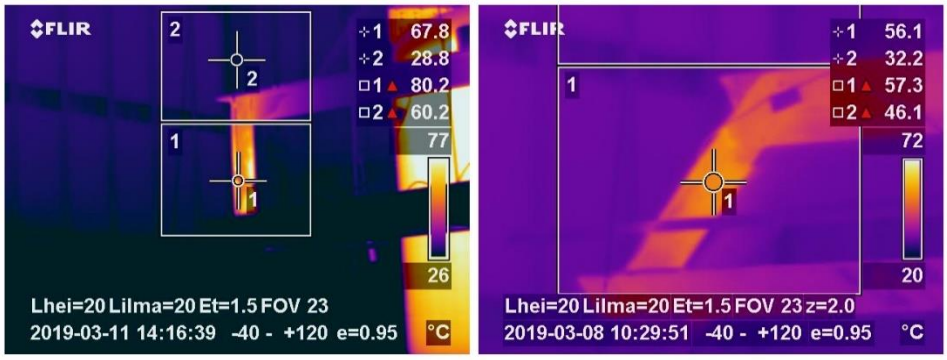

Figure 28. Thermal camera image of the steel loop at 90- and 45-degree angle

5.1.5 Total loss determination for loops from temperature measurements

It was noted during ANSYS simulations, that all loop losses could not be explained just as resistance losses caused by circulating current through the loop. This was the case for both steel and aluminium loops, but more so for the steel loop. There was a difference between the total loss of the loop and the loss caused by the circulating current. This implied that eddy currents had a larger effect than was originally thought. It was required then to determine the loop total loss using the acquired temperature measurement data. It would be important to know how much losses are caused by circulating current and how much due to eddy currents for different materials. The data can be then be compared to ANSYS simulations and it would be possible to verify the correctness of the simulations. The total loss for a loop was calculated as a combination of radiation and convection heat transfer.

The radiation heat from a loop surface was calculated using equation (19) (Stephan et al. 2010, 20 & 28). The degree of emission used in all calculations for steel was 0.276 and for aluminium 0.18 (Stephan et al. 2010, 951-952). The loop surface temperature was the average of the four thermocouple measurements and the ambient air temperature was the average of the two measurements. The steel loop surface area was calculated as 1.46 m^2 and the aluminium loop surface area was 0.98 m^2. Detailed calculations of surface areas are shown in appendix 4.

$$P_{\mathrm{R}} = \varepsilon\sigma\left(T_{\mathrm{surf}}^4 - T_{\mathrm{amb}}^4\right)A \tag{19}$$

P_{R} = radiation heat transfer [W]
ε = material degree of emission
σ = Stefan-Boltzmann constant [$5.6704 \cdot 10^{-8}$ $W/(m^2K^4)$]
T_{surf} = loop surface temperature [K]
T_{amb} = ambient air temperature [K]
A = total loop surface area [m^2]

The convection heat transfer calculation from a loop surface was more complex to calculate. The convection heat transfer was calculated for each individual rectangle shaped surfaces separately in a loop. This was required, since the calculation is different whether a surface position is vertical, horizontal or inclined. For horizontal and inclined surfaces, it also matters, if a surface faces up or down. For example, the steel loop at 0-degree angle (horizontal orientation) had 24 vertical surfaces, eight horizontal surfaces facing up and four horizontal surfaces facing down. However, many of the surfaces shared the same geometry, thus the convection coefficient could be calculated just for one of the similar surfaces and the convection heat transfer using the total area of the similar surfaces. Now, vertical surfaces of the steel loop at 0-degree angle were reduced to nine, horizontal surfaces facing up to four and horizontal surfaces facing down to two. Detailed calculations of all surfaces for steel and aluminium loops at 0, 45 and 90-degree angle are presented in appendix 4.

The general calculation procedure for the convection heat transfer from a loop surface is presented in table 7. Initial values required for the calculation includes: ambient temperature,

loop temperature, temperature difference between ambient and loop (ΔT), ambient air velocity, acceleration of gravity, characteristic length of a surface, area of the surface, properties of dry air in different temperatures and critical Rayleigh number value for 45-degree inclined surfaces. The ambient temperature used was the average of the two measurements and the loop temperature was the average of the four thermocouples. The ambient air velocity was assumed to be 0.15 m/s. The typical indoor air velocities are 0.1 m/s or higher (Zhang 2004, 255). The uncomfortable levels of draft indoors at 20 °C can range from about 0.11 m/s to 0.27 m/s (Vapaavuori & Kalliomäki 2012, 24). In the laboratory, there was a slight draft noticeable, thus the 0.15 m/s air velocity should be a good estimate. During laboratory tests, a trapdoor was opened at the roof to let warm air to escape around the reactor, thus the flow direction was suspected to be straight up. Properties of dry air required for the calculation are: kinematic viscosity, thermal diffusivity, isobaric volume expansion coefficient and thermal conductivity. Properties of dry air in a temperature range from 10 °C to 100 °C can be found in appendix 5.

Table 7. General calculation procedure for the convection heat transfer from a loop surface

Initial values
- Average ambient temperature [°C]
- Average loop temperature [°C]
- Average ΔT [°C]
- Ambient air velocity [m/s]
- Acceleration of gravity [9.81 m/s^2]
- Critical Rayleigh number for 45-degree inclined surfaces [7500000]
- Characteristic length of the surface [m]
- Area of the surface [m^2]
- Properties of dry air in different temperatures

Preliminary steps for the convection calculation
1. Calculate reference temperature [°C]
2. Interpolate properties of dry air from tables at the reference temperature
3. Calculate Prandtl number
4. Calculate Prandtl number function for vertical surfaces (f_1)
5. Calculate Prandtl number function for horizontal surfaces (f_2)

Vertical surfaces	**Horizontal surfaces**
1. Calculate Rayleigh number	1. Calculate Rayleigh number
2. Calculate Nusselt number for free convection	2. Calculate Nusselt number for free convection
3. Calculate Reynolds number	3. Calculate convection coefficient
4. Calculate Nusselt number for forced convection with laminar flow	4. Calculate convection heat transfer from the surface
5. Calculate Nusselt number for forced convection with turbulent flow	
6. Calculate combined Nusselt number for forced convection	
7. Calculate superimposed Nusselt number	
8. Calculate convection coefficient	
9. Calculate convection heat transfer from the surface	

Inclined surfaces
- Inclined surfaces with face down are calculated similarly to vertical surfaces
- Inclined surfaces with face up are calculated similarly to horizontal surfaces

Convection heat transfer calculations presented in the study precisely follow the book: VDI Heat Atlas 2010 by Stephan et al. from pages 663-671 and 713-714. For vertical surfaces and inclined surfaces facing down, superimposed free and forced convection was calculated. For horizontal surfaces, only free convection was calculated. This is because there are no valid equations for superimposed free and forced convection available for horizontal surfaces and the air velocity was assumed to be so low that it should not have much effect on horizontal surfaces. For inclined surfaces facing down, the superimposed calculation was implemented because it was suspected that the upward air flow would influence the heat transfer. The superimposed free and forced convection calculation method was not used for the inclined surfaces facing up.

Detailed calculations of steel and aluminium loops surface areas are shown in appendix 4, where also are calculated characteristic lengths. The characteristic length L for a vertical surface is directly the height of the surface and for a horizontal surface it is calculated with equation (20). The characteristic length value is used for the free convection calculations. For the forced convection, surface length parallel to the flow direction is used instead.

$$L = \frac{ab}{2(a+b)} \tag{20}$$

L = characteristic length [m]
a = surface length [m]
b = surface width [m]

For vertical surfaces on inclined loops, the characteristic length is calculated with equation (21) to account for the additional height caused by the inclination. For other inclined surfaces, the characteristic length is directly the surface height, as with vertical surfaces.

$$L = \frac{h}{\cos\theta} \tag{21}$$

L = characteristic length [m]
h = surface height [m]
θ = angle of inclination to vertical [degrees]

Different surface types and their characteristic lengths are explained in figure 29. It presents the surface types on the steel loop in horizontal orientation and at the 45-degree angle.

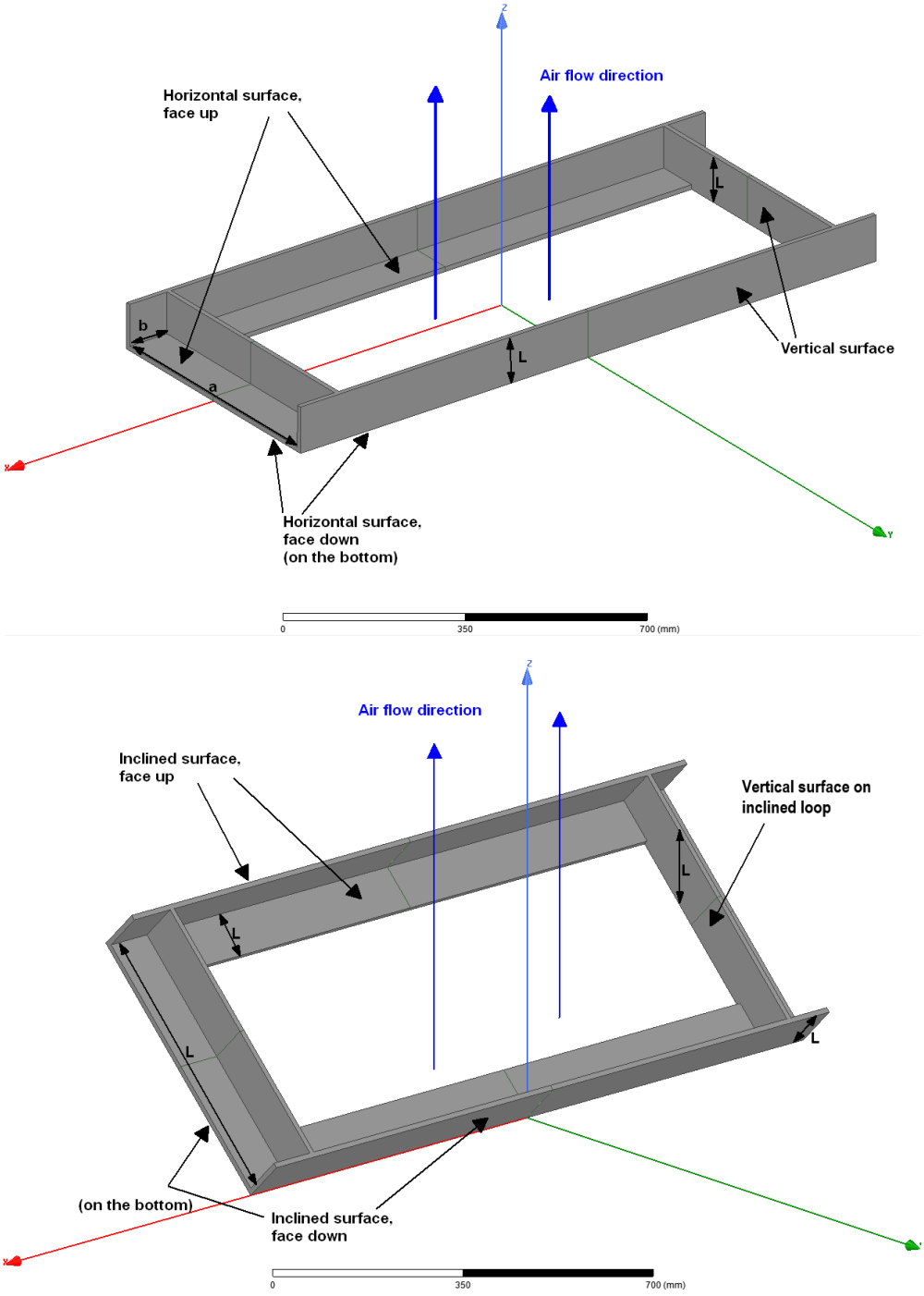

Figure 29. Different surface types and their characteristic lengths

Preliminary steps for the convection calculation included the calculation of the reference temperature, interpolating properties of dry air to the reference temperature, calculation of

the Prandtl number and Prandtl number functions. The reference temperature is the average temperature between the loop surface temperature and the ambient temperature. The properties of dry air are then interpolated to the reference temperature from the table which is found in appendix 5. The Prandtl number can be calculated using equation (22).

$$\mathrm{Pr} = \frac{\nu}{\kappa} \tag{22}$$

Pr = Prandtl number
ν = kinematic viscosity [m^2/s]
κ = thermal diffusivity [m^2/s]

The Prandtl number function $f_1(\mathrm{Pr})$ for vertical surfaces is calculated with equation (23).

$$f_1(\mathrm{Pr}) = \left[1 + \left(\frac{0.492^{\frac{9}{16}}}{\mathrm{Pr}}\right)\right]^{-\frac{16}{9}} \tag{23}$$

$f_1(\mathrm{Pr})$ = Prandtl number function for vertical surfaces
Pr = Prandtl number
Range of validity: $0.001 < \mathrm{Pr} < \infty$

The Prandtl number function $f_2(\mathrm{Pr})$ for horizontal surfaces is calculated with equation (24).

$$f_2(\mathrm{Pr}) = \left[1 + \left(\frac{0.322}{\mathrm{Pr}}\right)^{\frac{11}{20}}\right]^{-\frac{20}{11}} \tag{24}$$

$f_2(\mathrm{Pr})$ = Prandtl number function for horizontal surfaces
Pr = Prandtl number
Range of validity: $0 < \mathrm{Pr} < \infty$

Rayleigh number calculation for vertical and horizontal surfaces is similar, as shown in equation (25). The Rayleigh number is used for free convection calculations. One should be however careful to use the correct characteristic length L, depending whether the surface is

vertical or horizontal. The properties of dry air used in the equation: β, ν and κ, are at the reference temperature.

$$\mathrm{Ra} = \frac{\beta g \Delta T L^3}{\nu \kappa} \tag{25}$$

Ra = Rayleigh number
β = isobaric volume expansion coefficient [1/K]
g = acceleration of gravity [m/s^2]
ΔT = temperature difference between heated surface and ambient [°C]
L = characteristic length [m]
ν = kinematic viscosity [m^2/s]
κ = thermal diffusivity [m^2/s]

Rayleigh number for inclined surfaces can be calculated with equation (26). The "normal" Rayleigh number is calculated for the equation as for a vertical surface (characteristic length = surface height). The equation is not valid, if the heat transfer occurs at a heated upper surface. The transition into a turbulent flow happens in that case at a critical Rayleigh number Ra_c. Critical Rayleigh numbers in terms of angle of inclination is presented in appendix 5. The only critical Rayleigh number required for the convection calculations, is that at the 45-degree angle of inclination. Every surface of both loops is on vertical, horizontal or 45-degree angle orientation in all tests. The critical Rayleigh number for 45-degree angle of inclination to the vertical is obtained from the plot in appendix 5 and it is about $7.5 \cdot 10^6$.

$$\mathrm{Ra}_\theta = \mathrm{Ra} \cos\theta \tag{26}$$

Ra_θ = Rayleigh number for inclined surfaces
Ra = Rayleigh number
θ = angle of inclination to vertical [degrees]

The Nusselt number for free convection with laminar and turbulent flows near a vertical surface can be calculated using equation (27). This equation is also used for the case of

inclined surfaces facing down. Then the Rayleigh number Ra is replaced by the Rayleigh number for inclined surfaces Ra_θ in the equation.

$$\mathrm{Nu} = \left\{0.825 + 0.387[\mathrm{Ra} f_1(\mathrm{Pr})]^{\frac{1}{6}}\right\}^2 \qquad (27)$$

Nu = Nusselt number (free, laminar & turbulent, vertical surfaces)
Ra = Rayleigh number
f_1(Pr) = Prandtl number function for vertical surfaces
Range of validity: Ra = 10^{-1} to Ra = 10^{12}

Free convection Nusselt number for horizontal plane surfaces with heat emission at upper surfaces (horizontal surfaces facing up) and for laminar flow is calculated with equation (28). It is important to note the range of validity with this equation. If Ra·f_2(Pr) becomes larger than $7 \cdot 10^4$, the flow is turbulent and the Nusselt number is calculated with equation (29).

$$\mathrm{Nu} = 0.766[\mathrm{Ra} f_2(\mathrm{Pr})]^{\frac{1}{5}} \qquad (28)$$

Nu = Nusselt number (free, laminar, horizontal surfaces facing up)
Ra = Rayleigh number
f_2(Pr) = Prandtl number function for horizontal surfaces
Range of validity: Ra·f_2(Pr) < $7 \cdot 10^4$

Free convection Nusselt number for horizontal plane surfaces with heat emission at upper surfaces (horizontal surfaces facing up) and for turbulent flow is calculated with equation (29). It is important to note the range of validity also with this equation. If Ra·f_2(Pr) becomes less than $7 \cdot 10^4$, the flow is laminar and the Nusselt number is calculated with equation (28).

$$\mathrm{Nu} = 0.15[\mathrm{Ra} f_2(\mathrm{Pr})]^{\frac{1}{3}} \qquad (29)$$

Nu = Nusselt number (free, turbulent, horizontal surfaces facing up)
Ra = Rayleigh number

f_2(Pr) = Prandtl number function for horizontal surfaces
Range of validity: Ra·f_2(Pr) > $7 \cdot 10^4$

Free convection Nusselt number for horizontal plane surfaces with heat emission at lower surfaces (horizontal surfaces facing down) and for laminar flow is calculated using equation (30). There is no equation for turbulent flow, but the equation (30) has a wide range of validity in which all horizontal surfaces facing down reside. It should be noted, that even though the equation is for horizontal surfaces, the Prandtl number function f_1(Pr) is used.

$$\mathrm{Nu} = 0.6[\mathrm{Ra} f_1(\mathrm{Pr})]^{\frac{1}{5}} \tag{30}$$

Nu = Nusselt number (free, horizontal surfaces facing down)
Ra = Rayleigh number
f_1(Pr) = Prandtl number function for vertical surfaces

Free convection Nusselt number for inclined surfaces with heat emission at upper surfaces and for turbulent flow is calculated using equation (31). It was assumed that the flow was turbulent for all inclined surfaces facing up. There were only few small (total area < 0.040 m^2 for the steel loop and < 0.033 m^2 for the aluminium loop) inclined surfaces facing up where the flow could be laminar (Ra·f_2(Pr) < $7 \cdot 10^4$) for both loops, thus the error would be minimal even if the flow would be assumed turbulent for all the inclined surfaces facing up.

$$\mathrm{Nu} = 0.56(\mathrm{Ra_c} \cos\theta)^{\frac{1}{4}} + 0.13\left(\mathrm{Ra}^{\frac{1}{3}} - \mathrm{Ra_c}^{\frac{1}{3}}\right) \tag{31}$$

Nu = Nusselt number (free, inclined surfaces facing up)
$\mathrm{Ra_c}$ = critical Rayleigh number
θ = angle of inclination to vertical [degrees]
Ra = Rayleigh number

Reynolds number for the forced convection calculations is calculated with equation (32). The surface length l represents the length of a surface which is parallel to the air flow.

Because the air flow was assumed to be upward and the forced convection is not calculated for horizontal surfaces, the surface length for Reynolds number calculation is in all required cases also the characteristic length (vertical surfaces and inclined surfaces facing down).

$$\mathrm{Re} = \frac{\boldsymbol{wl}}{\boldsymbol{\nu}} \tag{32}$$

Re = Reynolds number
w = air velocity [m/s]
l = surface length [m]
ν = kinematic viscosity [m^2/s]

The Nusselt number for forced convection with laminar flow is calculated using equation (33). The equation is valid for a parallel flow along a flat plate and the entire surface is assumed at uniform temperature.

$$\mathrm{Nu} = 0.664\sqrt{\mathrm{Re}}\,\sqrt[3]{\mathrm{Pr}} \tag{33}$$

Nu = Nusselt number (forced, laminar)
Re = Reynolds number
Pr = Prandtl number
Range of validity: $\mathrm{Re} < 10^5$ and Pr = 0.6 - 2000

The Nusselt number for forced convection with turbulent flow is calculated with equation (34). Also, with this equation, the flow is parallel to a flat plate.

$$\mathrm{Nu} = \frac{0.037\mathrm{Re}^{0.8}\mathrm{Pr}}{1+2.443\mathrm{Re}^{-0.1}\left(\mathrm{Pr}^{\frac{2}{3}}-1\right)} \tag{34}$$

Nu = Nusselt number (forced, turbulent)
Re = Reynolds number
Pr = Prandtl number
Range of validity: $5\cdot10^5 < \mathrm{Re} < 10^7$ and $0.5 < \mathrm{Pr} < 2000$

In all cases where the forced convection was calculated, the flow should be laminar, according to the Nusselt number calculation range of validity. However, blunt leading edges and higher degrees of turbulence prevent the formation of a laminar boundary layer over the entire length of a surface. For that reason, a combined correlation for average Nusselt number coefficients for both turbulent and laminar flow over a plate was calculated using equation (35). Because of this reason, in all cases where the forced convection was calculated, Nusselt numbers for both laminar and turbulent flows had to calculated.

$$\mathrm{Nu} = \sqrt{\mathrm{Nu}_{\mathrm{lam}}^2 + \mathrm{Nu}_{\mathrm{turb}}^2} \tag{35}$$

Nu = Nusselt number (forced, combined laminar and turbulent)
$\mathrm{Nu}_{\mathrm{lam}}$ = Nusselt number for laminar flow (forced)
$\mathrm{Nu}_{\mathrm{turb}}$ = Nusselt number for turbulent flow (forced)
Range of validity: $10^1 < \mathrm{Re} < 10^7$ and $0.5 < \mathrm{Pr} < 2000$

For vertical surfaces and inclined surfaces facing down, the superimposed free and forced convection was calculated. The Nusselt number for superimposed free and forced convection is calculated with equation (36). The equation is valid for a case where the free convection is in the same direction as the forced convection. Because the air flow of 0.15 m/s was assumed to be straight up, the free and forced convection are in fact in the same direction. The Nusselt number for forced convection in the equation refers to the combined for average coefficients for both turbulent and laminar flow. The Nusselt number for free convection is either for laminar or turbulent flow depending on the surface. The superimposed calculation method was used because it was suspected, that the air flow was too low for just forced convection to give reliable results. But, due to the air flow, free convection only would not be reliable either.

$$\mathrm{Nu} = \left(\mathrm{Nu}_{\mathrm{forced}}^3 + \mathrm{Nu}_{\mathrm{free}}^3\right)^{\frac{1}{3}} \tag{36}$$

Nu = Nusselt number (superimposed)
$\mathrm{Nu}_{\mathrm{forced}}$ = Nusselt number for forced convection

Nu_{free} = Nusselt number for free convection

The convection coefficient is calculated in the same way for all surfaces of the loops, with equation (37). The Nusselt number used in the equation is of course different depending on the surface calculated. For vertical surfaces and inclined surfaces facing down, the Nusselt number in the equation (37) refers to the superimposed free and forced convection Nusselt number, equation (36). For horizontal surfaces facing up, the Nusselt number refers to the free convection Nusselt number for horizontal surface with heat emission at upper surface. It can be for the laminar or turbulent case, depending on the situation (equation 28 or 29). For horizontal surfaces facing down the Nusselt number refers to the equation (30) and for inclined surfaces facing up to the equation (31). The use of characteristic length in the equation (37) is valid for all cases, because only free convection is calculated for horizontal surfaces. The thermal conductivity of air λ, is at the reference temperature.

$$\alpha = \frac{\mathrm{Nu}\lambda}{L} \tag{37}$$

α = convection coefficient [W/(m^{2}K)]
Nu = Nusselt number
λ = thermal conductivity of air [W/(m·K)]
L = characteristic length [m]

Finally, the convection heat transfer from a surface can be calculated with equation (38). The total convection heat transfer from a loop surface could be calculated as a sum of the convection heat transfer from all rectangle shaped surfaces of the loop.

$$P_{\mathrm{C}} = \alpha \Delta T A \tag{38}$$

P_C = convection heat transfer [W]
α = convection coefficient [W/(m^{2}K)]
ΔT = temperature difference between heated surface and ambient [°C]
A = surface area [m^2]

The total convection coefficient for the whole steel and aluminium loops were calculated for each individual laboratory test with equation (39). The total convection coefficient is different for the same loop in different tests because the free convection is heavily dependent on the temperature difference between the surface and ambient air. The total convection coefficient was used for the loop temperature calculation in the simulations.

$$\alpha_{\text{total}} = \frac{P_{\text{C,total}}}{\Delta T A_{\text{total}}} \tag{39}$$

α_{total} = total convection coefficient of the loop [W/(m^{2}K)]
$P_{\text{C,total}}$ = total convection heat transfer from the loop [W]
ΔT = temperature difference between heated surface and ambient [°C]
A_{total} = total surface area of the loop [m^2]

Results of the radiation and convection heat transfer calculations are presented in tables 8, 9 and 10. These calculations cannot be however taken as an absolute truth, because there are many variables that can affect the results significantly. The degree of emission for the radiation heat transfer calculation is for example taken from a table in the VDI Heat Atlas book and it cannot be fully accurate. The major inaccuracies arise from the laboratory conditions. The air velocity in the laboratory could vary from the 0.15 m/s value. Changing the air velocity from 0.15 m/s to 0.2 m/s, the total loss of the loop can increase up to 10 %. The effect is emphasized with low ΔT values, because then the role of the forced convection is more significant. The ambient temperature in the laboratory did not stay uniform throughout the tests and it could vary several degrees even during a single test. The reactor could get over 100 °C, which would warm the surrounding ambient air. For this reason, it was difficult to get equilibrium between the loop temperature and the ambient temperature. This problem became significant with low ΔT values and therefore, total loss values of the cases where the temperature difference between the loop and the ambient was less than 2 °C must be looked with caution. For example, the calculated total loss of the aluminium loop in horizontal orientation and at a 5.0 m distance from the reactor was 7.1 W, but the calculated loss by the circulating current was 10.6 W. This cannot be the case. Some error must have happened in the temperature measurement. In other tests, the total loss was always larger than the loss by the circulating current.

Table 8. Uncut steel and aluminium loop in horizontal orientation, radiation and convection heat transfer

Loop distance [mm]	2000	3000	4000	5000	6000	
Heat transfer by radiation [W]	265.2	29.3	7.0	2.6	1.5	Steel
	218.3	29.6	6.7	1.3	0.8	Aluminium
Heat transfer by convection [W]	768.5	90.0	19.2	6.8	3.9	Steel
	963.6	173.5	36.9	5.8	3.7	Aluminium
Total heat transfer by radiation and convection [W]	1033.7	119.3	26.1	9.4	5.4	Steel
	1181.9	203.1	43.5	7.1	4.5	Aluminium
Loop total convection coefficient [W/(m^{2}K)]	6.8	5.3	4.6	4.2	4.1	Steel
	8.4	6.8	5.8	5.0	4.9	Aluminium

Table 9. Uncut steel and aluminium loop in different orientations, radiation and convection heat transfer

Loop angle [degrees]	45	90	
Heat transfer by radiation [W]	51.4	96.8	Steel
	27.1	1.8	Aluminium
Heat transfer by convection [W]	156.0	279.5	Steel
	153.6	9.4	Aluminium
Total heat transfer by radiation and convection [W]	207.4	376.4	Steel
	180.7	11.2	Aluminium
Loop total convection coefficient [W/(m^{2}K)]	5.6	5.7	Steel
	6.8	5.3	Aluminium

Table 10. Cut steel and aluminium loop in different orientations, radiation and convection heat transfer

Loop angle [degrees]	0	45	90	
Heat transfer by radiation [W]	1.7	37.2	87.0	Steel
	3.1	2.9	2.5	Aluminium
Heat transfer by convection [W]	4.6	116.4	263.3	Steel
	16.7	14.8	13.8	Aluminium
Total heat transfer by radiation and convection [W]	6.3	153.6	350.2	Steel
	19.8	17.7	16.3	Aluminium
Loop total convection coefficient [W/(m^{2}K)]	4.1	5.4	5.7	Steel
	5.4	5.1	5.5	Aluminium

5.1.6 Combining laboratory test results

After the tests, for each individual case, DC and AC resistances were calculated separately to account for the material resistance dependency on the temperature. Maximum loop temperatures could reach well over 100 °C at close distances from the reactor and that temperature affects the material resistance significantly. The calculation of the loop loss by circulating current might give inaccurate results if the loop resistance is wrong. The effect of the temperature could be seen in the laboratory tests. The measured loop AC current would drop as the loop was reaching its maximum temperature. The calculation of the DC and AC resistance for each case individually was also important because these values were used to calculate the circulating current losses and electrical conductivities in the simulations. With ANSYS, it was possibly to calculate the total loss of the loop, but without the knowledge of the AC resistance value, ANSYS could not separate the losses which are from circulating current and eddy currents. The DC resistance values were on the other hand used to determine the correct electrical conductivities in the simulations. According to (Valtanen 2012, 353), the temperature dependency of the resistance can be calculated with equation (40). The reference temperature T_0 refers to the temperature where the DC and AC resistance measurements were conducted. It was 20 °C in this case. According to (Valtanen 2012, 353), the resistivity temperature coefficient ϑ for iron is 0.0066 1/°C and for aluminium 0.0043 1/°C. The value for iron was assumed to be good enough approximation for steel.

$$R = R_0[1 + \vartheta(T - T_0] \tag{40}$$

R = resistance at temperature T [Ω]
R_0 = resistance at temperature T_0 [Ω]
ϑ = material resistivity temperature coefficient [1/°C]
T = loop temperature [°C]
T_0 = reference temperature [°C]

The loop loss by the circulating current in the loop was calculated with equation (41).

$$P_{\text{circ}} = I^2 R_{\text{AC}} \tag{41}$$

P_{circ} = loop loss by the circulating current [W]

I = measured RMS AC current in the loop [A]

R_{AC} = loop AC resistance at its final temperature [Ω]

The final results of the laboratory measurements and the related calculations are presented in tables 11, 12 and 13. The loop total loss is the addition of the convection and radiation heat transfer from the loop. The average ΔT is the temperature difference between the average ambient temperature and the average loop temperature. The max ΔT is the temperature difference between the average ambient temperature and the maximum measured loop temperature.

Table 11. Uncut steel and aluminium loop in horizontal orientation, laboratory test calculations

Loop distance [mm]	**2000**	**3000**	**4000**	**5000**	**6000**	
Loop DC resistance [mΩ]	0.641	0.459	0.440	0.429	0.426	Steel
	0.226	0.164	0.152	0.154	0.151	Aluminium
Loop AC resistance [mΩ]	1.21	0.870	0.833	0.812	0.807	Steel
	0.268	0.195	0.180	0.182	0.179	Aluminium
Loop total loss [W]	1033.7	119.3	26.1	9.4	5.4	Steel
	1181.9	203.1	43.5	7.1	4.5	Aluminium
Loop loss by circulating current [W]	711.3	60.2	16.1	6.1	4.3	Steel
	1067.5	174.3	38.2	10.6	3.9	Aluminium
Loop loss by eddy currents [W]	322.5	59.2	10.0	3.3	1.1	Steel
	114.4	28.8	5.3	-3.5	0.7	Aluminium
Ambient temperature, avg [°C]	22.5	22.2	23.8	21.8	21.2	Steel
	25.5	19.2	18.9	28.0	23.4	Aluminium
Loop temperature, avg [°C]	99.2	33.9	26.7	22.9	21.9	Steel
	142.0	45.1	25.4	29.1	24.2	Aluminium
Average ΔT [°C]	76.7	11.7	2.9	1.1	0.7	Steel
	116.5	25.9	6.5	1.2	0.8	Aluminium
Max ΔT [°C]	88.3	15.3	4.3	2.0	1.6	Steel
	138.2	28.0	7.2	1.3	0.9	Aluminium

Table 12. Uncut steel and aluminium loop in different orientations, laboratory test calculations

Loop angle [degrees]	45	90	
Loop DC resistance [mΩ]	0.492	0.530	Steel
	0.165	0.147	Aluminium
Loop AC resistance [mΩ]	0.933	1.00	Steel
	0.195	0.174	Aluminium
Loop total loss [W]	207.4	376.4	Steel
	180.7	11.2	Aluminium
Loop loss by circulating current [W]	38.1	0.6	Steel
	138.8	4.8	Aluminium
Loop loss by eddy currents [W]	169.3	375.8	Steel
	41.9	6.4	Aluminium
Ambient temperature, avg [°C]	26.8	25.5	Steel
	23.1	16.5	Aluminium
Loop temperature, avg [°C]	45.7	59.1	Steel
	46.2	18.3	Aluminium
Average ΔT [°C]	19.0	33.6	Steel
	23.1	1.8	Aluminium
Max ΔT [°C]	28.5	61.1	Steel
	25.7	2.8	Aluminium

Table 13. Cut steel and aluminium loop in different orientations, laboratory test calculations

Loop angle [degrees]	0	45	90	
Loop DC resistance [mΩ]	0.418	0.465	0.512	Steel
	0.148	0.147	0.147	Aluminium
Loop AC resistance [mΩ]	0.792	0.881	0.969	Steel
	0.176	0.174	0.173	Aluminium
Loop total loss [W]	6.3	153.6	350.2	Steel
	19.8	17.7	16.3	Aluminium
Loop loss by circulating current [W]	0.1	0.3	0.2	Steel
	0.0	0.0	0.0	Aluminium
Loop loss by eddy currents [W]	6.2	153.3	350.1	Steel
	19.8	17.6	16.3	Aluminium
Ambient temperature, avg [°C]	18.2	21.1	20.9	Steel
	16.8	15.2	14.5	Aluminium
Loop temperature, avg [°C]	19.0	35.9	52.7	Steel
	19.9	18.1	17.0	Aluminium
Average ΔT [°C]	0.8	14.8	31.8	Steel
	3.1	2.9	2.6	Aluminium
Max ΔT [°C]	1.6	27.2	60.6	Steel
	6.3	4.8	3.9	Aluminium

5.2 ANSYS simulations

Two ANSYS programs were used to do the simulations: ANSYS Electronics 19.2 and ANSYS Mechanical 19.2. These programs could be interconnected via ANSYS Workbench. ANSYS Electronics was used to calculate the electromagnetic fields of the system and via them, the total loss of the loop. More specifically, ANSYS Maxwell 3D design was used within the ANSYS Electronics. ANSYS Maxwell is well optimized for low frequency electromagnetic field simulations. ANSYS Maxwell uses finite element method to solve static, frequency-domain and time-varying electromagnetic and electric fields. It contains many solution types for specific needs: magnetic transient, AC electromagnetic, magnetostatic and electric field. (ANSYS 2019a) For the cases of this study, the magnetic transient solution type was used, since the reactor produces a changing magnetic field. The lighter AC electromagnetic solution type was briefly tested, but the loop losses became less than half, compared to the losses calculated from the laboratory test results, even though the AC electromagnetic module calculated the current very accurately. As a whole, the transient solution type seemed to give better results concerning both; the induced current and losses, although it was much more demanding. The magnetostatic solution type was however used to simulate the magnetic field around the reactor when there was not a loop present. In that case, transient solution type is not necessary because induction to a loop is not calculated. From the calculated total loss with ANSYS Maxwell, the ANSYS Mechanical was able to calculate the surface temperature of the loop. The loop surface temperature simulation with ANSYS Mechanical was done as a steady-state problem. This reduces simulation time significantly. The ANSYS Mechanical also utilizes finite element method for solving thermal and structural mechanics problems. (ANSYS 2019b)

5.2.1 Finite element method

The finite element method; FEM is a numerical method that finds an approximated solution of the distribution of field variables in the problem domain. The finite element method can be used when the solution is too difficult to obtain analytically. The problem domain is divided into small parts which are called elements. This procedure is also known as the

meshing of the domain. Proper meshing of the domain is very important for achieving a converged solution. If the mesh is too sparse, the solution becomes inaccurate and too dense mesh might result in too long computation time. If the meshing can be done using a set of grids or nodes, the solution variation within an element is possible to be approximated easily with simple functions such as polynomials. The solution variation for the whole problem domain is formed by the collective variations of the solutions for each element. (Liu & Quek 2014, 3-6)

After the mesh formation, physical principles or laws are applied for each element. Depending on the generated mesh, a set of discrete simultaneous equations are formulated using existing procedures. The simultaneous equations can be formulated in few different ways that include energy principles, such as Hamilton's principle and the minimum potential energy principle, the weighted residual method, approach based on the Taylor series and approach based on the control of conservation laws on each finite volume (elements) in the domain. Based on the problem, a proper theory must be selected for discretising the governing equations. The created FEM model is then fed into a solver that solves the discretised system of equations. Different algorithms are used by different software's for solving the equations, depending on the physical phenomenon that is simulated. Direct methods and iterative methods are the two main types of methods for solving simultaneous equations. Direct methods can be used for relatively small equation systems and for larger systems and nonlinear problems, iterative methods should be used. Time-dependent problems require time stepping, where the time history of the solution is computed by marching forward to the next time steps until the final time step is reach. (Liu & Quek 2014, 3-9)

Figure 30 presents a finite element approximation for a one-dimensional case. The *F(x)* represents a continuous function that is approximated using piecewise linear functions in each element/sub-domain. Nodes are the ends of each element in the one-dimensional case of the figure 30. The unknown variables in the finite element method are the discrete values of the field variable at the nodes. (Liu & Quek 2014, 3)

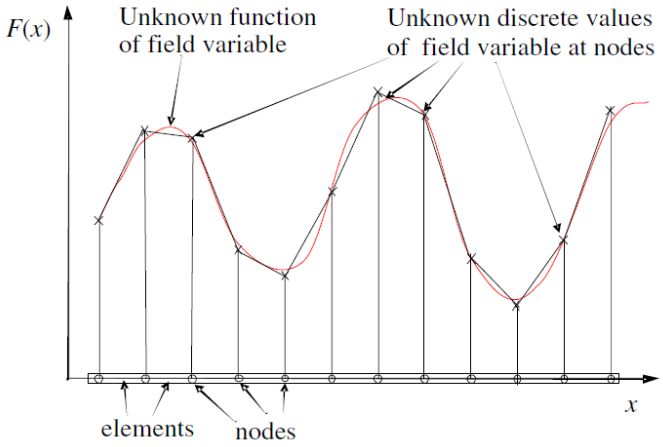

Figure 30. Finite element approximation (Liu & Quek 2014, 3)

5.2.2 Reactor coil and loop ANSYS models

The air core reactor model selected for the thesis had to be simplified for the ANSYS simulations. The reactor was modelled with only one cylinder, and without spider-arms or post insulators. The position of the coil in the ANSYS modelling coordinate system was set so it would match the real reactor with post insulators. The center point of the ANSYS model coil was at 1727 mm height from the origin. The height of the coil was calculated by multiplying the average number of turns and average winding pitch of the real reactor. 79 turns with a pitch of 21 mm gave 1682 mm for the coil height. The single cylinder of the model had a mean diameter of 2383 mm, which is the average between the outer diameter (2765 mm) and bore (2000 mm) of the real reactor. Figure 31 presents the simplified air core reactor ANSYS model.

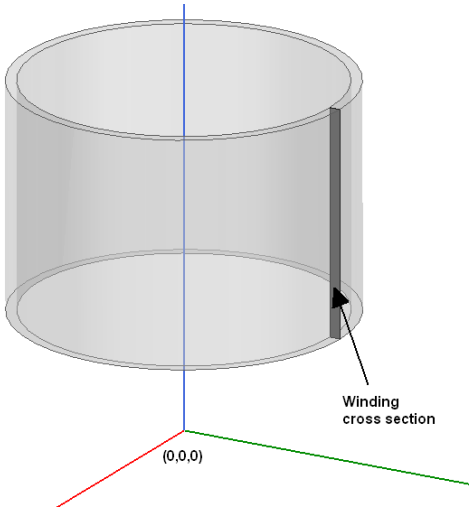

Figure 31. Air core reactor coil model used for ANSYS simulations

The width of the winding cross section was calculated using equation (42). The winding was assumed to be pure solid aluminium for the calculation, thus density of 2700 kg/m^3 (Valtanen 2012, 367) was used. Since it was assumed that winding is solid aluminium, for the equation winding mass of 2700 kg was used. Coil height was 1.68 m and mean diameter of the coil was 2.38 m. With these values, the winding cross section width was calculated as 79 mm. Of course, in reality winding cannot be solid material, but for simulations it is accurate enough approximation. The focus was in any case in the induction to the loop and magnetic field outside the $\mathbf{m_x}$. The conductivity for the winding was chosen as 3.8·10^7 S/m, which is the conductivity for aluminium in ANSYS Electronics 19.2 database.

$$x = \frac{m}{\pi \rho h D_{\mathrm{m}}} \tag{42}$$

x = winding cross section width [m]
m = winding mass [kg]
ρ = density [kg/m^3]
h = winding/coil height [m]
D_{m} = mean diameter of the coil [m]

Steel and aluminium loops were attempted to model in ANSYS as close as possible compared to their real counterparts, to ensure accurate enough induction current and heat production in loops. ANSYS models of the used steel and aluminium loops are presented in

figure 32. The dimensions of the models are the same as the real loops with 5 mm tolerance. The cuts in cut loops was modeled in the same locations as in their real counterparts and the width of the cuts was 5 mm in both steel and aluminium loop.

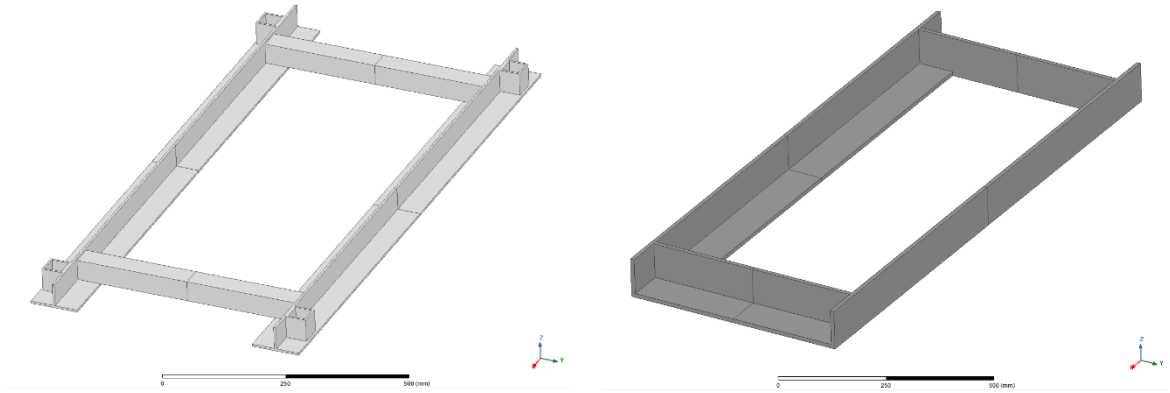

Figure 32. ANSYS models of the aluminium loop (left) and steel loop (right)

5.2.3 Reactor coil magnetic field simulation

The magnetostatic solution type in the ANSYS Electronics was used to calculate the magnetic flux density around the reactor. This simulation was conducted to validate the simplified reactor model. In the magnetostatic solver, 118500 A of DC current was set through the cross-section of the reactor model. This simulates a case where 1500 A RMS of AC current is flowing through a coil with 79 turns. To simulate a case with 3000 A RMS of AC current through the coil, 237000 A of DC current must be set in the cross-section of the reactor model. The magnitude of the magnetic flux density can be calculated for any distance from the reactor with ANSYS, but results were obtained from the simulation for the same distances as were measured in the laboratory tests. The distances in the laboratory tests were from 3.1 m to 11.0 m from the center of the reactor for the 1500 A reactor current and from 4.0 m to 11.0 m for the 3000 A. As in the laboratory tests, the simulation results were obtained from 1.5 m height from the origin. The simulation boundary was a sphere with a diameter of 40.0 m. The boundary condition used at the edge of the calculation space was the Neumann boundary or natural boundary condition. Flux is not allowed to cross the boundary. Because of the natural boundary condition, the calculation space must be

significantly larger than the farthest measurement point. Close to the boundary, the magnetic field would be distorted, and it appears to be larger than it would really be. The medium inside the sphere boundary was selected as air and the default properties from ANSYS were used. The simulation results are presented in table 14. The meshing setup is not very important with the magnetostatic solver, because it uses adaptive meshing. It refines the mesh automatically after every iteration where it is needed until the energy error of the system reaches the desired level.

Table 14. Simulation results of the magnetic flux density magnitude caused by the reactor coil

Initial values		**Calculation results**
Reactor simulation current, DC [A]	Simulation distance [mm]	Magnetic flux density [mT]
1500	3100	1.85
1500	4000	0.86
1500	5000	0.45
1500	6000	0.26
1500	7000	0.17
1500	8000	0.12
1500	9000	0.09
1500	10000	0.07
1500	11000	0.05
3000	4000	1.72
3000	5000	0.90
3000	6000	0.53
3000	7000	0.34
3000	8000	0.23
3000	9000	0.17
3000	10000	0.13
3000	11000	0.11

5.2.4 Electrical conductivity determination for the loops

The electrical conductivity (S/m) of the material in ANSYS Maxwell simulation is one of the most important parameters, which defines the final result of the calculation. It describes the resistivity (Ω·m) of the material, thus how easily current can flow through it. Because the conductivity value affects the simulation that much, it was necessary to determine the

electrical conductivity for steel and aluminium loops more accurately than just use values from material tables. This was done by using ANSYS Maxwell 3D, DC conduction solution type. Cut steel and aluminium loop models were used to determine the correct conductivity for these loop materials. The small cut in a loop creates two cross-section areas in the loop, which can be used as terminals to apply voltage difference between them, as shown in figure 33.

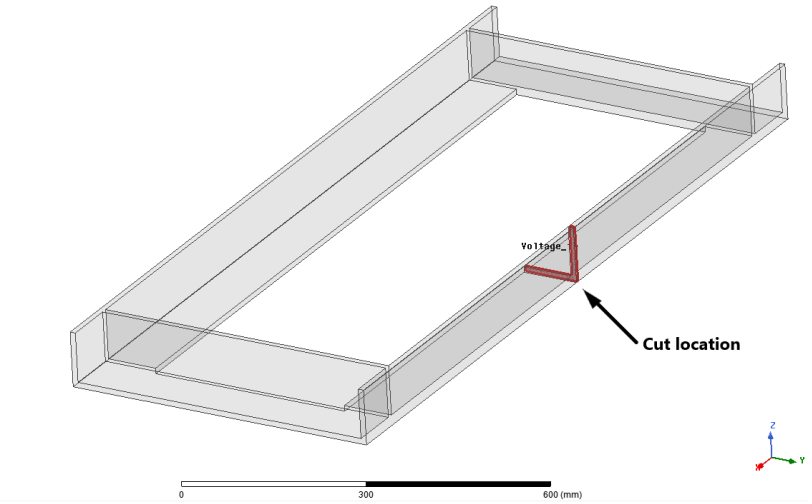

Figure 33. Terminals in the cut steel loop for electrical conductivity determination

The applied voltage difference, which was selected as one volt, causes current to flow through the loop. After simulation, ANSYS field calculator can be used to calculate the current flowing through a cross-section at any point of the loop. From the voltage difference between the terminals and current through the loop, resistance can be calculated using equation (43).

$$R = \frac{\Delta U}{I} \tag{43}$$

R = resistance [Ω]

ΔU = voltage difference between terminals [V]

I = current [A]

The parameter that can be changed in ANSYS, is the bulk conductivity of the material. Testing different conductivities for steel and aluminium loops gives different resistances for the loops, because the current value changes. In laboratory tests, the DC resistance for the loops was measured. This was used as a reference for the simulation to determine the correct electrical conductivity for the loops. For the steel loop, conductivities from $4.4 \cdot 10^6$ S/m to $2.6 \cdot 10^6$ S/m were simulated, and for the aluminium loop, from $2.8 \cdot 10^7$ S/m to $1.0 \cdot 10^7$ S/m. Ten simulations were conducted for both loops. Results of the calculations is presented in figure 34, and more accurate results in appendix 6. From the calculated loop resistances, the correct electrical conductivity can be determined using linear interpolation, with measured loop resistance from laboratory tests as reference. The measured DC resistance for the steel loop at 20 °C was 0.421 mΩ and for the aluminium loop 0.148 mΩ. Thus, the corresponding conductivity for the steel loop at 20 °C would be about $4.17 \cdot 10^6$ S/m and for the aluminium loop about $2.53 \cdot 10^7$ S/m. With this method, also temperature dependency of the material resistivity can be considered. For ANSYS Maxwell simulations, electrical conductivity of the material was interpolated for each individual case separately, so that temperature dependency of the resistance was considered also for the simulations.

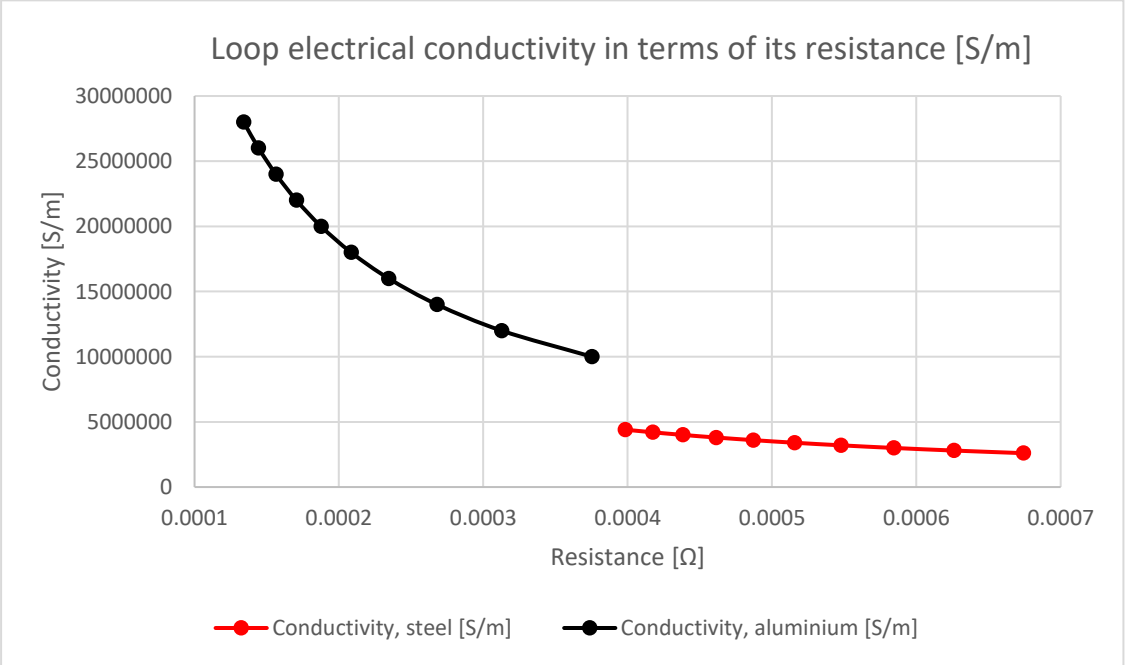

Figure 34. Steel and aluminium loop electrical conductivity in terms of resistance

5.2.5 ANSYS loop induction simulations

The same loop induction test cases were simulated with ANSYS as were conducted in the laboratory tests. These included simulations of the steel and aluminium loops in horizontal orientation with one meter spacing at distances from 2.0 m to 6.0 m, simulations of the loops in 45- and 90-degree angles at 3.0 m distance from the reactor and simulations of the cut loops in 0-, 45- and 90-degree angles at a distance of 3.0 m. As in the laboratory test, the loop height was in all simulations 1.5 m from the bottom edge of the loop to the origin and the loop distances were measured from the center point of the reactor to the closest edge of the loop. The AC frequency was 50 Hz and the RMS current was exactly 3000 A in all simulations. The simulation setup for a horizontal case is presented in figure 35. The idea was to test how well ANSYS simulations compare to the laboratory tests. If the simulation results become close enough to the laboratory tests, ANSYS can be used to simulate other cases as well.

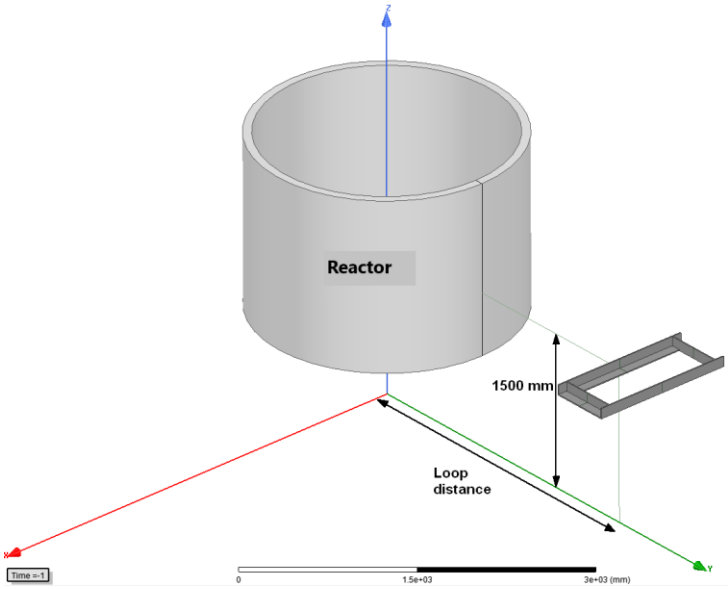

Figure 35. ANSYS Electronics setup for the loop induction simulations

As mentioned before, the electrical conductivity of the loop material was the main parameter in the electromagnetic simulation that was adjusted prior the simulation. The conductivity of the loop was set in each simulation to match the resistance at the average temperature of the loop in the corresponding laboratory test. The conductivities used in the simulations are

shown among the calculation results, which are in tables 15, 16 and 17. A *B*-*H* curve for the steel S355J0 was used to model the relative permeability in the simulations. The *B*-*H* curve was the default curve for the steel 1010 found in the ANSYS material property data. Data points for the *B*-*H* curve can be found in appendix 7. The relative permeability for the aluminium was ≈1. Hysteresis losses were assumed to be minimal for the steel. Empirical Steinmetz's formula, equation (44), was used to verify that hysteresis losses are not significant with these relatively low *B*-fields and frequencies (Étienne et al. 2005, 93). Even when the steel loop was assumed to be pure iron in the equation, with a hysteresis loss per cycle value (k_n) of 500 J/m^3 (Mitchell 2004, 614), the hysteresis losses were only 47 W at 2.0 m distance from the reactor. This is only 4 % of the simulated total loss of 1073 W (table 15), without hysteresis losses. The hysteresis loss per cycle is for carbon steel much lower ($B_r \cdot H_c$ = 3.8 J/m^3) than for iron (Mitchell 2004, 619) and it is therefore safe to say that hysteresis losses can be neglected. The average magnetic flux density in the loop was calculated with the fields calculator at 15 ms, when the *B*-field was strongest. It had a value of about 0.5 T (2.0 m distance). The Steinmetz's constant α of 1.9 (Étienne et al. 2005, 93) was used and the steel loop volume was about 0.007 m^3.

$$P_h = k_n f \boldsymbol{B}_m^{\alpha} V \tag{44}$$

P_h = hysteresis loss [W]
k_n = hysteresis loss per cycle [J/m^3]
f = frequency [Hz]
B_m = medium peak magnetic flux density [T]
α = Steinmetz's constant
V = volume [m^3]

The simulation boundary was a sphere with a diameter of 40.0 m as in the chapter 5.2.3 "Reactor coil magnetic field simulation" and the boundary condition was the same. The medium inside the sphere boundary was also air and the default properties from ANSYS were used. The maximum element size in the background sphere volume was 2000 mm. The simulation time of the electromagnetic fields was in all simulations 22 ms and the timestep 0.5 ms. The simulation time only included one full AC cycle (20 ms), but longer simulations

were not possible due to the time consumed by one simulation and the available storage. Especially simulating the ferromagnetic steel, the simulation could take up to 10 hours and the amount of data for both steel and aluminium loops was about 11 Gb per simulation. The total number of elements in the problem domain was tried to be kept under 450000 in the simulations to minimize problems concerning time and storage availability. Meshing of the ANSYS Electronics loop induction simulations is presented in appendix 8. Because of the strong skin effect in the ferromagnetic steel, the mesh for the steel loop was refined close to the outer edges of the loop with a skin depth meshing method. 2 mm skin depth was used and the mesher would create at least 2 layers of mesh within the 2 mm skin depth. Maximum surface element length was set as 16 mm. For the aluminium loop, 10 mm element length was used throughout the loop.

ANSYS fields calculator was used to calculate the total loss of the loop and the circulating current in the loop from the electromagnetic fields. The total loss of the loop was calculated by integrating power density [W/m^3] over the loop volume and the circulating current was calculated by integrating current density [A/m^2] over the cross-section area of the loop. An example calculation of the total loss and circulating current at a timestep of 12.0 ms for the steel loop in horizontal orientation at 3.0 m distance with the fields calculator is presented in appendix 9. With the fields calculator, it was only possible to calculate the total loss or the current for one timestep at a time. Calculated total losses for the steel and aluminium loops in horizontal orientation at 3.0 m distance at simulation time range from 0 ms to 20 ms are shown in figure 36. The figure 36 shows that one cycle of AC was not enough to stabilize the system, but longer simulations could not be conducted due to the time and storage availability. Total loss curves for both loops are quite close to a sin wave, which was expected. Naturally the loop current would also follow the same curve. However, the curve peaks do not match with the maximum peak value of the magnetic flux density *B* produced by the reactor. The peak values of the *B*-field would be at timesteps 5.0 and 15.0 ms. The cause for this phenomenon comes from the Faraday's induction law. The induced current circulating in the loop creates its own magnetic field around the loop that opposes the magnetic field produced by the reactor. The magnetic field caused by the circulating current in the loop becomes so strong that the maximum current in the loop, and thus the losses, occurs before the peak value of the reactors *B*-field. Hysteresis effect causes delay in the

change of electromagnetic fields in the ferromagnetic steel loop, even though the hysteresis losses are not calculated.

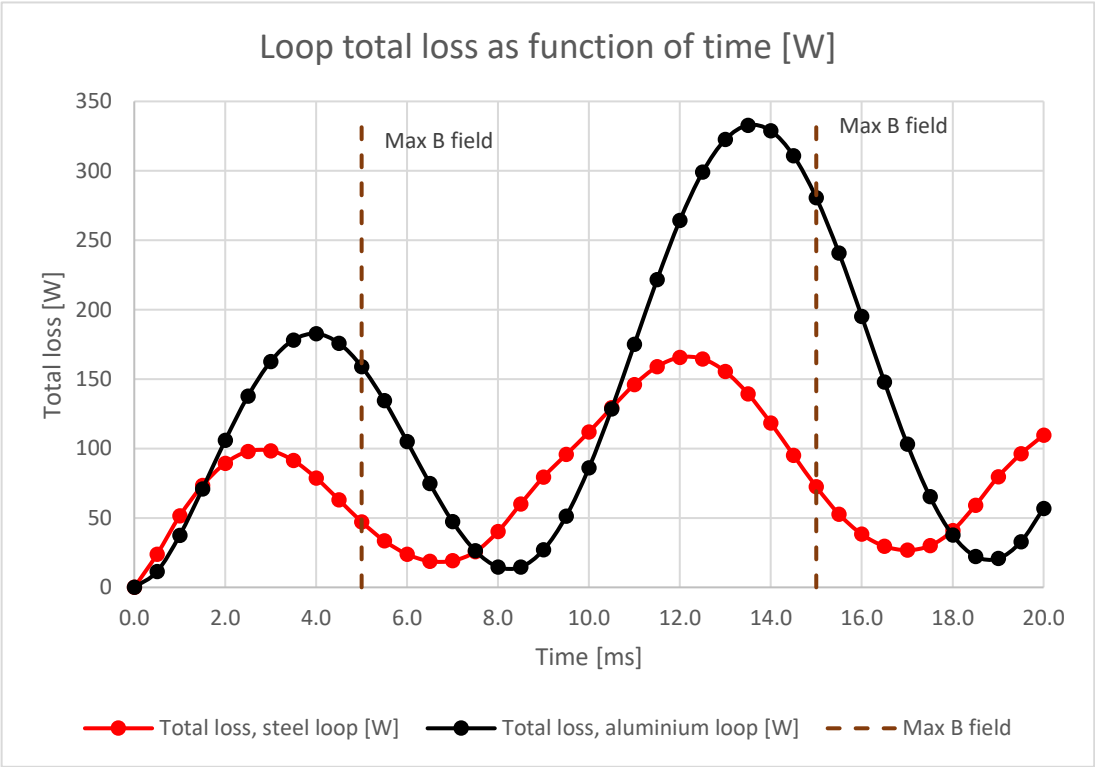

Figure 36. Steel and aluminium loop total loss as function of time at 3.0 m distance

Because the total loss and current waveforms of the loop follow a sin waveform closely, the RMS values for the total loss and circulating current can be calculated with equations (45) and (46). The peak values in the equations are the average of the two peaks that occur during the simulation time from 0.0 ms to 22.0 ms. The peak values occurred in most cases for the steel loop at timesteps 3.0 ms and 12.0 ms. For the aluminium loop the peaks were often at timesteps 4.0 ms and 13.5 ms. The total loss and current curves of the loop did not stabilize during one cycle of 50 Hz AC, thus the average of the two peaks had to be used. It was tested that the final peak values of the losses and current would stabilize somewhere between the two peaks of the first AC cycle. The possible error of the total loss with this method for the steel loop could be on average about 26 % and for the aluminium loop 29 %. Even though the possible error could be quite high, the average value of the two peak values must be considered accurate enough approximation, because longer simulation times were not possible. The loop loss by circulating current was calculated in the same manner as in the

laboratory test calculations, with equation (41) (page 69). The same AC resistance values were used for the equation as in the laboratory test calculations, because the ANSYS field calculator does not display the impedance value. The current value in the equation (41) was the RMS value of the of the current for the ANSYS calculations.

$$P_{\text{total,RMS}} = \frac{P_{\text{peak}}}{\sqrt{2}} \tag{45}$$

$P_{\text{total,RMS}}$ = RMS value of the total loss [W]
$P_{\text{total,peak}}$ = peak value of the total loss [W]

$$I_{\text{RMS}} = \frac{I_{\text{peak}}}{\sqrt{2}} \tag{46}$$

I_{RMS} = RMS value of the current [A]
I_{peak} = peak value of the current [A]

The strong skin effect in the ferromagnetic steel became evident during the AC resistance measurement of the steel loop in the laboratory tests. The AC resistance value was much greater than the DC resistance value. Simulations supported the theory that the skin effect is the reason for the different DC and AC resistance values for the loops. Figure 37 shows the current density distribution in the cross-section of the steel and aluminium loop. The current is much more evenly distributed in the cross-section of the aluminium loop than in the steel loop cross-section. In the case of the steel loop, most of the current is flowing couple millimeters inward from the edges and in the middle of the cross-section, very little current is flowing.

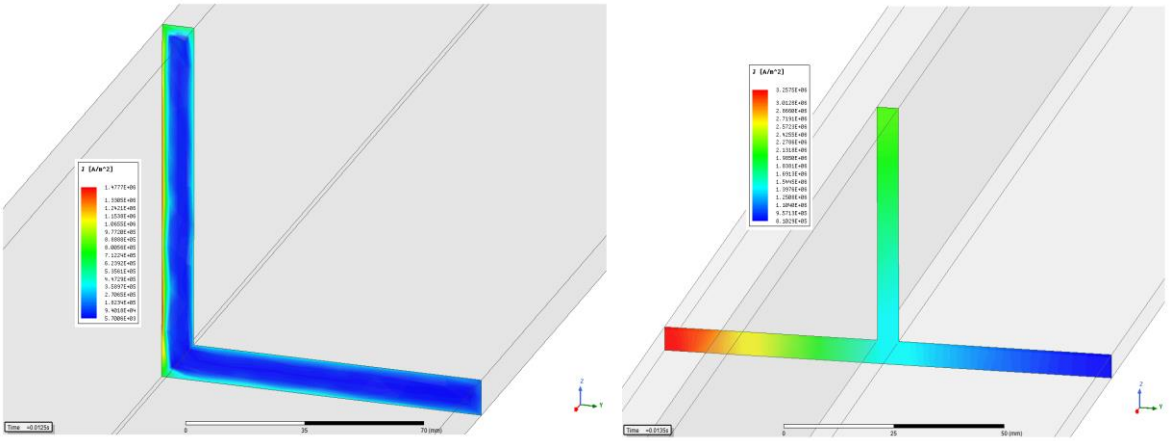

Figure 37. Current density distribution in the cross-section of the steel loop (left) and aluminium loop (right)

In the laboratory tests it was noticed that upright sides of the steel loop that were parallel to the magnetic field direction heated significantly, even though the AC current probe did not indicate current flowing through the loop. Figure 38 shows how eddy currents are circulating around the cross-section of the vertical L-beam in the cut steel loop. The current is strong at the edges of the cross-section and weak in the middle. The skin effect forces the current close to the edges that makes the current to follow cross-section edges almost perfectly.

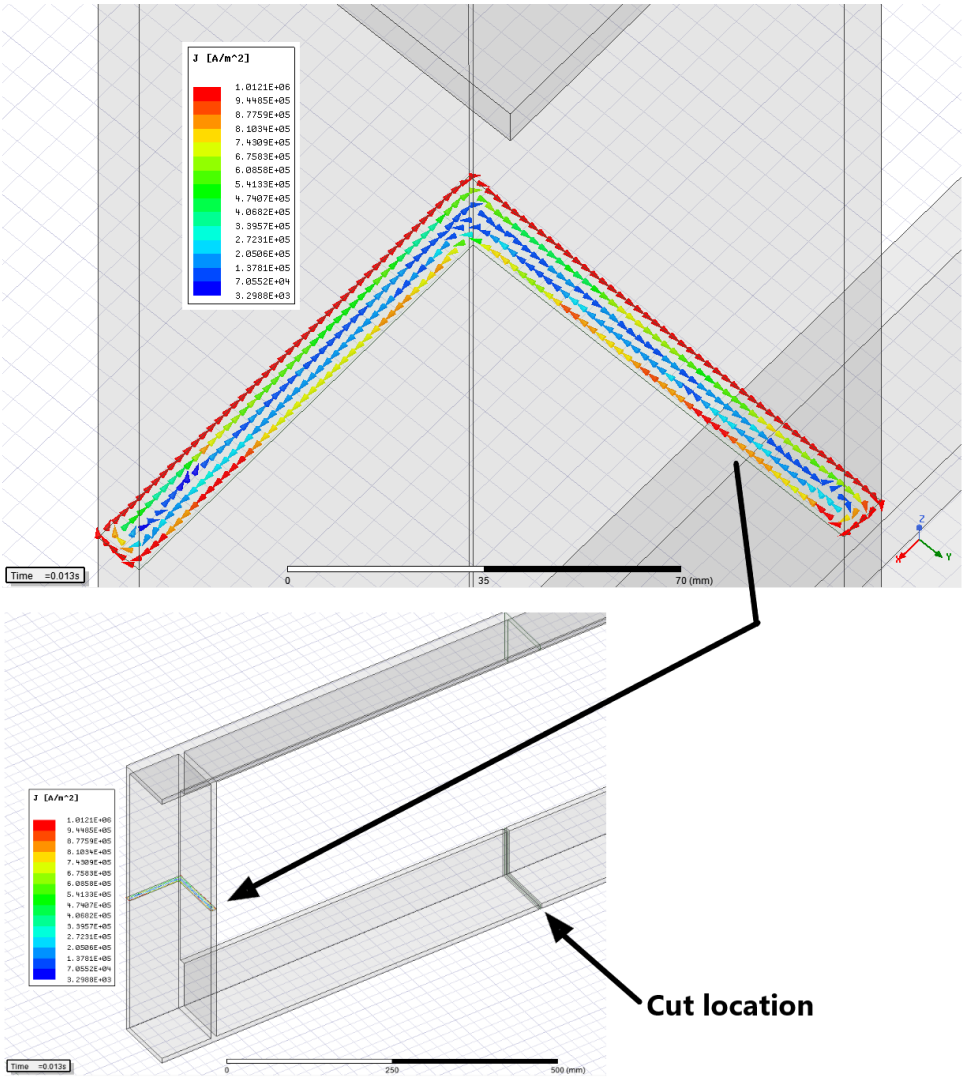

Figure 38. Eddy currents in the cut steel loop in vertical orientation

ANSYS Workbench could be used to couple the electromagnetic field solutions to the ANSYS Mechanical thermal analysis. Via Workbench it was possible to simulate the temperatures as a steady-state problem even though the electromagnetic simulations were conducted as transient problems. This feature was crucially important because 22 ms would not be enough for the thermal simulation to reach equilibrium. The total loss of the loop was imported to the ANSYS Mechanical. For the loop, own mesh was created in the Mechanical and the total loss power density [W/m^3] was imported from the electromagnetic field calculation nodes to the mesh in the ANSYS Mechanical. It was important to create fine enough mesh for the loop in the Mechanical to achieve accurate data mapping. The steel loop required finer mesh because of the skin depth meshing method in the ANSYS

Electronics and 1,5 mm element size in the Mechanical was used. For the aluminium loop 10 mm element size was enough. After importing the heat generation, Mechanical notifies the scaling factor on how successful the data mapping was. The closer it is to one, the better. The importation integrates the total loss of the loop over desired period of simulation time. The whole simulation time was used for the importation, which was from 0.0 ms to 22.0 ms. The time-varying total loss from the electromagnetic field simulation is transformed to a static heat generation via the importation. The imported total loss is comparable to the calculated RMS value of the total loss in the electromagnetic field simulations. Because the electromagnetic simulation did not fully stabilize, there was slight differences between the imported load to the Mechanical and the calculated total loss from the electromagnetic field simulation. As an average, the imported load was about 10 % smaller for the steel loop and about 25 % smaller for the aluminium loop, compared to the calculated total loss. This affects somewhat to the calculated temperatures with ANSYS and it increases the gap for temperatures between the laboratory tests and simulations. In some cases, for example, total losses came quite close to each other between laboratory test results and simulations, but loop temperatures would differ more due to this issue.

Figure 39 presents the result of the uncut aluminium loop temperature calculation. The loop is in horizontal orientation and at 3.0 m distance. The hottest side is closest to the reactor and where the magnetic field is strongest. Initial values required for the temperature simulation included convection coefficient, degree of emission, thermal conductivity and setting ambient temperature. The convection coefficient for each simulation was taken from the loop convection calculations regarding to the laboratory tests. The convection coefficient for each case was different and they are presented in tables 8-10 in page 68 (Loop total convection coefficient). The degree of emission used for the steel was 0.276 and for the aluminium 0.18 (Stephan et al. 2010, 951-952). The thermal conductivity for the steel was selected as 52 W/(m·K) (MatWeb 2019a) and for the aluminium 137 W/(m·K) (MatWeb 2019b). The ambient temperature was set for all simulations at 20 °C.

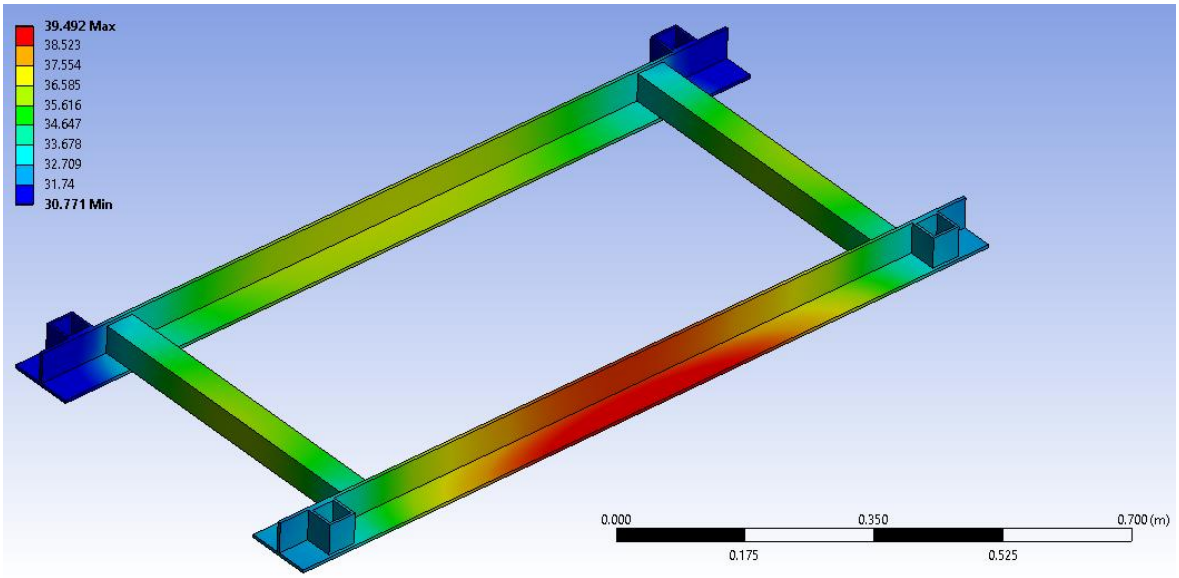

Figure 39. Temperature distribution of the uncut aluminium loop in horizontal orientation

All results of the electromagnetic and thermal simulations for the steel and aluminium loops are presented in tables 15, 16 and 17.

Table 15. Uncut steel and aluminium loop in horizontal orientation, simulation results

Loop distance [mm]	2000	3000	4000	5000	6000	
Loop conductivity [S/m]	$2.74 \cdot 10^6$	$3.82 \cdot 10^6$	$3.99 \cdot 10^6$	$4.09 \cdot 10^6$	$4.12 \cdot 10^6$	Steel
	$1.66 \cdot 10^7$	$2.29 \cdot 10^7$	$2.48 \cdot 10^7$	$2.44 \cdot 10^7$	$2.49 \cdot 10^7$	Aluminium
Loop circulating current, RMS [A]	536.5	176.4	85.6	48.2	30.0	Steel
	2240.5	837.2	386.7	209.3	128.2	Aluminium
Loop total loss, RMS [W]	1073.1	93.3	18.8	5.8	2.3	Steel
	1754.7	182.2	36.2	10.7	3.9	Aluminium
Loop loss by circulating current, RMS [W]	349.4	27.1	6.1	1.9	0.7	Steel
	1343.7	136.3	26.9	8.0	2.9	Aluminium
Loop loss by eddy currents [W]	723.6	66.3	12.7	3.9	1.5	Steel
	411.0	45.9	9.3	2.7	1.0	Aluminium
Loop imported load [W]	900.0	84.0	17.7	5.3	2.0	Steel
	1328.1	136.2	27.0	8.0	2.9	Aluminium
Loop temperature, min [°C]	72.8	27.1	21.7	20.6	20.2	Steel
	94.7	30.8	22.6	20.9	20.3	Aluminium
Loop temperature, max [°C]	121.6	31.8	22.5	20.7	20.3	Steel
	166.9	39.5	24.3	21.4	20.5	Aluminium
Loop temperature, avg [°C]	93.0	28.4	22.0	20.6	20.2	Steel
	133.0	35.1	23.4	21.2	20.4	Aluminium

Table 16. Uncut steel and aluminium loop in different orientations, simulation results

Loop angle [degrees]	45	90	
Loop conductivity [S/m]	$3.56 \cdot 10^6$	$3.31 \cdot 10^6$	Steel
	$2.28 \cdot 10^7$	$2.55 \cdot 10^7$	Aluminium
Loop circulating current, RMS [A]	133.0	12.9	Steel
	639.2	70.4	Aluminium
Loop total loss, RMS [W]	180.5	354.6	Steel
	109.5	18.2	Aluminium
Loop loss by circulating current, RMS [W]	16.5	0.2	Steel
	79.8	0.9	Aluminium
Loop loss by eddy currents [W]	164.0	354.4	Steel
	29.7	17.4	Aluminium
Loop imported load [W]	158.6	298.6	Steel
	83.3	15.5	Aluminium
Loop temperature, min [°C]	25.1	26.1	Steel
	26.9	21.6	Aluminium
Loop temperature, max [°C]	50.0	86.9	Steel
	32.0	22.9	Aluminium
Loop temperature, avg [°C]	35.1	48.1	Steel
	29.3	22.1	Aluminium

Table 17. Cut steel and aluminium loop in different orientations, simulation results

Loop angle [degrees]	0	45	90	
Loop conductivity [S/m]	$4.19 \cdot 10^6$	$3.77 \cdot 10^6$	$3.43 \cdot 10^6$	Steel
	$2.53 \cdot 10^7$	$2.55 \cdot 10^7$	$2.56 \cdot 10^7$	Aluminium
Loop circulating current, RMS [A]	1.1	0.4	0.4	Steel
	3.6	3.9	1.4	Aluminium
Loop total loss, RMS [W]	28.2	138.3	370.7	Steel
	24.5	19.2	17.4	Aluminium
Loop loss by circulating current, RMS [W]	0.0	0.0	0.0	Steel
	0.0	0.0	0.0	Aluminium
Loop loss by eddy currents [W]	28.2	138.3	370.7	Steel
	24.5	19.2	17.4	Aluminium
Loop imported load [W]	26.4	119.9	311.6	Steel
	20.3	16.0	14.5	Aluminium
Loop temperature, min [°C]	21.5	22.3	25.9	Steel
	21.3	21.4	21.4	Aluminium
Loop temperature, max [°C]	25.7	46.0	89.0	Steel
	24.9	23.4	22.7	Aluminium
Loop temperature, avg [°C]	23.2	31.8	49.5	Steel
	22.8	22.3	22.0	Aluminium

5.3 Laboratory tests and simulations comparison and analysis

In this chapter laboratory test and simulation results are compared to each other, concerning the magnetic field produced by the reactor and the induction tests for the loops, which were extracted from the capacitor racks. It was a concern, would the simplified reactor model for ANSYS be accurate enough representation of the real reactor. If the simplified, one-cylinder reactor creates too inaccurate magnetic field around the reactor, also the loop induction simulations would go wrong. However, it was found out that the simulations generated very similar results compared to the laboratory tests.

5.3.1 Reactor B-field

The reactor magnetic field laboratory measurements and ANSYS magnetostatic simulation results became very close to each other. Figure 40 shows a magnitude of the magnetic flux density produced by the reactor in terms of distance for the laboratory tests and simulations. In the figure 40 both current levels; 1500 A and 3000 A are presented. The curves for both current levels are almost identical between the laboratory measurements and simulations. The results prove that the simplified reactor model in the simulations creates accurate enough approximation of the magnetic field around the reactor. The very accurate magnetic field simulation results are significant also for the reason, that ANSYS could be implemented for pure magnetic field studies and not just for induction simulations, which were the main target for the thesis.

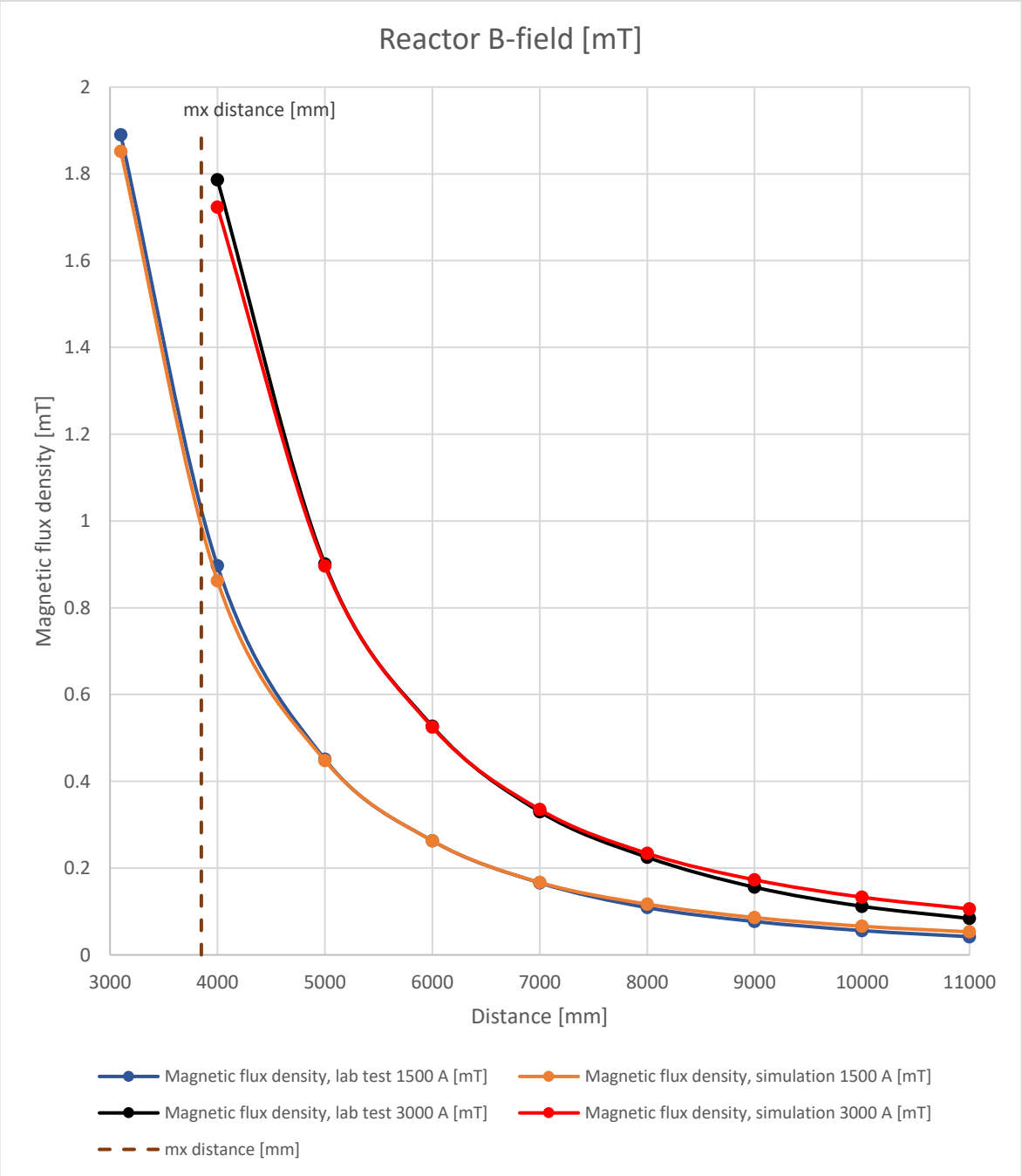

Figure 40. Magnitude of the magnetic flux density created by the reactor in terms of distance

Figure 41 shows a difference in the magnetic flux density between the laboratory measurements and simulations. The simulation results are compared to the laboratory test measurements. The difference stays minimal until 7.0 m distance, but then the percentage of error starts to rapidly increase for the measurements further away from the reactor. The error is almost the same for both current levels; 1500 A and 3000 A. This happens due to the Neumann boundary condition for the simulation calculation space. Flux is not allowed to

cross the boundary which increases the *B*-field for the simulations close to the boundary. At 11.0 m distance from the reactor, the error reaches already about 26 %. The increasing error shows that the simulation calculation space must be significantly larger than the objects which are simulated. Also, the percentual defects in the laboratory test measurements at longer distances can be greater, because the magnetic flux densities are low and even small inaccuracy in the measurement can result in substantial percentual error.

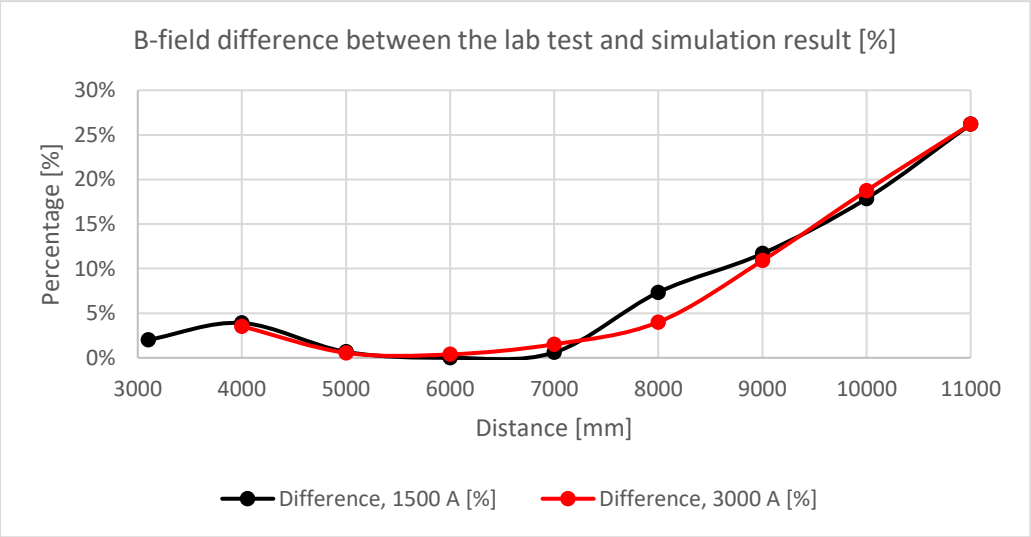

Figure 41. Difference of the magnetic flux density between the laboratory tests and simulations

5.3.2 Uncut loops in horizontal orientation

The circulating current in the steel and aluminium loop for uncut loops in horizontal orientation at different distances for laboratory measurements and simulations is presented in figure 42. The current levels between the laboratory tests and simulations compared quite well for both loops. For both loops, the current in the laboratory tests was larger than in the corresponding simulation, except for the aluminium loop at 2.0 m distance. The strong reactor magnetic field close to the reactor pushed the aluminium loop back about 30 cm from the reactor during the laboratory test, thus the correct distance would be about 2.3 m. The measured current in the laboratory for the aluminium loop at 2.0 m distance should be larger than what was measured. The difference between the simulations compared to the laboratory measurements for the steel loop was on average about 41 % and for the aluminium loop

about 13 %. The average difference for the steel loop seems quite high, but the current levels for the steel were altogether much lower than for the aluminium. However, the percentage of error for the steel loop increased steadily from 30 % at 2.0 m distance to 59 % at 6.0 m distance. It should be noted that the current level for the aluminium loop is noticeably larger than for the steel loop. The resistance of the aluminium loop is very low, thus more current can induce into it than in the steel loop. The current level for the aluminium loop at the $\mathbf{m_x}$ distance was still around 500 A, even though the loop was quite small. The result indicates that even small loops with high electrical conductivity should be avoided also outside the $\mathbf{m_x}$ distance. The results between the steel and aluminium loops of course are not fully comparable because the geometry of the loops was different.

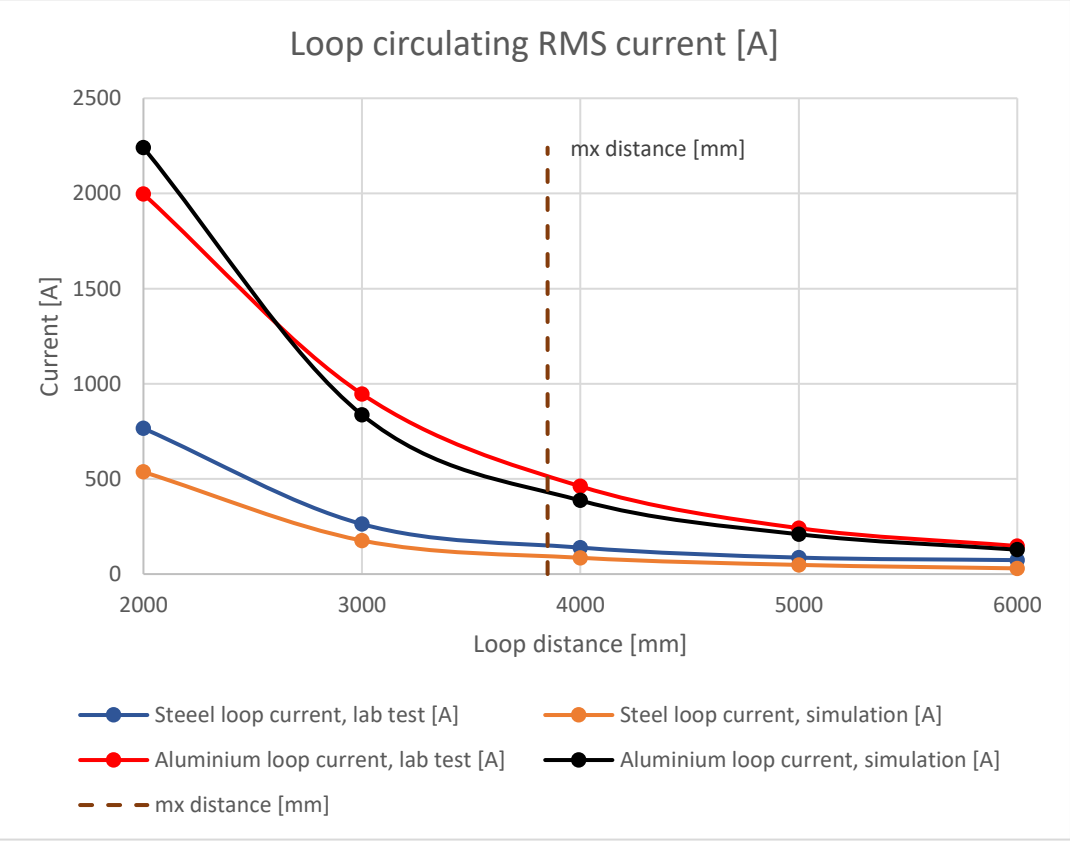

Figure 42. Circulating current in the loop at horizontal orientation in terms of distance

Figure 43 presents the total loss of the steel and aluminium loop in horizontal orientation at different distances for the laboratory measurements and simulations. The total loss of the loops decreases exponentially in terms of the distance. At the $\mathbf{m_x}$ distance, the losses are for both loops only a few dozen watts, even though the circulating current level can be relatively

high at the same distance. That amount of losses should not be a problem from a reactor efficiency point of view or cause any significant heating. However, both loops have high material thickness and the situation might change if the loop is fully or partially thin. That case is studied later in the report. The losses also match quite well between the laboratory measurements and simulations. The difference between the simulations compared to the laboratory measurements for the aluminium loop was on average about 13 %, neglecting the results from 2.0 m and 5.0 m distances for the reasons explained in this chapter and in the chapter 5.1.5 “Total loss determination for loops from temperature measurements”, page 67. The error between the laboratory measurements and simulations for both; the circulating current and total loss is about 13 %, which indicates that the electromagnetic simulations for the aluminium loop were successful. The error of the total loss between the laboratory measurements and simulations for the steel loop increased steadily from 4 % at 2.0 m distance to 58 % at 6.0 m distance.

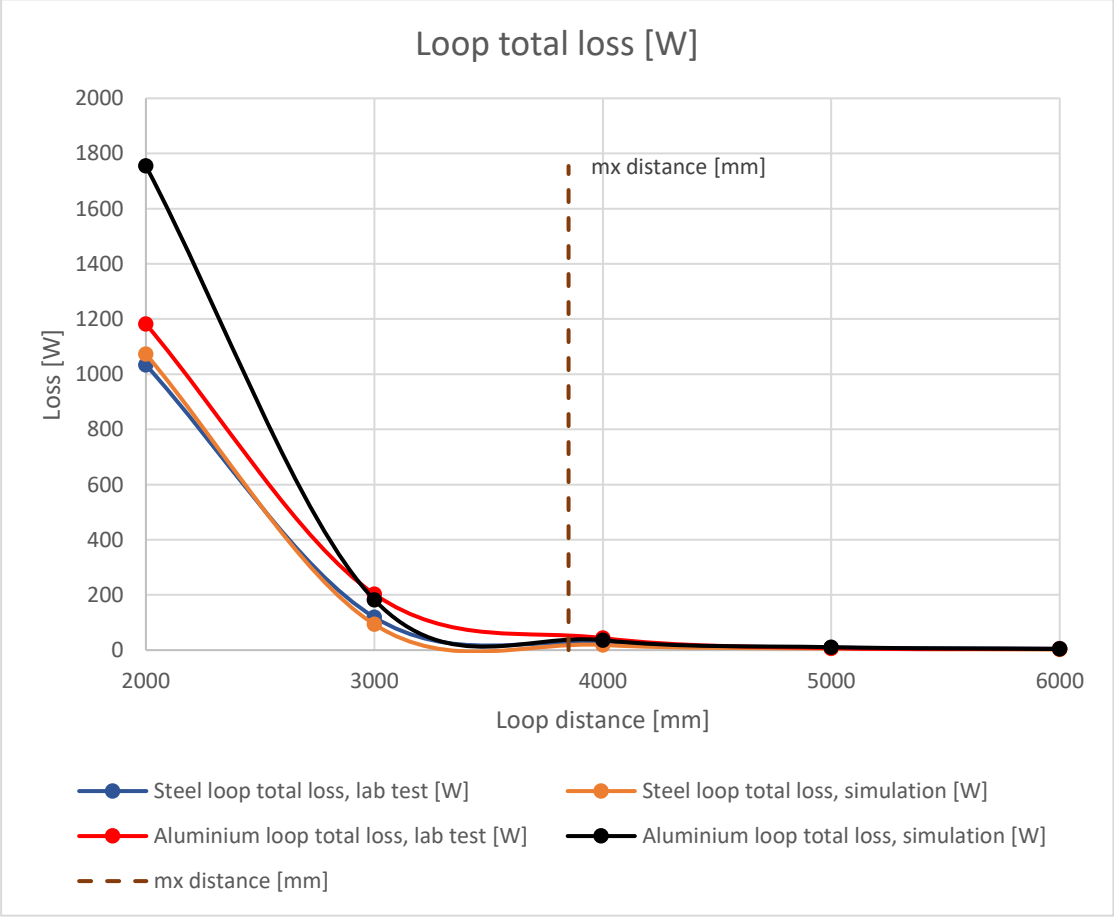

Figure 43. Total loss of the loop at horizontal orientation in terms of distance

The increasing error of the current and total loss for the steel loop as the distance increases gave suspicion that the magnetic properties of the real steel loop were not as strong as was used in the simulations. Weaker magnetic properties and therefore weaker skin effect would result in more current to circulate through the loop, as the AC resistance of the loop decreases. The total loss error at close distances from the reactor is low, because high eddy currents in the simulations compensate for the difference in the circulating current. It was tested how it would affect the simulation results of the steel loop, if the magnetic properties of the material would be reduced. One test was conducted on the steel loop in horizontal orientation at 3.0 m distance. The *B* value in the *B-H* curve was reduced 30 % from the original curve. The original and reduced *B-H* curve data points for the steel are presented in appendix 7. The results of the simulation with reduced magnetic properties are presented in appendix 10. The circulating current value increased about 17 % to 207 A, from the original 176 A and the difference between the laboratory measurement and simulation decreased from 33 % to 21 %. The total loss of the loop increased about 16 % to 109 W, from the original 93 W and the difference of the lab test and simulation decreased just to 9 %, from the original 22 %. The results became significantly closer together between the laboratory measurements and simulations, thus shows that magnetic properties of the material have big effect on the induced current. The results also showed that it is difficult to know the correctness of all the variables required for simulations. Using inaccurate initial values in the simulations, could result in totally wrong results. Laboratory tests are of course not always available, which leads to an estimation of some variables required for simulations. The simulation results should not be taken as an absolute truth, but as an approximation and the results should be interpreted with caution.

Figure 44 presents the hot spot temperature difference between the loops and ambient temperature, for the loops in horizontal orientation at different distances. The curve forms are very similar to the ones for the total loss, which was expected. The loop temperatures became significant only at very close distances from the reactor and structures would not be allowed to be build that close to reactors anyway. At the $\mathbf{m_x}$ distance, both loops heated from the ambient temperature only few degrees. But again, the material thickness of the loops was high, and the loops would probably heat more if they had thinner parts in them. The error between the lab tests and simulations was a bit higher than for the total loss due to the losses

importation issue to the ANSYS mechanical, explained in the chapter 5.2.5 “ANSYS loop induction simulations”, pages 86-87.

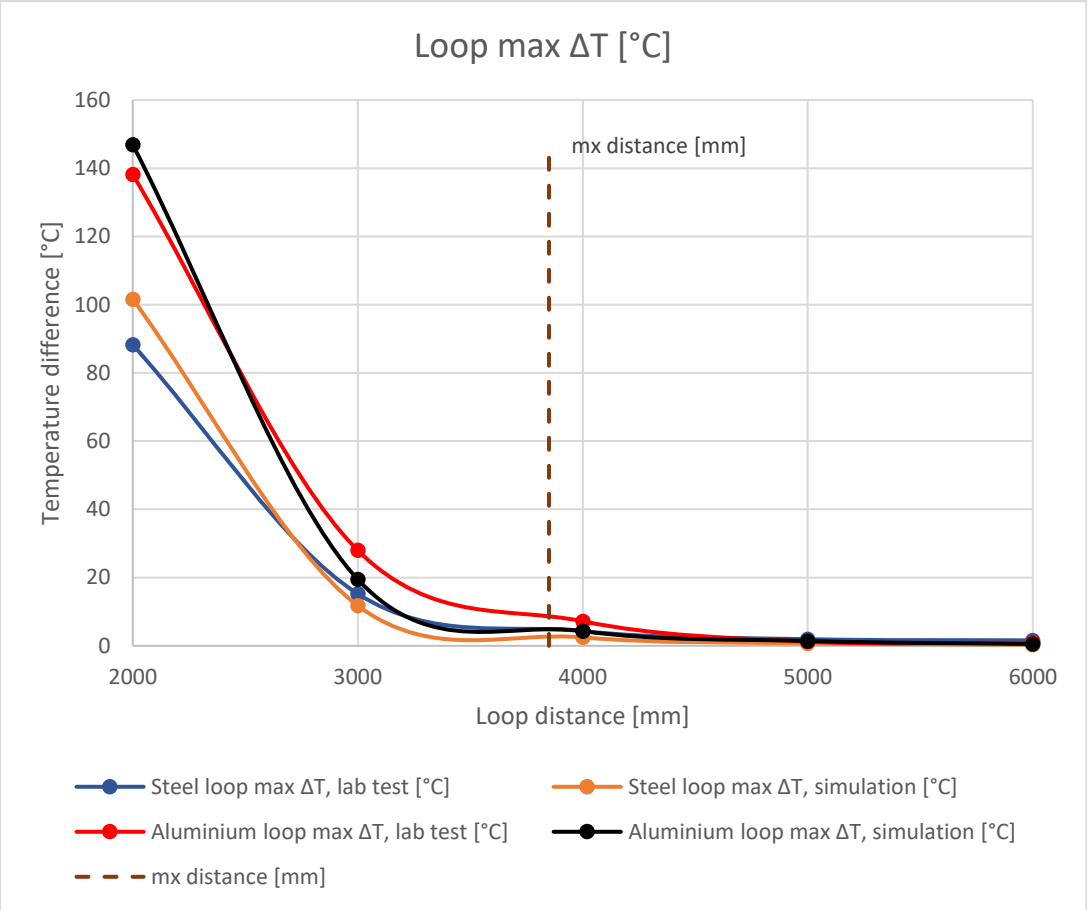

Figure 44. Temperature difference between the loop and ambient at horizontal orientation in terms of distance

5.3.3 Uncut loops in different orientations

Figure 45 presents the circulating current in the uncut steel and aluminium loops at 3.0 m distance from the reactor at 0-, 45- and 90-degree loop angles. When the loops are at 0-degree angle or in horizontal orientation, maximum amount of the magnetic flux created by the reactor crosses the area enclosed by the loop. This results in maximum induced current in the loop. At 45-degree angle the induced current in the loops starts to decrease, because the amount of magnetic flux crossing the loop area decreases. At the loop height (1.5 m), direction of the magnetic field created by the reactor was almost vertical according to

simulations. In vertical orientation, the induced circulating current in both loops diminished to a fraction of what it was in horizontal orientation. The difference in the circulating current between the lab tests and simulations for the steel loop was between 33 and 47 %. For the aluminium loop the difference was between 12 and 57 %. The high percentage of error in some cases can be explained by the inaccuracies in the laboratory measurements. For example, even minimal change on the loop angle at vertical orientation would affect significantly on the induced current.

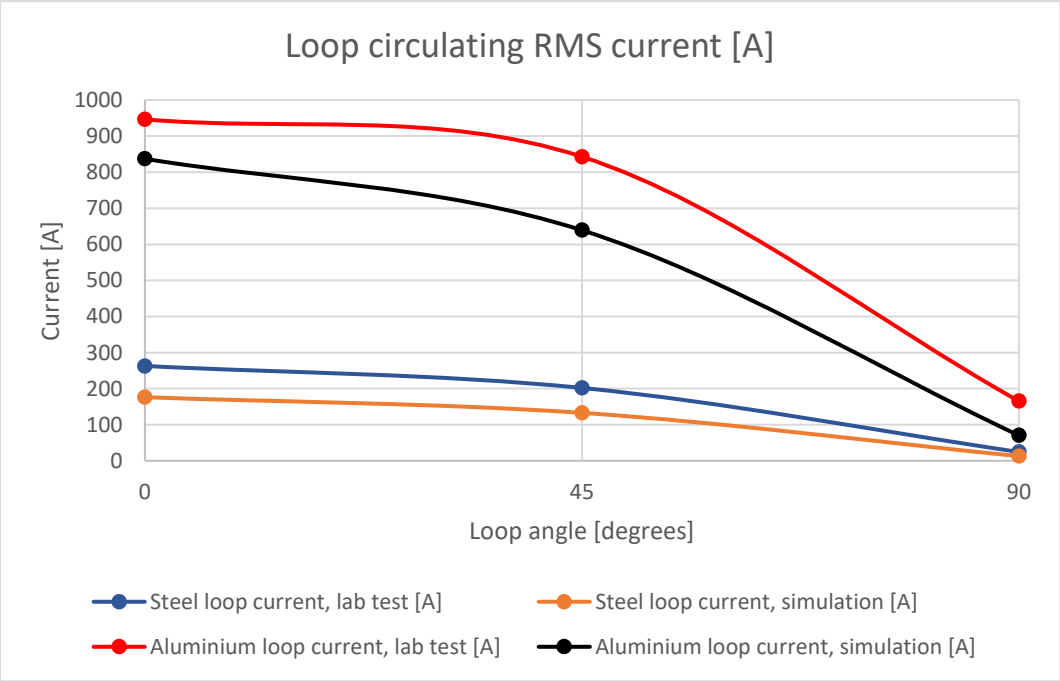

Figure 45. Circulating current in the loop at 3.0 m distance in terms of loop angle

The angle on which the area enclosed by the loop is relative to the external magnetic field has a major effect on how much circulating current is induced to the loop. One must be aware on how the magnetic field lines of reactors or other equipment are formed in STATCOM or SVC substations. There are two identical horizontal planes at different heights in figure 46, that can be thought as areas enclosed by conducting loops 1 and 2. They both are at the same horizontal distance (5.0 m) from a reactor coil that produces a changing magnetic field. The magnetic field crossing the loop 1 is almost perpendicular to the loop, thus large amount of magnetic flux crosses the loop area. Therefore, high current could induce to it. However, even though the loop 2 is at the same horizontal distance, the magnetic field lines are almost parallel to the loop area at its height. The current induced to the loop 2 would be minimal

compared to the loop 1. Therefore, it is important to know also the direction of the magnetic field and not just the intensity of it at specific distances.

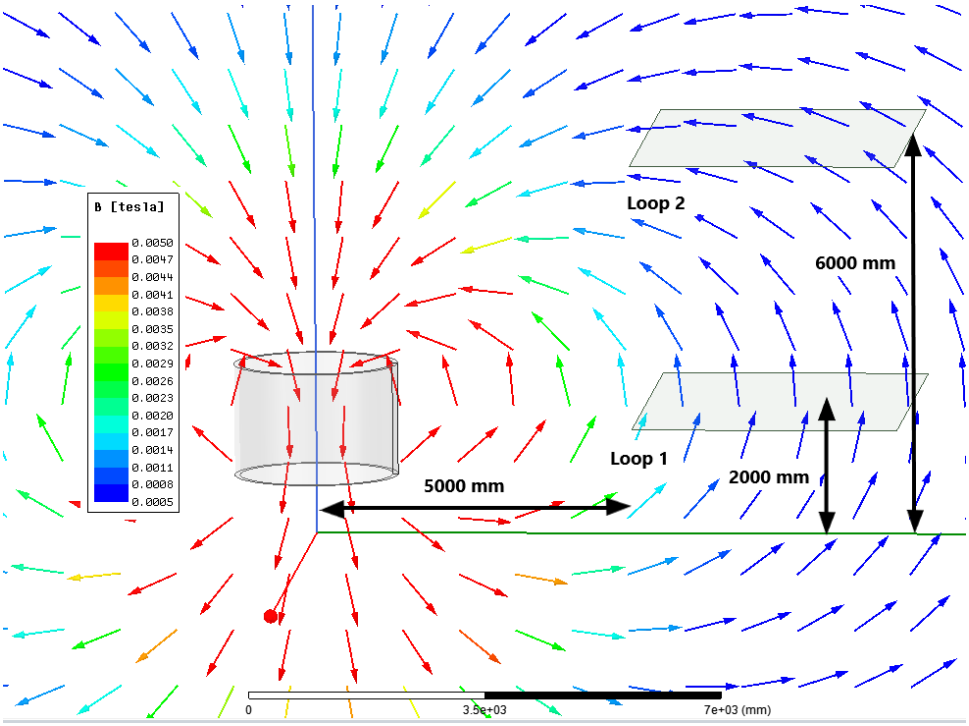

Figure 46. Reactor B-field direction at different heights

Figure 47 shows the total loss of the uncut steel and aluminium loops at 3.0 m distance from the reactor at 0-, 45- and 90-degree loop angles. For the aluminium loop, the total loss curve form looks similar to the circulating current curve. The losses of the aluminium loop decrease as the loop angle increases and in vertical orientation, the losses were less than 20 W. The losses for the steel loop are however increasing as the loop angle increases. In vertical orientation the losses for the steel loop are the highest, even though there is not much current flowing around the loop. At the loop height (1.5 m) the magnetic field is almost parallel to the upright sides of the loop. As explained before, the ferromagnetic steel intensifies the magnetic flux inside the material and causes high eddy currents to circulate around the cross-section of the upright sides. The losses of the steel loop in vertical orientation were over 350 W due to the eddy currents. It is then obvious that for ferromagnetic materials as carbon steel, the induced eddy currents can be actually a bigger concern than the induced current that circulates around the whole loop. Strong eddy currents

can occur in ferromagnetic structures that are parallel to the magnetic field. These structures include for example supporting carbon steel beams in buildings.

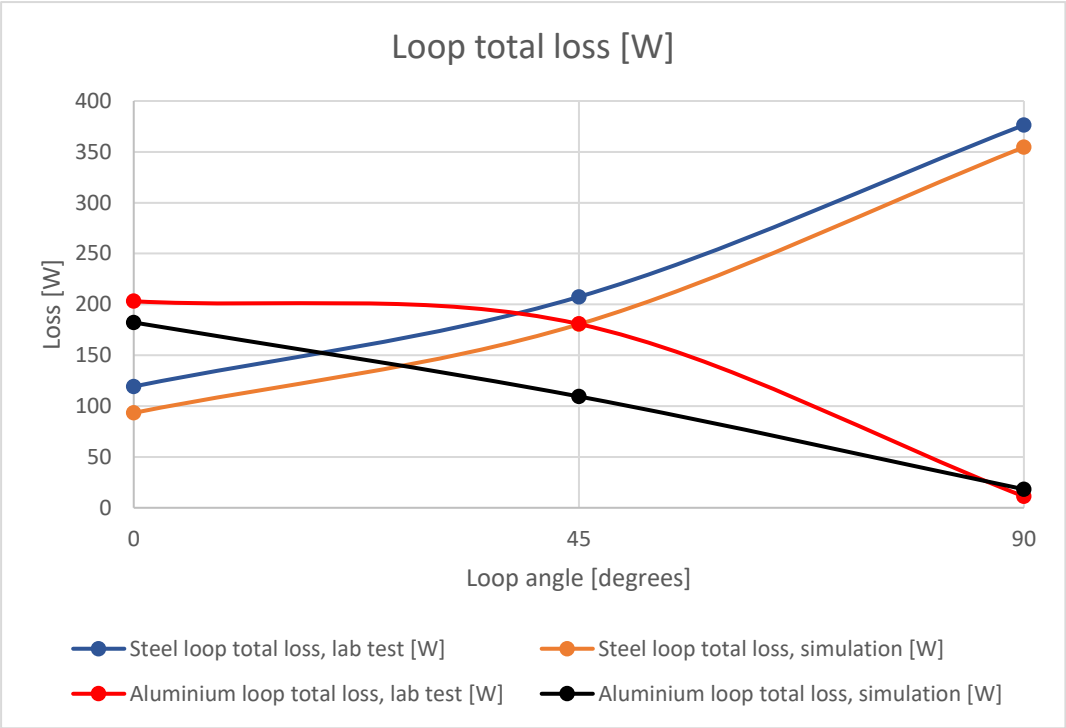

Figure 47. Total loss of the loop at 3.0 m distance in terms of loop angle

The temperature curves in figure 48 are very similar to the total loss curves as expected. The temperature rose from the ambient for the steel loop more than 60 °C in vertical orientation. The produced heat in the steel loop is quite significant, but it was achieved inside the $\mathbf{m_x}$ distance of the reactor.

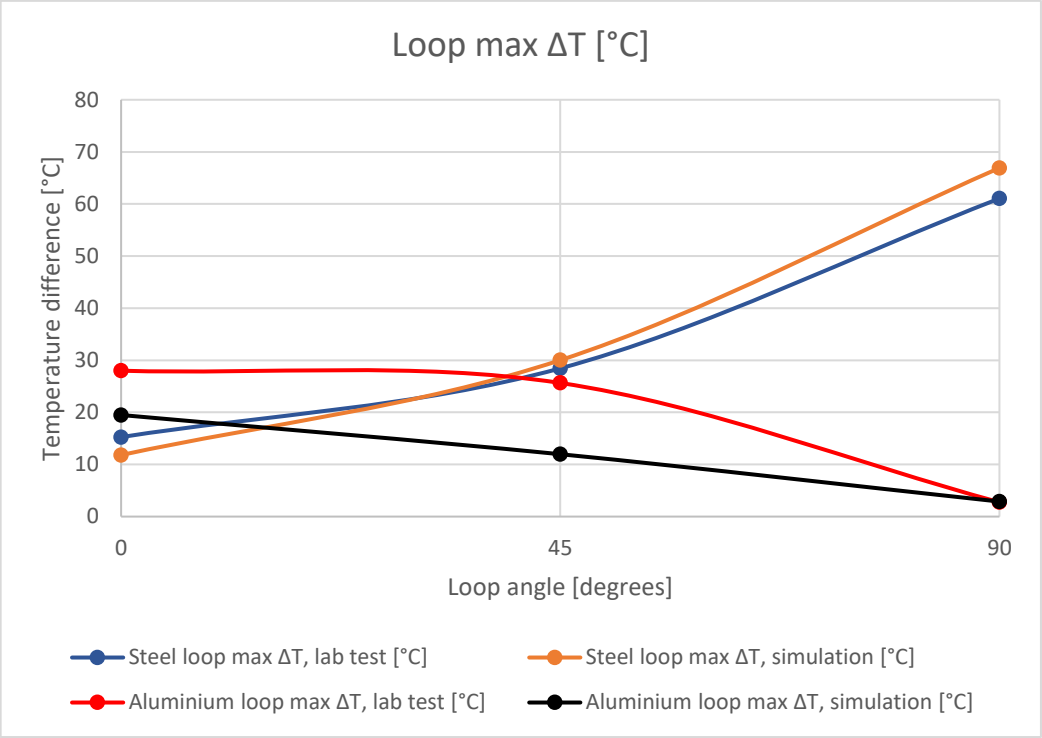

Figure 48. Temperature difference between the loop and ambient at 3.0 m distance in terms of loop angle

5.3.4 Cut loops in different orientations

The circulating current in the cut steel and aluminium loops at 3.0 m distance from the reactor at 0-, 45- and 90-degree loop angles is shown in figure 49. The cut eliminates the induced circulating current totally. The laboratory test results in the figure 49 are not accurate due to method on how the YOKOGAWA DL850 scope calculates the RMS current from the measurement. Because the circulating current in the loops was basically almost zero, the scope used previously measured values for the calculation which distorts the actual results. The small amount of current showing in the simulation results is from the eddy currents. Cutting the loop is obviously then a good way to prevent the current flow around the loop.

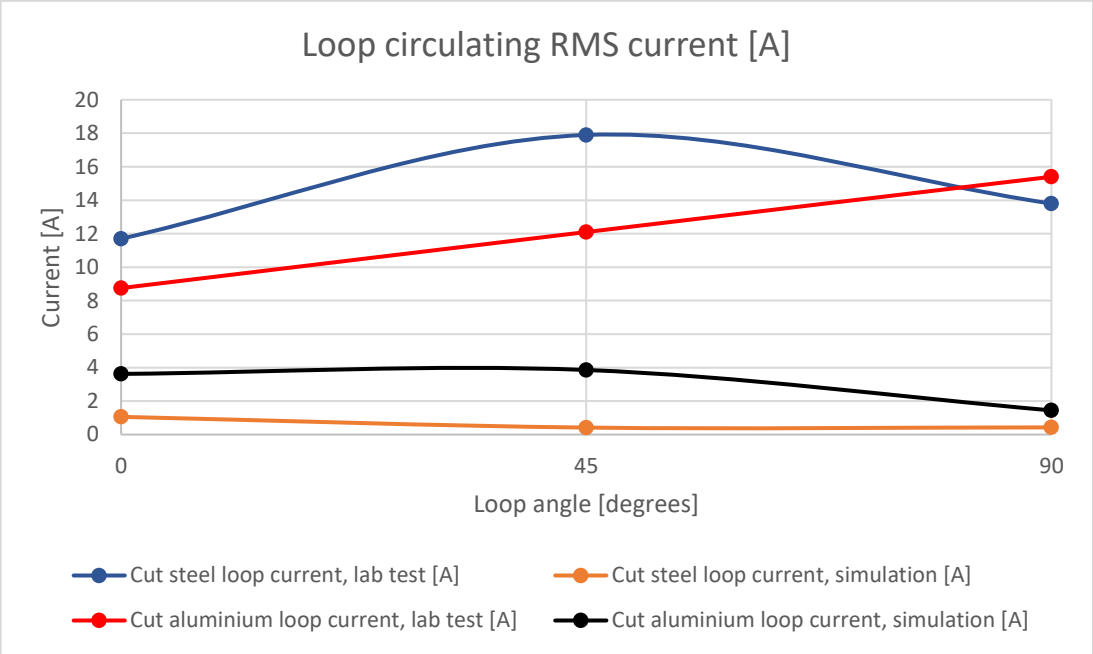

Figure 49. Circulating current in the cut loop at 3.0 m distance in terms of loop angle

The losses and temperatures for the cut loops match well between the laboratory tests and simulations, as can be seen in figures 50 and 51. The cut eliminates losses and heating for the aluminium loop almost completely in every orientation. Only small amount of eddy current losses is present, and they stay similar regardless of the loop orientation. In horizontal orientation, the total loss for the cut steel loop was also minimal, but at 45-degree, the losses were already about 150 W. The losses for the cut steel loop in vertical orientation reached the same values as the uncut loop, about 350 W. In conclusion, cutting a loop made of non-ferromagnetic material (aluminium) is a great way to avoid any current flow and losses in the loop. For a ferromagnetic material as carbon steel, cutting the loop might not be enough for avoiding losses and heating due to the strong eddy currents. The amount of eddy currents formed in a ferromagnetic material is however heavily dependent on the ferromagnetic material structure and the magnetic flux direction relative to the structure. The strongest eddy currents are formed in a long ferromagnetic structure, as a carbon steel beam, that is parallel to the magnetic field.

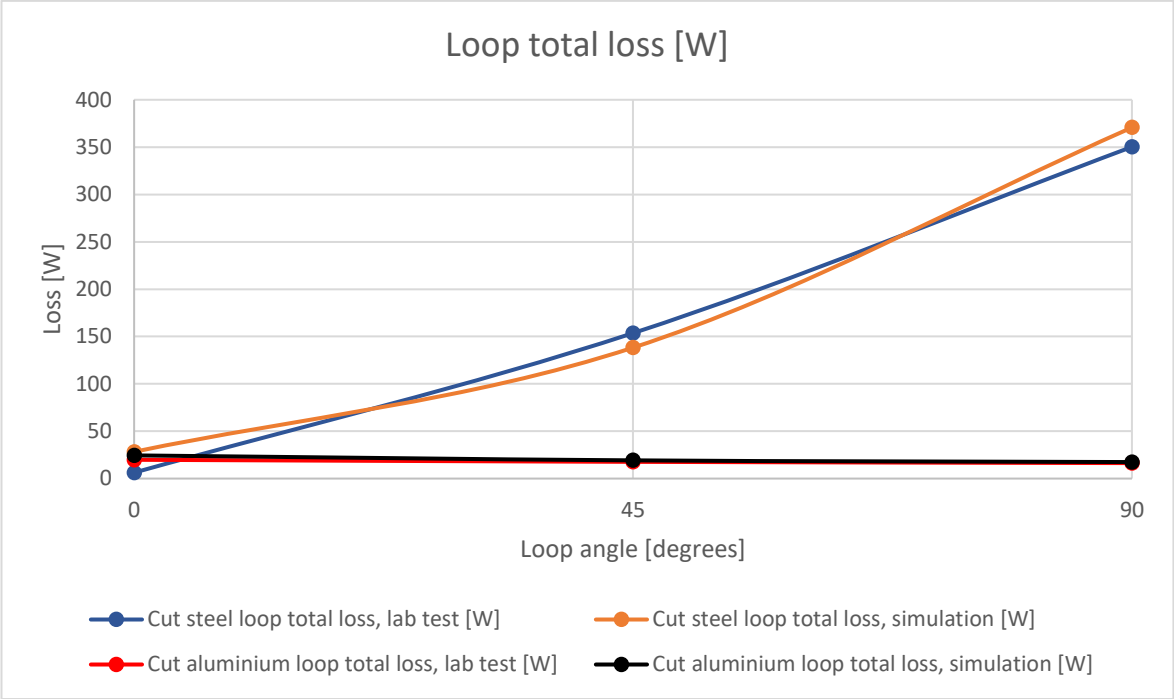

Figure 50. Total loss of the cut loop at 3.0 m distance in terms of loop angle

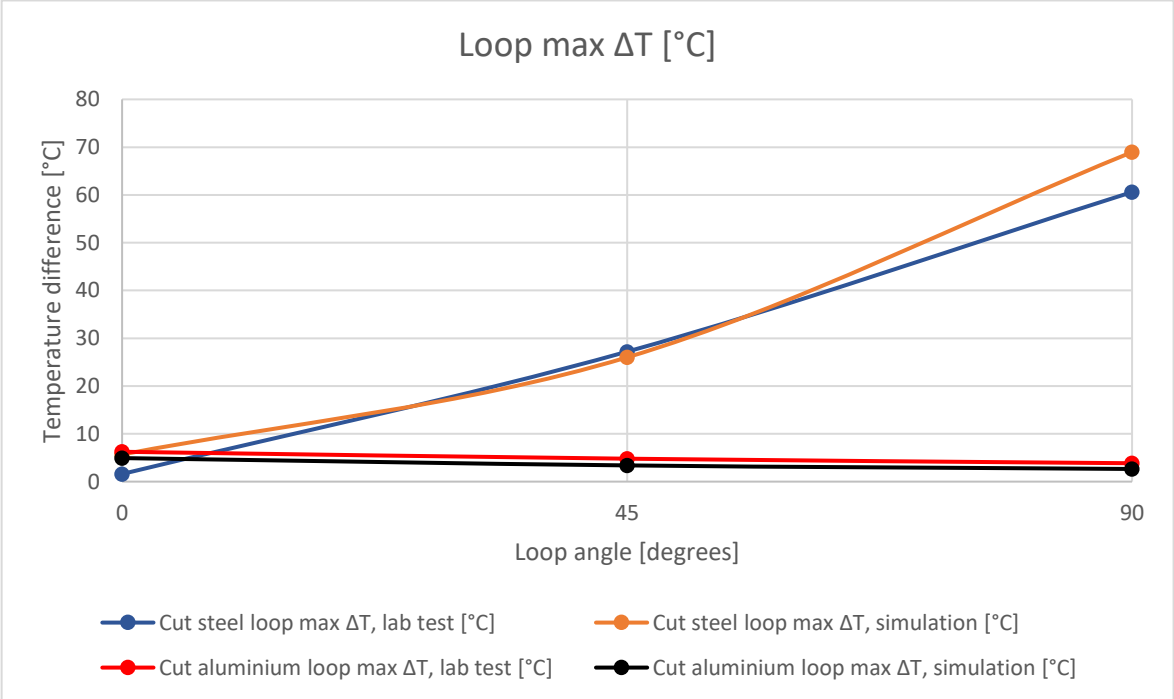

Figure 51. Temperature difference between the cut loop and ambient at 3.0 m distance in terms of loop angle

5.4 Simulations of geometrically identical steel and aluminium loops

Because the laboratory measurement results and simulations compared well with each other concerning the loop induction tests, it was decided to simulate geometrically identical steel and aluminium loops in different sizes. The idea was to test how the loop size affects to amount of the induced current, losses and heating. These simulations should also give a definitive answer on which material would be worse in forming loops in STATCOM or SVC stations. Then for the worse material, one side of the loop was made thinner to see the effects if the loop cross-section would not stay uniform for the whole loop. The loops were simulated in horizontal orientation and at 1.5 m height from the origin. At that height, the magnetic field direction was almost vertical, which ensured maximum amount flux crossing the area enclosed by the loops. The magnitude of the magnetic flux density at the closest edge of the loops relative to the reactor would be about 1.5 mT.

The basic simulation methods were the same as in the chapter 5.2.5 “ANSYS loop induction simulations”. The calculation space for the electromagnetic simulations was a sphere with 40.0 m diameter and the medium inside the sphere was air with default properties. The *B-H* curve points for the steel loop can be found from appendix 7 and the default permeability for the aluminium was used. The electromagnetic simulation time was also 22 ms with 0.5 ms timestep for these simulations. The loss importation to the ANSYS Mechanical for the temperature analysis was conducted similarly with same issues as explained before. The RMS current and total loss were calculated with same methods as in the chapter 5.2.5 “ANSYS loop induction simulations”. The electrical conductivity for the steel was selected as $4.17 \cdot 10^6$ S/m and for the aluminium $2.53 \cdot 10^7$ S/m. These values correspond to the conductivities for the steel and aluminium loops from the capacitor racks at 20 °C. The same thermal conductivities were used; 52 W/(m·K) for the steel and 137 W/(m·K) for the aluminium. The convection coefficient of 5 W/(m^2K) was used for all cases, because it was about the average what was calculated for the capacitor rack loops from the lab test results. The degree of emission used for the steel was 0.276 and for the aluminium 0.18, as before. The ambient temperature in the ANSYS Mechanical was set as 20 °C. The skin depth method was used in electromagnetic simulations for mesh creation for both, steel and aluminium loops. The surface element length was set as 15 mm and the skin depth for the

steel was 2 mm and for the aluminium 5 mm. Meshing in the cross-section of the loops is presented in appendix 11. The mesh creation for the reactor and background volume was similar as in previous simulations. The element length in the ANSYS Mechanical was selected as 3 mm for both materials. The reactor model was the same as in previous simulations, except the reactor rated current of 2577 A was used in these simulations, instead of 3000 A. The AC frequency was 50 Hz.

5.4.1 Simulations for loop sizes from 1x1 m to 6x6 m

To see the effects on how the loop size affects to the induced current, six different loop sizes were simulated for both materials; steel and aluminium. All loops were squares with the same length and width. The loop size was increased in one-meter intervals from 1x1 m size to 6x6 m size. The cross-section of the loops was a square with 20 mm edge length. Figure 52 shows the loop sizes and their locations relative to the reactor for the simulations. Each loop was simulated of course separately, although all sizes are presented in the same figure. The distance from the center of the reactor to the closest edge of all loops was 4.0 m. All loops are located outside the $\mathbf{m_x}$ distance (3850 mm) specified by the coil manufacturer, which means that conductive structures are allowed at these distances, from the reactor point of view. The height of the loops was 1.5 m from the bottom edge of the loop to the origin.

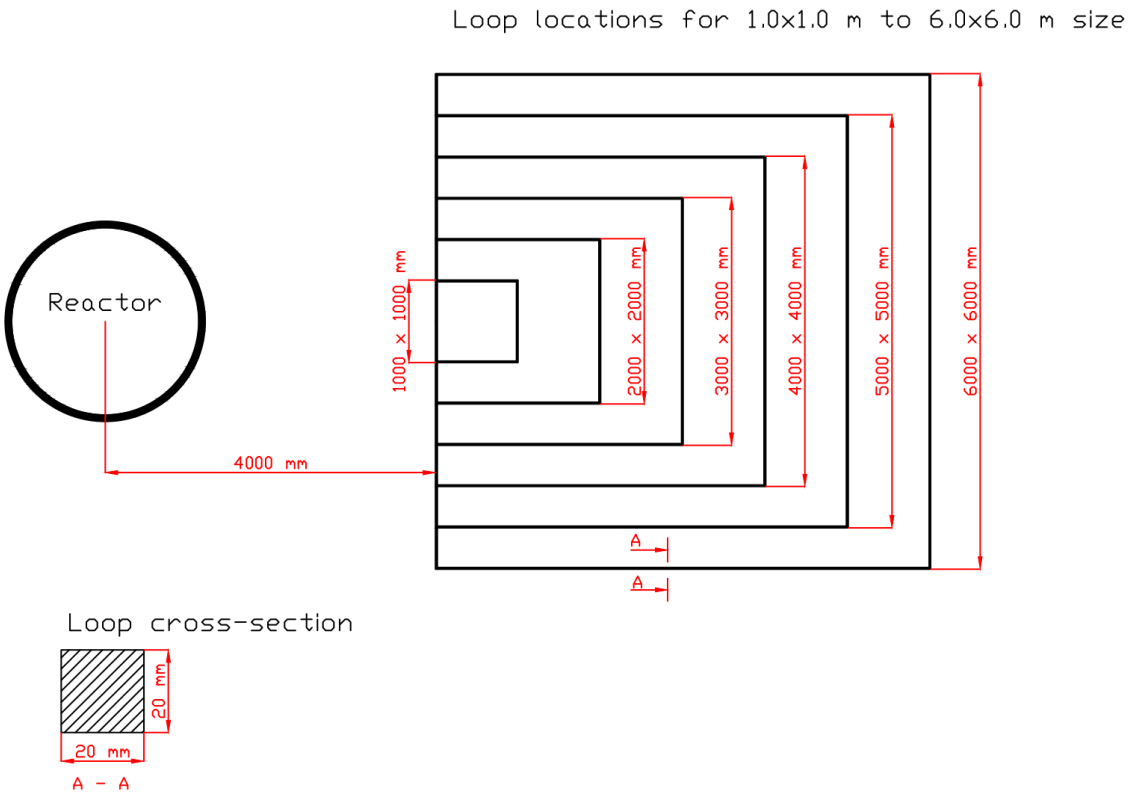

Figure 52. Simulation loop locations for the steel and aluminium loops from 1x1 m to 6x6 m size

Figure 53 shows the induced the induced current in the loop in terms of area enclosed by the loop. It can be clearly seen that much more current was induced to aluminium loops for every loop size. In fact, the induced current in the aluminium loops was on average about 750 % larger than the current in the steel loops. This was expected, because the conductivity of the aluminium is much larger than for the steel and the strong skin effect of the ferromagnetic steel increases the resistance of the steel loops. The maximum current of about 270 A for the aluminium was for the 5x5 m loop, but it should be noted that the current value did not rise significantly for larger than 3x3 m loops. The current for the steel loops did not exceed 33 A. As the loop size increases, the current value does not increase after a point, because the resistance of the loops also increases. Also, the reactor magnetic field weakens rapidly in terms of distance.

If it was assumed that these loops would be a part of some structure in a STATCOM or SVC station, for example a part of fence or some structural member of a building, the high current levels of the aluminium could be a problem for the ground cabling. The current in the ground

wires is tried to be kept in a few dozen amps and too high current could cause the thin cables to heat or even melt. The circulating current in steel loops would not be such a problem for the ground cabling, because the current levels were low. (Hernesniemi 2019)

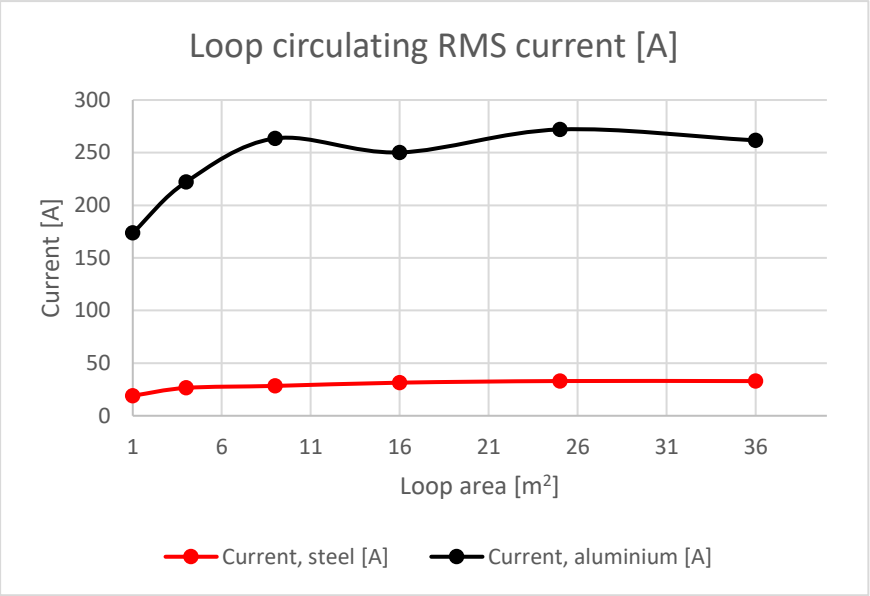

Figure 53. Circulating current in the loop in terms of loop size

The total loss of the steel and aluminium loops in terms of the area enclosed by the loop is presented in figure 54. The losses increase as the loop size increases, but the curves start to level out due to the weakening reactor magnetic field in terms of distance. The losses are much greater for the aluminium than for the steel, though the difference between materials was not as big as for the current. As an average, the losses for the aluminium loops were about 260 % higher than for the steel loops. The losses for the 6x6 m loops reached a value of 229 W for the aluminium and 74 W for the steel. The temperature curves are shown in figure 55. The temperature curves are similar to the current curves. However, the average difference between the aluminium and steel was reduced to about 165 %. The maximum temperature difference between the loop and ambient temperature was about 15 °C for the aluminium and about 7 °C for the steel. It must be noted that the loss importation error to the ANSYS Mechanical is larger for the aluminium than for the steel, as explained in the chapter 5.2.5 “ANSYS loop induction simulations”, pages 86-87. It can be seen from the figure 55, that for these geometrically simple loops, surface temperature differences of a loop are small. The average ΔT and the maximum ΔT of a loop are very close to each other in every simulation. The loops did not heat too much, but the cross-section area of the loops

was relatively large, and it needs to be investigated further what happens if the cross-section does not stay uniform. The simulation results in a table form can be found in appendix 11.

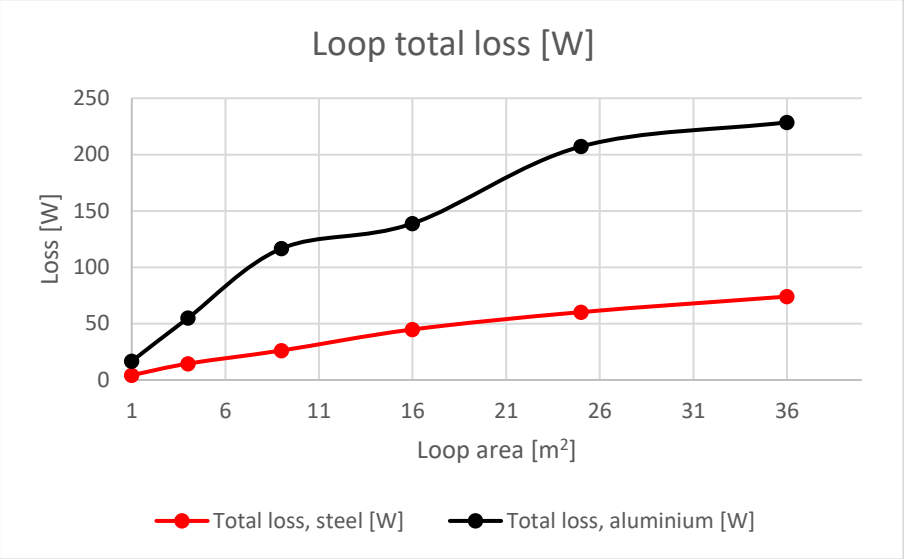

Figure 54. Total loss of the loop in terms of loop size

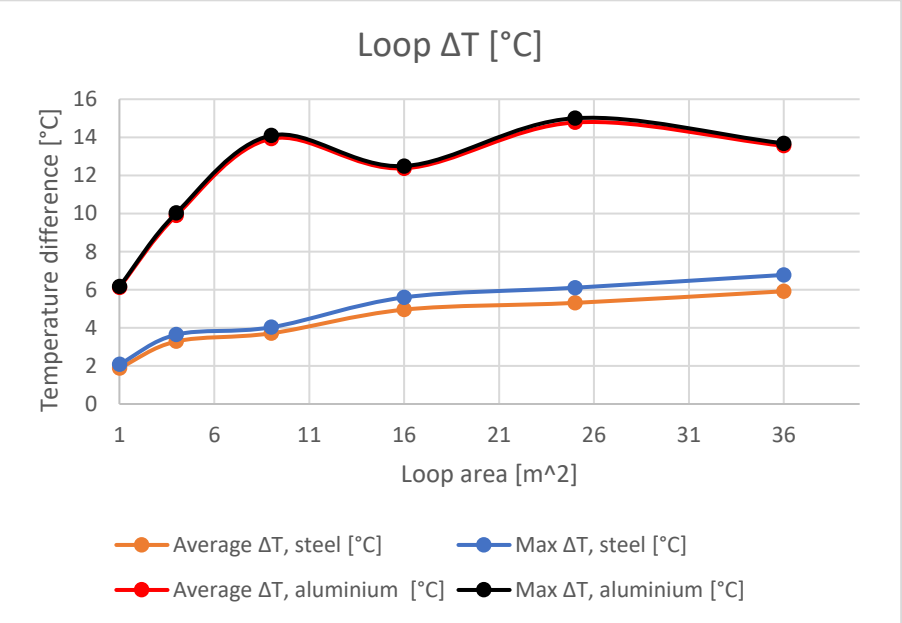

Figure 55. Temperature difference between the loop and ambient in terms of loop size

Based on the simulation results, aluminium was clearly inferior material compared to steel, regarding on forming loops in the presence of a changing magnetic field. There were more induced current, losses and heating in the aluminium loops. The results indicate also that high currents can be induced to structures forming loops even outside the $\mathbf{m}_x$ distance of the

reactor. In conclusion, structures forming loops with high electrical conductivity should be avoided in STATCOM or SVC substations. It is difficult to give definite answer on what size loops can exist at specific distances from reactor, because there are many variables to be considered. Even for the relatively small, 1x1 m size aluminium loop outside the $\mathbf{m_x}$, the induced current reached a value of 174 A in the simulation. It should be noted, that even if the losses of one conductive loop would be acceptable, a combined effect of several highly conductive loops could become a problem.

5.4.2 Aluminium loop simulation with one thin side

Because the aluminium proved to be the worse material in forming loops, it was tested what would happen to the induced current, losses and loop temperature, if one side of the 3x3 m size aluminium loop was made thinner. The 3x3 m size loop was selected for these simulations, because the induced current value was not any larger for bigger loops. The position of the loop was the same as presented in the figure 52 and the loop height was also the same, 1.5 m from the origin. The cross-section of the loop for three sides was the previously used square with 20 mm edge length. The fourth side of the loop was made thinner and the location of the thin side was at the left side of the loop when looked from the reactor. Two different size cross-sections were tested for the thinner side of the loop: 10x10 mm square and 5x5 mm square. The simulation setup was otherwise the same as in previous simulations.

The circulating current and total loss of the loop is presented in figure 56, as a function of the loop smallest cross-section area. The first point, where the smallest cross-section area is 400 mm^2, refers to the situation where the cross-section of the loop is uniformly 20x20 mm. When the cross-section of one side of the loop was reduced to 10x10 mm (100 mm^2), the current value decreased 21 %, because the resistance of the loop increases. The total loss increased about 8 %. However, when the smallest cross-section was reduced to 5x5 mm (25 mm^2), the total loss increased significantly. The increase was about 52 % compared to the non-reduced loop. With the 5x5 mm reduction, the current value decreased about 44 % from the non-reduced loop.

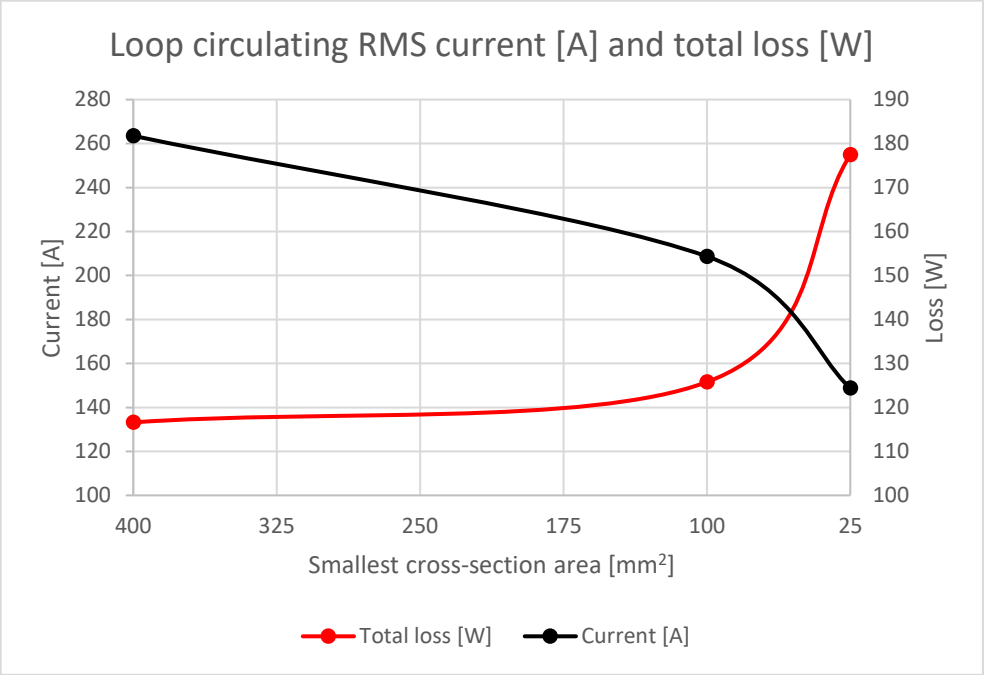

Figure 56. Circulating current and total loss of the loop in terms of minimum loop cross-section

Figure 57 shows the average and maximum temperature difference between the loop and ambient temperature. The average temperature difference stays quite similar throughout the simulations. The maximum temperature difference between the loop and ambient was very high for the loop with 5x5 mm reduced cross-section. The curve form looks very similar to the total loss curve, but the increase in the loop maximum ΔT compared to the non-reduced loop was 1816 %. The side with 5x5 mm cross-section reached a max ΔT value of about 270 °C, but the three other sides with 20x20 mm cross-section heated only about 6 °C from the ambient temperature. The temperature distribution of the 3x3 m aluminium loop with the smallest cross-section of 5x5 mm is presented in figure 58.

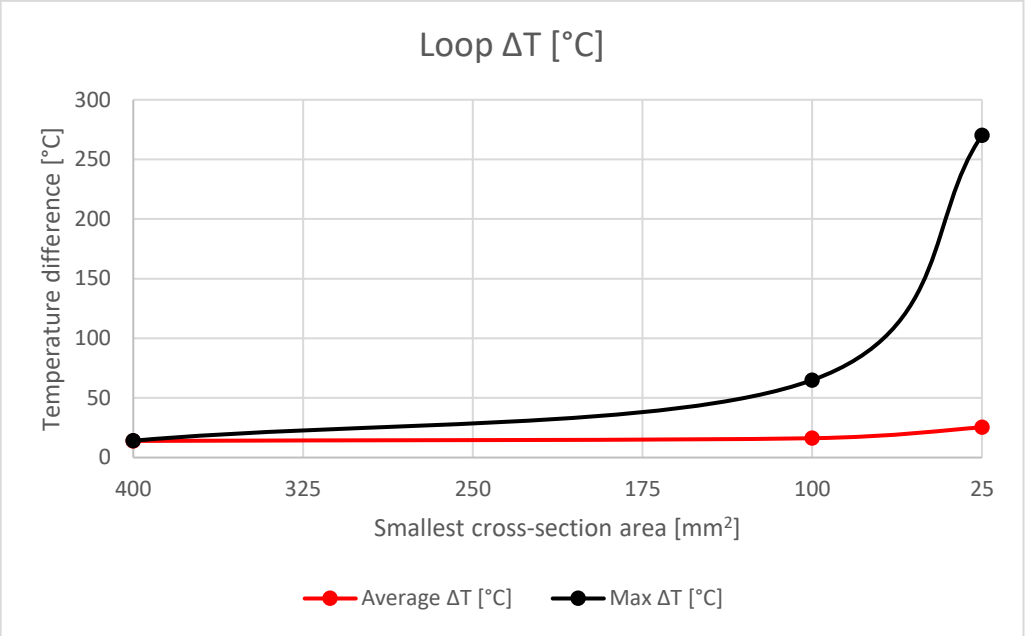

Figure 57. Temperature difference between the loop and ambient in terms of minimum loop cross-section

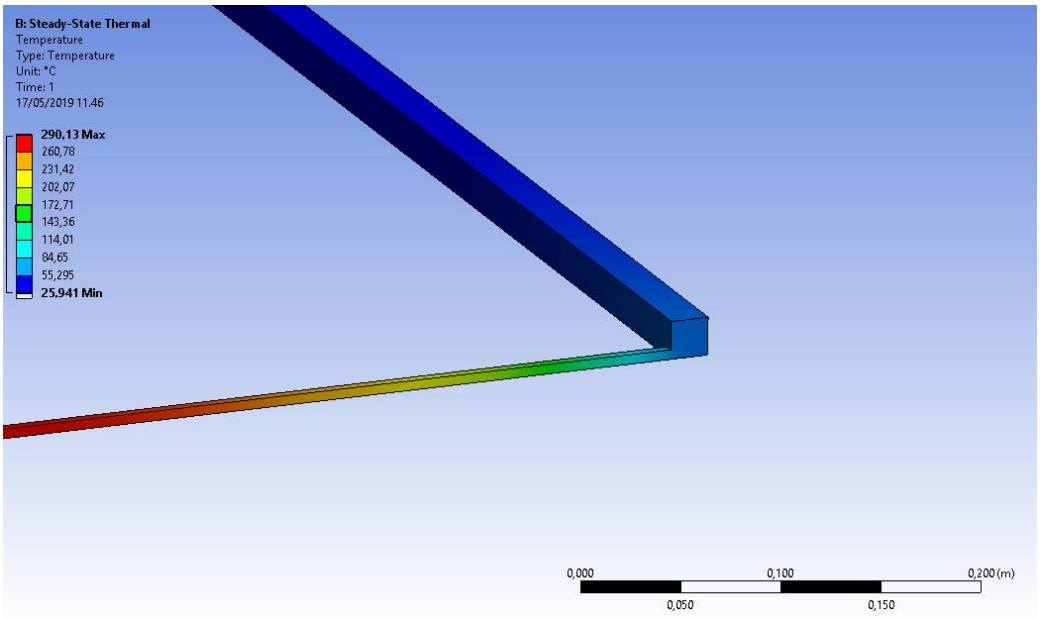

Figure 58. Temperature distribution of the 3x3 m size aluminium loop with a minimum cross-section area of 25 mm^2

The obtained results from the simulations shows, that the most important parameter is not necessarily the loop size (area enclosed by the loop) that defines the losses and heating of the loop in a presence of a changing magnetic field. The material thickness of the loop might actually have a bigger impact on how losses and heat are generated in the loop. The simulations showed that when a loop was made partially thinner, the thin part could heat

significantly more than the rest of the loop. The simulations could refer to a situation, where for example, there is an aluminium fence forming a loop or the loop could be a part of some structure in a building. The thin part could be some bolt connection where the effective cross-section reduces considerably or the structure forming the loop could be otherwise partially thinner. Even if most of a structure forming a loop in a STATCOM or SVC substation would have high enough material thickness not to cause any significant heating, one bolt connection or other reduction to the cross-section area can be enough to cause problems. The highly conductive material could get hot enough to start fire, if there is flammable material next to it, or the material itself could even melt. Unintentional hot surfaces can be hazardous for people working in a substation, if one comes into contact with one. Of course, heat means also unnecessary losses for the system.

5.4.3 Recommendations

The simulations showed, that for highly conductive big loops outside the $\mathbf{m_x}$ distance, the losses could rise to the magnitude of several hundred watts, even though the loop temperature would not be at dangerous level. Also, when the aluminium loop was made partially thinner, the thin part could heat significantly and generate considerably more losses. As a conclusion, it should be avoided constructing structures that form whole loops in STATCOM or SVC substations from materials with high electrical conductivity, as aluminium. There are many variables that determine would a loop become an issue in a substation: material electrical conductivity, loop size, loop material thickness, loop angle relative to the magnetic field and magnetic field intensity at the loop location. Thus, if there is uncertainty whether a loop would become a problem or not, it would be advisable to avoid it altogether. However, if a problematic loop is formed anyhow, the laboratory tests and simulations showed that cutting the loop is an effective way to prevent induced circulating current in the loop. Though, the cut would not be effective against eddy currents.

5.5 Vertical steel beam simulation

Because there was substantial heating and losses noticeable in the ferromagnetic structures that were parallel to the magnetic field (upright) during the laboratory tests and simulations, it was decided to simulate a vertical carbon steel I-beam, just outside the $\mathbf{m_x}$ distance of the reactor and further away. The steel I-beam represents a common structure, that can be found in STATCOM or SVC substations, for example as a supporting beam for buildings. The simulated I-beam had a profile length of 200 mm and flange width of 65 mm. Both web and flange thickness of the I-beam was 10 mm. The height of the beam was 4.0 m from the origin. Two simulations were conducted for two different beam distances from the reactor: 4.0 m and 5.8 m distance from the center point of the reactor to the closest edge of the beam. The 5.8 m distance was selected for a reason that at 5.8 m distance from the reactor, the magnitude of the magnetic flux density should be about 0.5 mT. The reactor model producing the magnetic field was the same as used in previous simulations. The reactor current used, was the rated current of 2577 A RMS at 50 Hz frequency.

The basic simulation setup and calculation methods for the electromagnetic and thermal simulations were the same as used in the chapter: 5.2.5 “ANSYS loop induction simulations”. The electrical conductivity for the steel was selected as $4.17 \cdot 10^6$ S/m, as in previous chapter (5.4). The hysteresis curve for the ferromagnetic steel was the same as for the steel 1010 in the ANSYS material database. The *B-H* curve points are presented in appendix 7. The meshing method used in the electromagnetic simulations for the I-beam, was the skin depth method with 2 mm skin depth and 16 mm surface element length. The meshing methods for the reactor and background volume were the same as previously used. For the thermal analysis in ANSYS Mechanical, 10 mm element length for the mesh was required to be used. The thermal calculation did not converge with finer mesh, with the hardware that was available. The profile of the I-beam and the mesh of the beam cross-section, for the electromagnetic simulations can be found in appendix 12. The thermal conductivity, convection coefficient and the degree of emission for the steel were the same as used in the previous chapter (5.4): 52 W/(m·K), 5 W/(m^2K) and 0.276. The ambient temperature for the thermal simulations was set at 20 °C.

Figure 59 shows the temperature distribution of the steel I-beam at 4.0 m distance from the reactor. The magnitude of the magnetic flux density at that distance from the reactor would be about 1.5 mT. The simulation result showed that the maximum temperature difference between the beam and ambient temperature was about 27 °C. The calculated losses were about 330 W. The temperature distribution of the beam was very similar to what was seen in the laboratory tests and previous simulations for the vertical sides of the steel loop. Most of the heat and losses are generated about in the middle of the beam. The direction of the external magnetic flux in the middle of the beam is almost parallel to the beam. At the 5.8 m distance from the reactor, where the magnitude of the magnetic flux density was about 0.5 mT, the beam heated only about 3 °C, from the ambient at its peak. The beam losses reduced to 44 W. The increase in distance from 4.0 m to 5.8 m, is about 45 %, but the reduction in losses was 87 %. The strength of the magnetic field produced by the reactor weakens very rapidly, thus even small increase to the structure distance from the reactor can reduce losses significantly. The simulation results are presented in appendix 12.

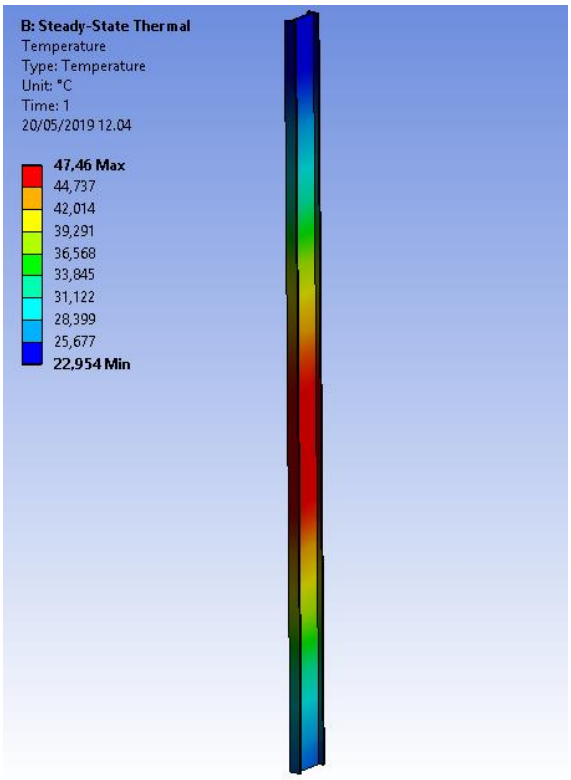

Figure 59. Temperature distribution of the vertical steel I-beam at 4.0 m distance

5.5.1 Recommendations

The simulations showed, that large ferromagnetic structures that are parallel to the magnetic field created by a reactor, can still heat and produce unnecessary losses due to eddy currents just outside the $\mathbf{m_x}$ distance of the reactor. Therefore, it is not recommended to place long ferromagnetic structures, as carbon steel beams, to an area where is a changing magnetic field present, with a strength of 1 mT or more. Of course, the orientation of the structure relative to the magnetic field must be also taken into account, when evaluating the adverse effects of the eddy currents. The 0.5 mT can be thought as a safe limit even for large ferromagnetic structures regarding to eddy currents. If it is necessary however to build, for example, a large supporting structure close to reactors, it would be recommended to use non-ferromagnetic materials as stainless steel. The vertical sides of the aluminium loop did not heat during laboratory tests and simulations, thus shows that eddy currents are not a major problem for non-ferromagnetic materials. It should be noted, that even if the eddy current losses of one carbon steel beam would be on acceptable levels, there are usually many structural members for instance in a building. The combined eddy current losses of several structures could become a problem if the building is placed too close to the reactors.

6 SUMMARY

The object of the thesis was to analyze magnetic fields created by air core reactor coils and especially study the effects of a changing magnetic field to surrounding conductive structures. Laboratory tests and simulations were conducted to determine the magnetic field of a reactor coil and to define the induced current, losses and heating for different structures and materials due to the changing magnetic field. A major part of the thesis was also determining the suitability of the ANSYS software for Grid Solutions in simulating reactor magnetic fields and the effects of current induction to conductive structures.

The reactor magnetic field simulation with ANSYS magnetostatic solver was very accurate representation of a magnetic field produced by a real reactor. The results proved that the simplified reactor model in simulations is accurate enough approximation of a real reactor and the ANSYS can be used for a reactor magnetic field analysis. ANSYS also calculated the induced current and the effects of it for conductive loops and other structures relatively accurately, compared to the results obtained from the laboratory tests. The transient solver proved to be the best option for solving the electromagnetic fields in current induction simulations. The transient solver in ANSYS Electronics is however, very demanding. ANSYS proved to be a good tool for evaluating the effects of the induced current in different structures and materials. One should keep in mind that, when simulations are conducted without any laboratory testing verifying the results, some variables, for example material magnetic properties and electrical conductivity must be estimates. The final results of simulations can vary significantly depending on the initial values used, thus the simulation results should be always interpreted with caution.

According to the laboratory tests and simulations, aluminium turned out be inferior material compared to steel, in structures that form loops in a presence of a changing magnetic field. There were more induced circulating current, losses and heat in the whole aluminium loops, when the direction of the external magnetic flux was close to perpendicular to the loop window. There are many variables that determine would a loop become an issue: material electrical conductivity, loop size, loop material thickness, loop angle relative to the magnetic field and magnetic field intensity at the loop location. For this reason, it is difficult to define

exact distances on what size loops can exist on specific distances from a reactor. Thus, if there is uncertainty whether a loop would become a problem or not, it would be advisable to avoid it altogether. A loop built from highly conductive material as aluminium, can heat significantly even relatively far away from the reactor, depending on the structure of the loop.

For ferromagnetic materials as carbon steel, eddy currents proved to be more problematic than the circulating current through a structure that forms a loop. Significant amount of eddy currents can form to long ferromagnetic structures that are parallel to the external magnetic flux direction. There were significant eddy current losses and heating noticeable in the carbon steel I-beam just outside the $\mathbf{m_x}$ distance of the reactor. Therefore, the reactor $\mathbf{m_x}$ distance should be interpreted with caution for large ferromagnetic structures. The simulations showed, that the 0.5 mT limit for the magnetic field strength should be safe even for large ferromagnetic structures, regarding to eddy currents.

REFERENCES

Aebischer H & Friedli H. 2018. Analytical Approximation for the Inductance of Circularly Cylindrical Two-Wire Transmission Lines with Proximity Effect. Advanced Electromagnetics, Vol 7, No. 1. LEGIC Identsystems AG, Switzerland.

Ahoranta J. 2017. Sähkötekniikka. Helsinki. Sanoma Pro Oy. ISBN 978-952-63-5109-4

ANSYS Inc. 2019a. ANSYS Maxwell Capabilities. [Website]. [Cited 2019-04-11]. Available: https://www.ansys.com/products/electronics/ansys-maxwell/maxwell-capabilities

ANSYS Inc. 2019b. ANSYS Structures. [Website]. [Cited 2019-05-15]. Available: https://www.ansys.com/products/structures

Étienne du Trémolet de Lacheisserie, Gignoux D & Sclenker M. 2005. Magnetism; Materials and Applications. Boston. Springer Science + Business Media, Inc. ISBN 0-387-23063.

Hernesniemi Matti. 2019. Master of Science in electrical engineering. Lead Mechanical Component Engineer, REN GS-FACTS-Technology, Grid Solutions Oy. Tampere. Discussion of how induced current in a loop can affect to the ground cabling, 14.05.2019.

Ida N. 2015. Engineering Electromagnetics. 3rd edition. Heidelberg New York. Springer International Publishing Switzerland. ISBN 978-3-319-07806-9.

Kauppi M. 2018. Civil Works Guideline; STATCOM and SVC. GE Grid Solutions PET Finland. [unpublished]

Keikko Tommi. 2018. Doctor of Science in electrical engineering. Sr Lead Electrical Engineer, REN GS-PQP-Technology, Grid Solutions Oy. Tampere. Air Core Reactor Training. Asiantuntijaluento kelan magneettikentistä, GE lecture, Kaapelikatu 3 Tampere Finland, 20.11.2018. [unpublished]

Kraus J & Carver K. 1973. Electromagnetics. 2nd edition. McGraw-Hill Kogakusha, Ltd. Japan. ISBN 0-07-035396-4.

Kurka A. 2017a. STATCOM vs. SVC. Internal GE Grid Solutions PowerPoint. [unpublished]

Kurka A. 2017b. How STATCOM can solve dynamic grid problems. Internal GE Grid Solutions PowerPoint. [unpublished]

Kähkönen A. 2019. SVC & MRSVC & STATCOM. Internal GE Grid Solutions PowerPoint. [unpublished]

Kähkönen A. 2016a. Technical presentation of GE FACTS Portfolio. Internal GE Grid Solutions PowerPoint. [unpublished]

Kähkönen A. 2016b. GE STATCOM technology. Internal GE Grid Solutions PowerPoint. [unpublished]

Kähkönen A. 2016c. An introduction to the STATCOM MMC Valve. Internal GE Grid Solutions PowerPoint. [unpublished]

Kähkönen A. 2016d. STATCOM Studies and Configurations. Internal GE Grid Solutions PowerPoint. [unpublished]

Lehner G. 2010. Electromagnetic Field Theory for Engineers and Physicist. New York. Springer. ISBN 978-3-540-76305-5.

Lupi S, Forzan M & Aliferov A. 2015. Induction and Direct Resistance Heating; Theory and Numerical Modeling. Switzerland. Springer International Publishing. ISBN 978-3-319-03479-9.

Makarov S, Ludwig R & Bitar S. 2016. Practical Electrical Engineering. Switzerland. Springer International Publishing AG. ISBN 978-3-319-21173-2.

Martin JP. 2014. Measuring Resistance/Impedance with the Four-Wire Kelvin Method. [Website]. [Cited 2019-04-17 and 2019-08-26]. Available: https://www.aemc.com/userfiles/files/resources/applications/micro-ohmmeter/APP-4WireKelvin.pdf

MatWeb. 2019a. Material Property Data. EN S355J0 High Manganese, Structural, Hot Rolled, Quality Steel. [Website]. [Cited 2019-05-29]. Available: http://www.matweb.com/search/DataSheet.aspx?MatGUID=1dc0414bd1ea4061a5dc09382c455e2a&ckck=1

MatWeb. 2019b. Material Property Data. 7020-T6 Aluminium. [Website]. [Cited 2019-05-29]. Available: http://www.matweb.com/search/DataSheet.aspx?MatGUID=c66e13c1d36445c29bb9f852ccf2da17

Mitchell B. 2004. An Introduction to Materials Engineering and Science. Hoboken, New Jersey. John Wiley & Sons, Inc. ISBN 0-471-43623-2.

Oinonen V. 2017. GE STATCOM General Information. Internal GE Grid Solutions PowerPoint. [unpublished]

Pyrhönen J & Nerg J. 2004. Sähkömagnetismi. Lappeenrannan teknillinen korkeakoulu. ISBN 951-764-625-9.

Silva F & Bak C. 2013. Electromagnetic Transients in Power Cables. London. Springer-Verlag London. ISBN 978-1-4471-5236-1.

Stephan P, Kabelac S, Kind M, Martin H, Mewes D & Schaber K. 2010. VDI Heat Atlas. 2nd edition. Berlin. Springer. ISBN 978-3-540-77877-6.

Liu G & Quek S. 2014. The Finite Element Method A Practical Course. 2nd edition. Butterworth-Heinemann. ISBN 978-0-08-098356-1.

Tornberg Joel. 2019. Master of Science in electrical engineering, Production Quality Control Specialist, Grid Solutions Oy. Tampere. Discussion of TCR harmonics, 5.1.2019.

Ulaby T, Michielssen E & Ravaioli U. 1997. Fundamentals of Applied Electromagnetics. 6th edition. Upper Saddle River, NJ, USA. Prentice Hall. ISBN 0-13-577388-1.

Valtanen E. 2012. Tekniikan Taulukkokirja. 19th edition. Mikkeli. Genesis-Kirjat Oy. ISBN 978-952-9867-36-3.

Vapaavuori J & Kalliomäki P. 2012. D2 Suomen rakentamismääräyskokoelma Ympäristöministeriö, Rakennetun ympärisön osasto. Rakennusten sisäilmasto ja ilmanvaihto, Määräykset ja ohjeet 2012. Helsinki.

Zaidi H, Santandrea L, Guillaume K, Bihan Y & Demaldent E. 2014. FEM Technique for Modeling Eddy-Current Testing of Ferromagnetic Media With Small Skin Depth. IEEE Transactions on magnetics, Vol 50, No. 2. University of Paris-Sud.

Zhang Y. 2004. Indoor Air Quality Engineering. New York. CRC Press. ISBN 978-1-56670-674-2.

CAD drawings of the capacitor racks

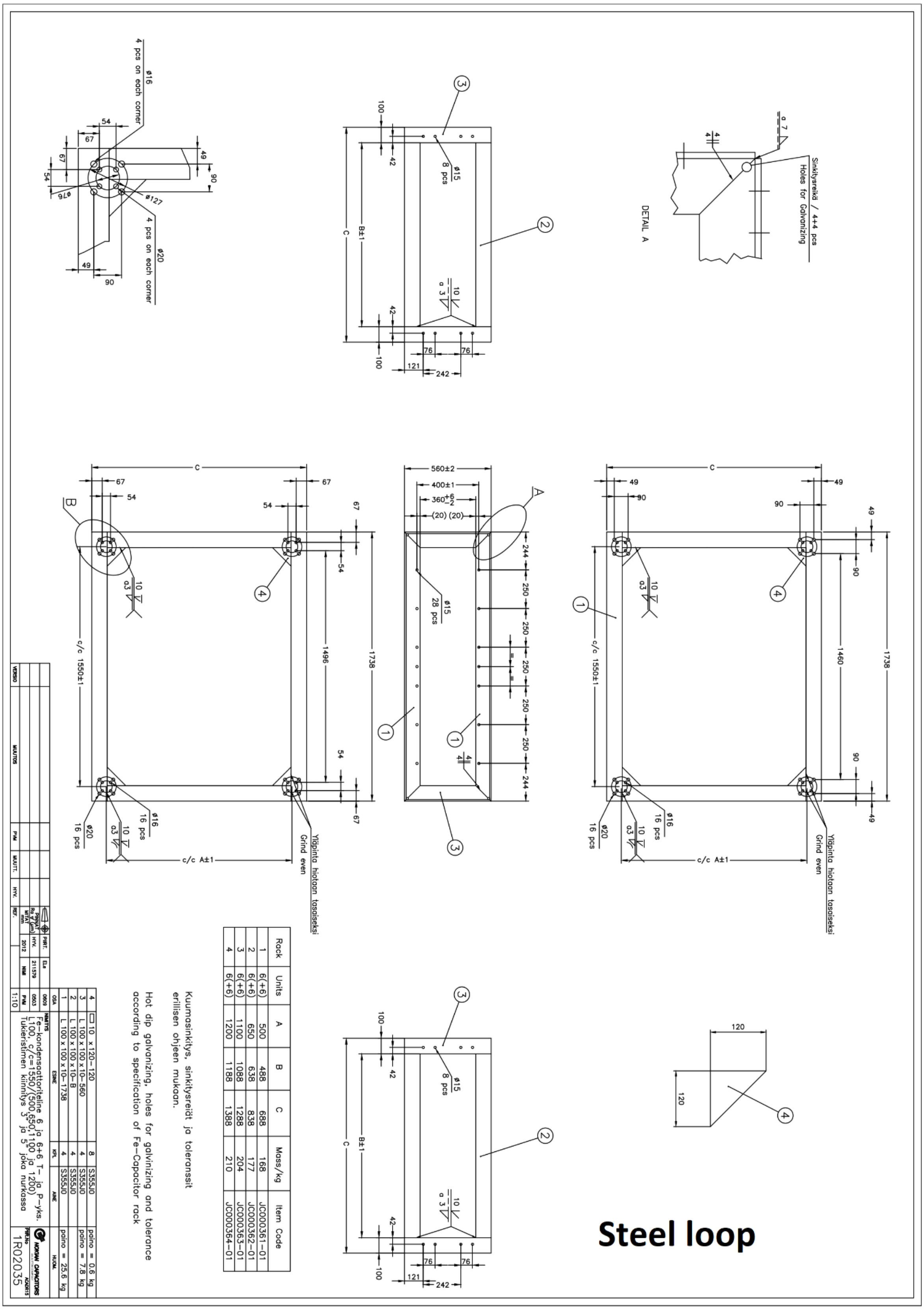

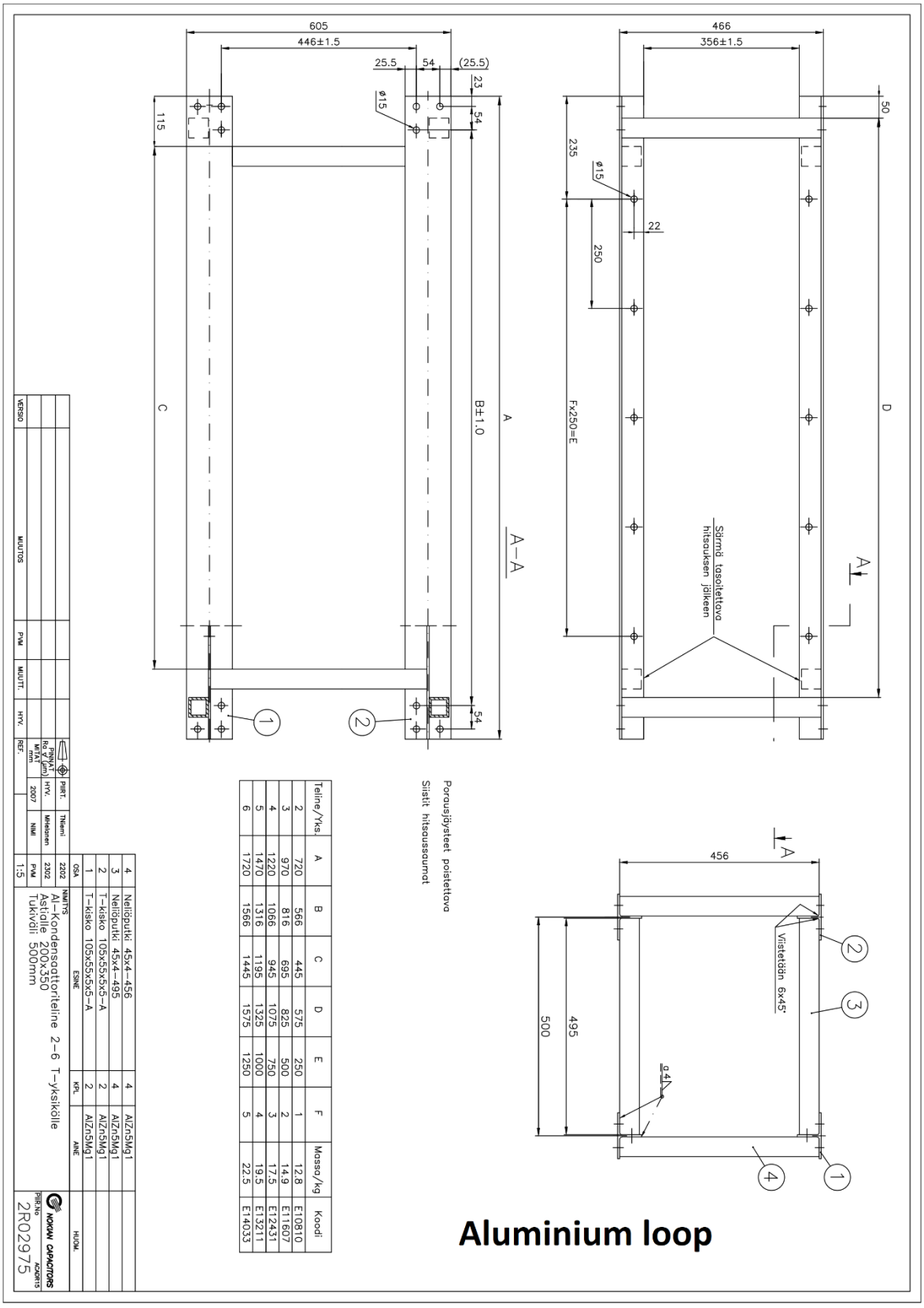

Teline/Yks.	A	B	C	D	E	F	Massa/kg	Koodi
2	720	566	445	575	250	1	12.8	E10810
3	970	816	695	825	500	2	14.9	E11607
4	1220	1066	945	1075	750	3	17.5	E12431
5	1470	1316	1195	1325	1000	4	19.5	E13211
6	1720	1566	1445	1575	1250	5	22.5	E14033

VERSIO	MUUTOS	PVM	MUUTT.	HYV.	REF.	PINNAT. Ra (µm) Rz (µm) mm	PIIRT. HYV. 2007	TNtemi Mihkelsonen	NIMI PVM 2302	OSA 2202	NIMITYS Al–Kondensaattoriteline 2–6 T–yksiköille Astialle 200x350 Tukivälit 500mm	ESINE	KPL	AINE	HUOM.
												4	Neliöputki 45x4–456	4	AlZn5Mg1	
												3	Neliöputki 45x4–495	4	AlZn5Mg1	
												2	T–kisko 105x55x5–A	2	AlZn5Mg1	
												1	T–kisko 105x55x5–A	2	AlZn5Mg1	

NOKIAN CAPACITORS

PIIR.No 2R02975 ACADRIS

Laboratory tests equipment

Test circuit equipment

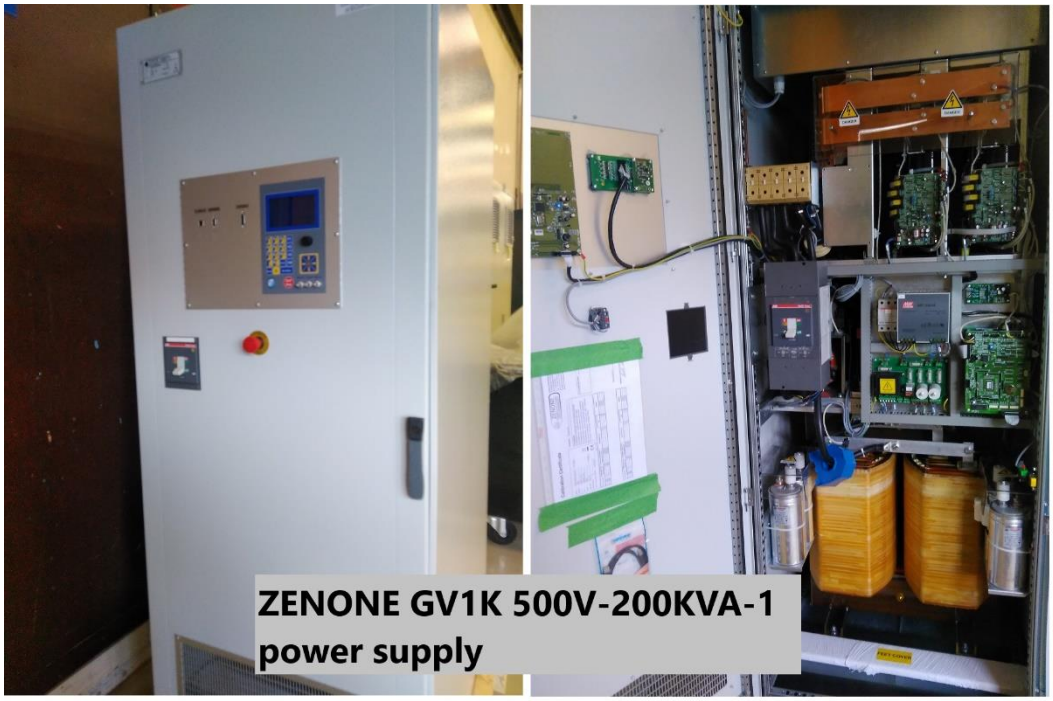

ZENONE GV1K 500V-200KVA-1
power supply

GBE transformer

GBE info plate

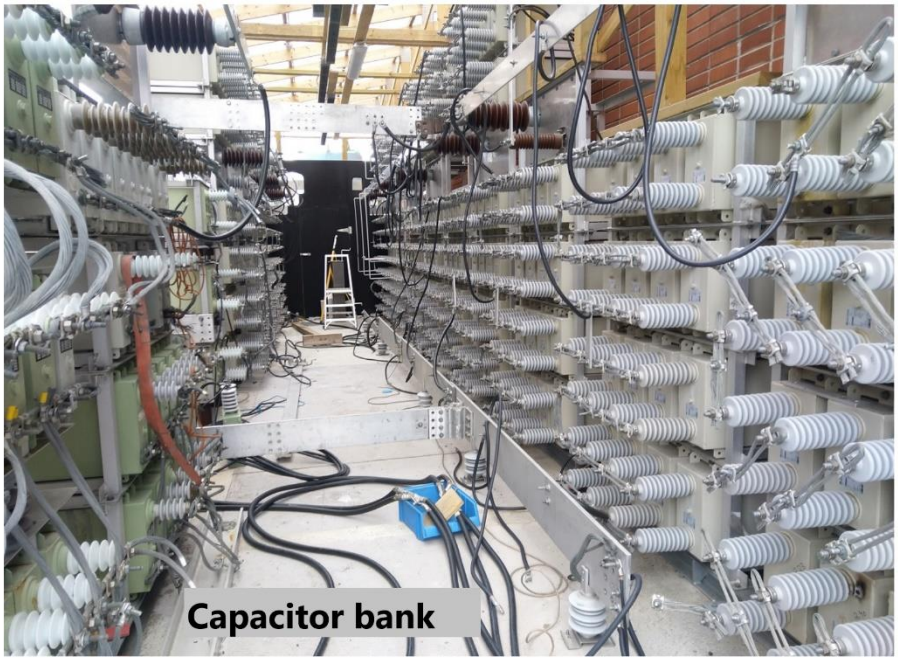
Capacitor bank


Inductor = Reactor coil


AC supply for the
Reactor

Reactor coil current measurement equipment in the laboratory tests

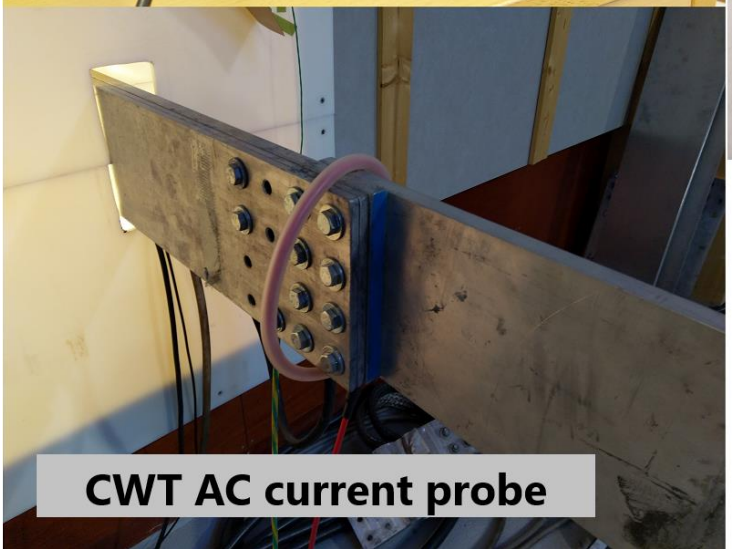

Current measuring equipment for loops in the laboratory tests

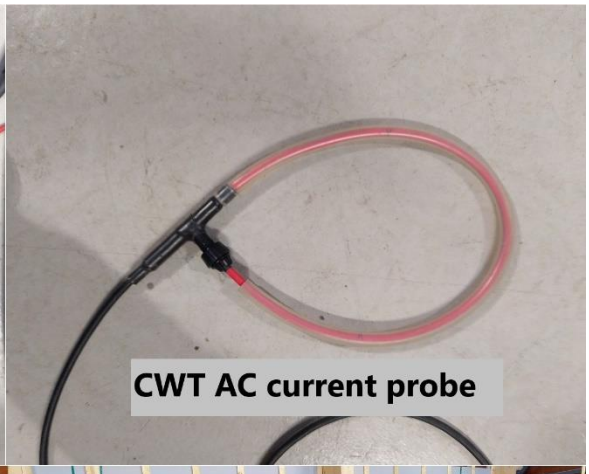

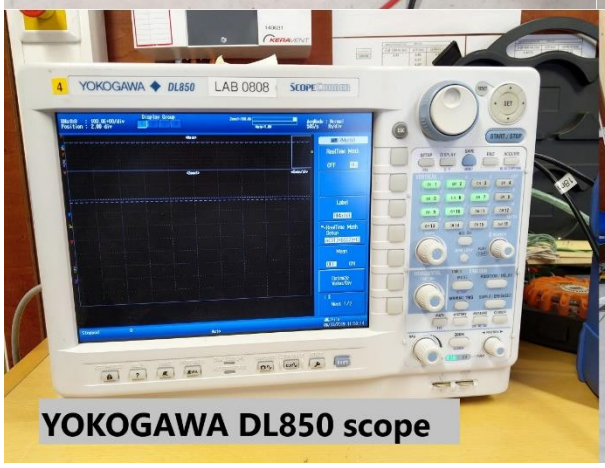

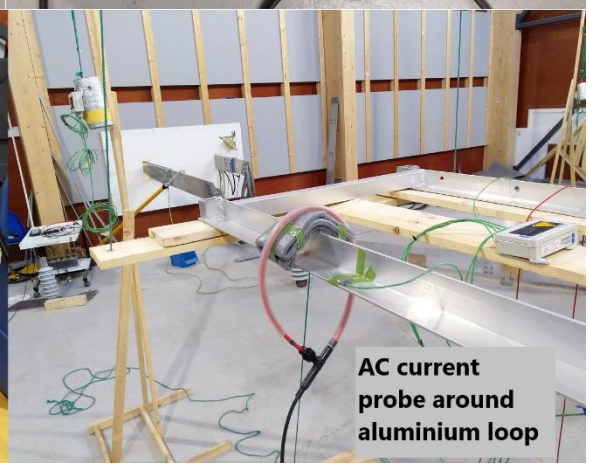

Steel and aluminium loops DC and AC resistance measurement equipment

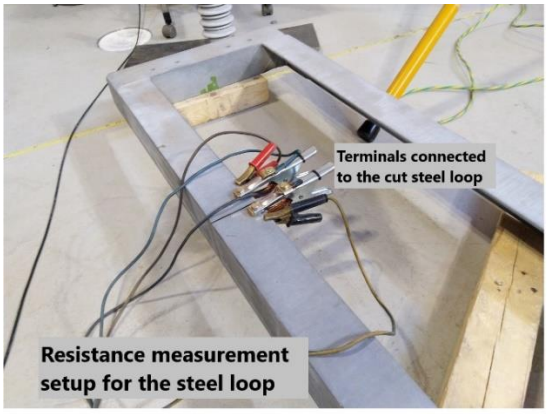

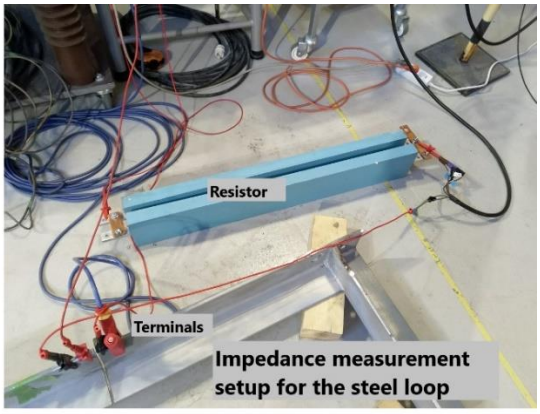

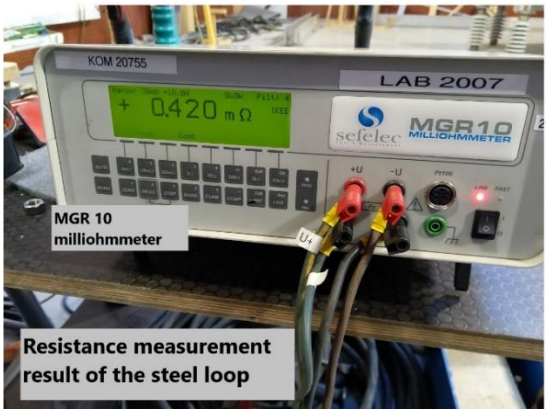

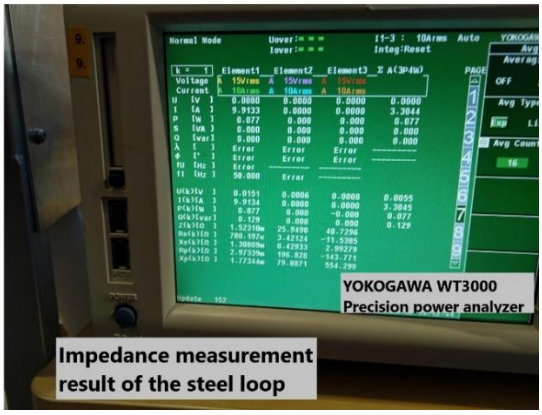

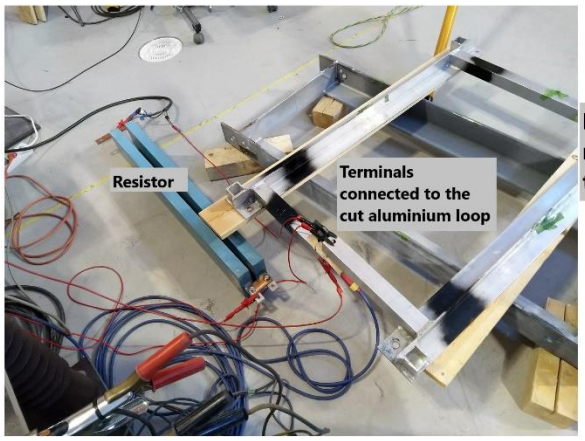

Impedance measurement setup for the aluminium loop

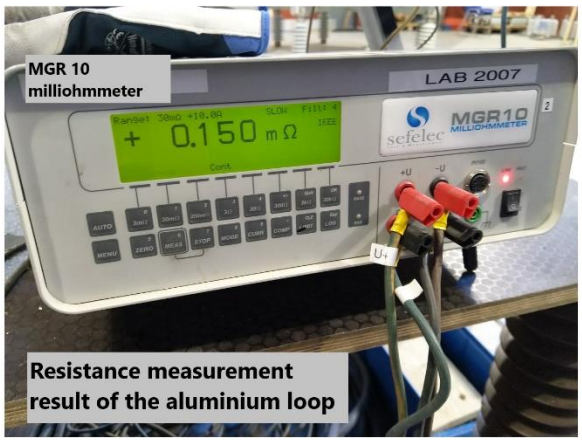

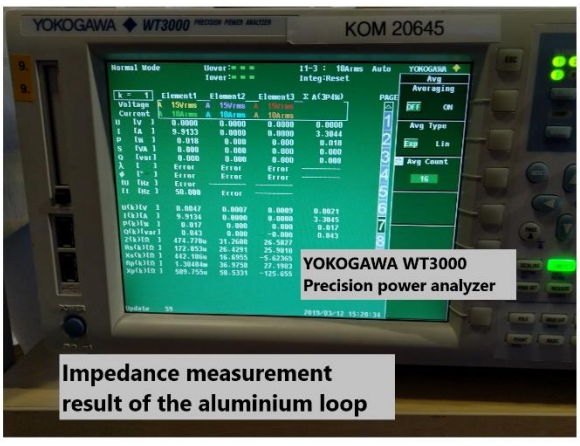

HIOKI 3470 Magnetic field HiTester with 2 mT sensor

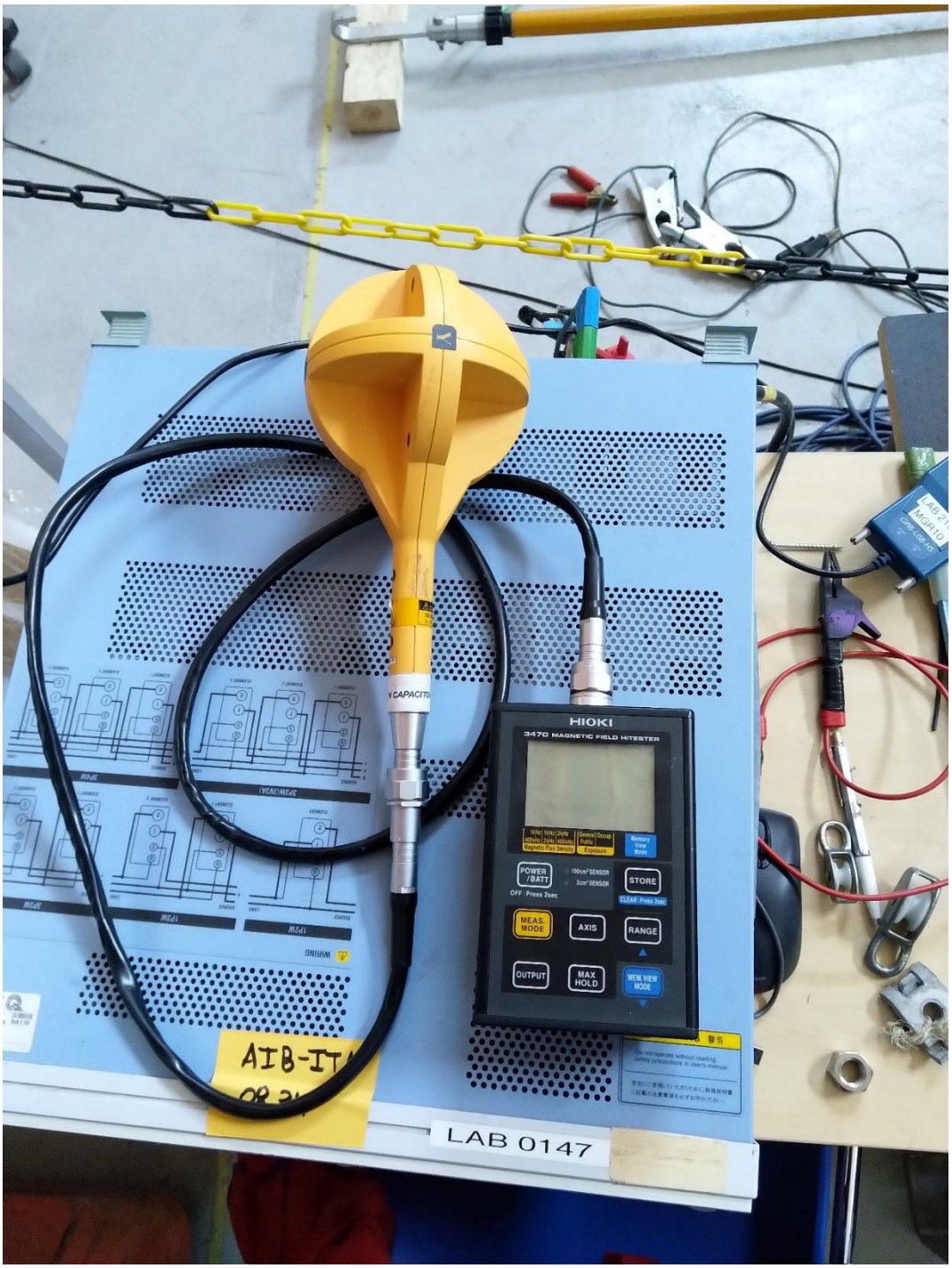

Temperature measurements in the laboratory tests

Ambient temperature measurement in the laboratory tests

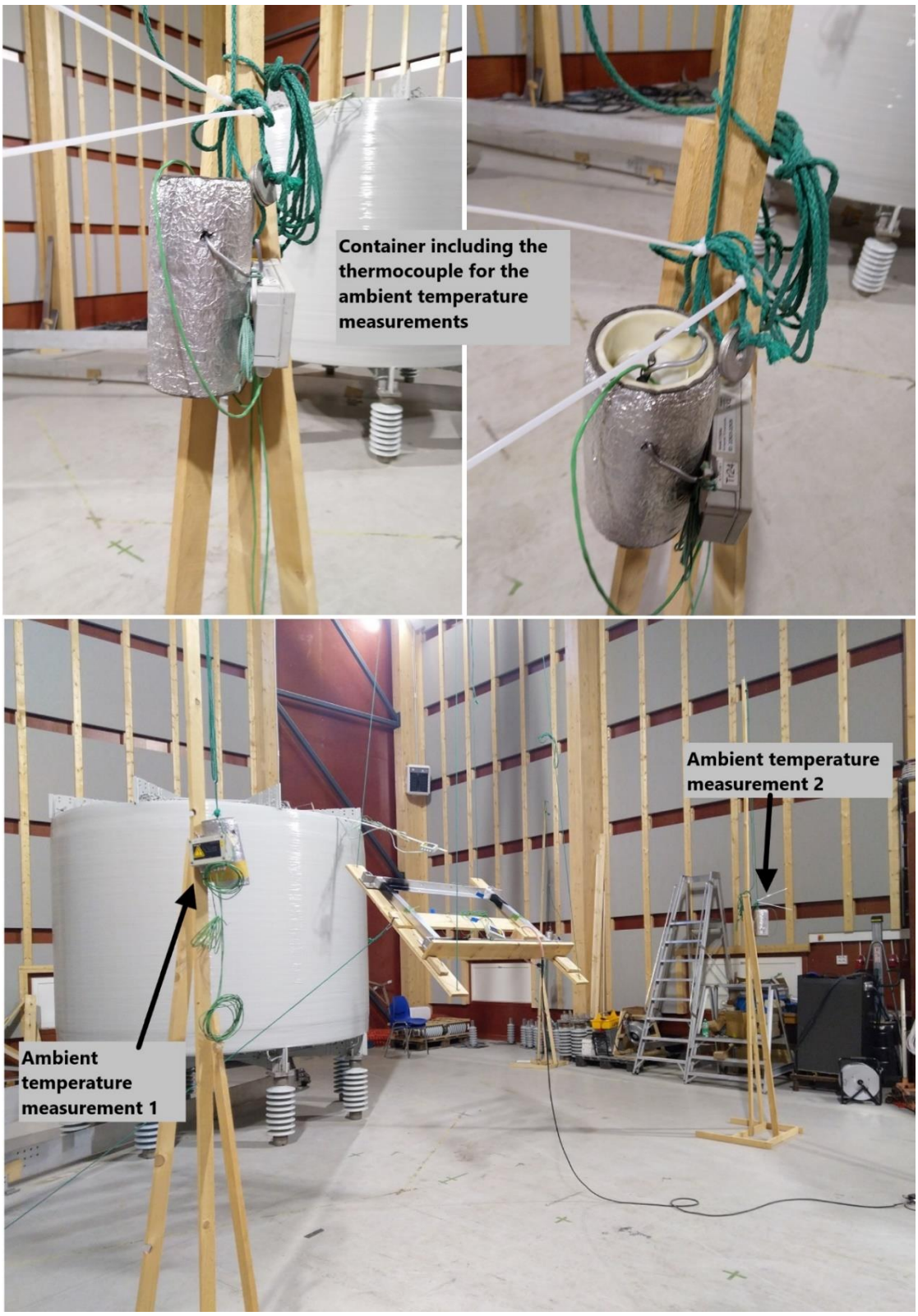

Temperature measurement of the loops in the laboratory tests

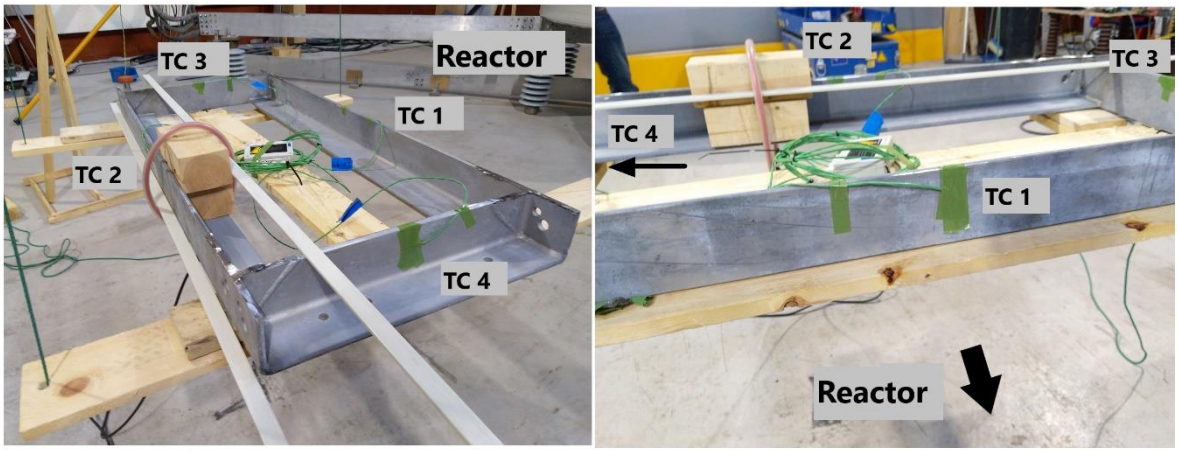

Steel loop

TC = thermocouple

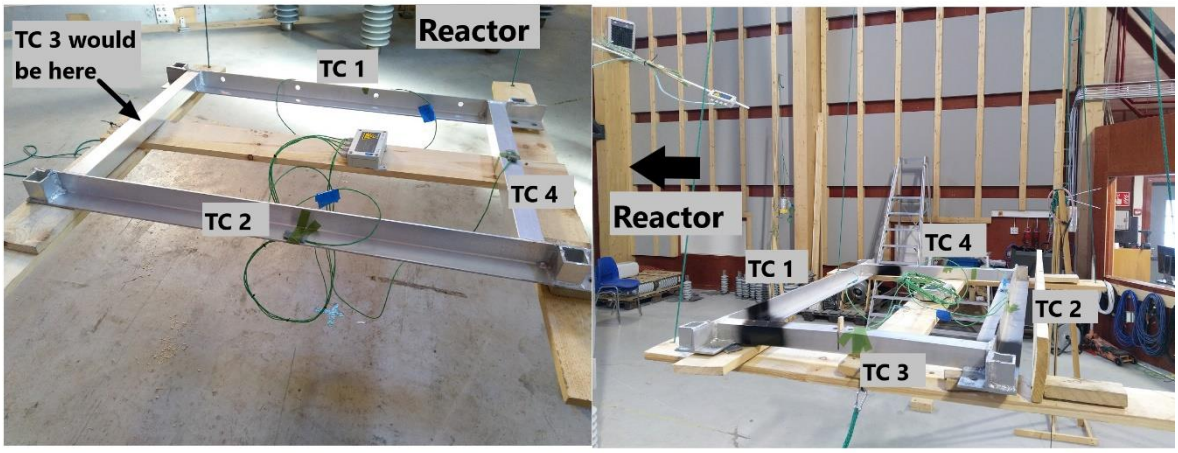

Aluminum loop **Cut aluminium loop**

Steel and aluminium loop surfaces

Steel loop geometry for horizontal orientation

Vertical surfaces

Surface	Length [m]	Height [m]	Number	Area for single surface [m^2]	Total area [m^2]	Characteristic length [m]
S1	1,388	0,1	2	0,1388	0,2776	0,1
S2	1,188	0,09	2	0,10692	0,21384	0,09
S3	0,54	0,09	2	0,0486	0,0972	0,09
S4	0,36	0,1	2	0,036	0,072	0,1
S5	0,09	0,09	4	0,0081	0,0324	0,09
S6	0,09	0,09	4	0,0081	0,0324	0,09
S7	1,188	0,01	2	0,01188	0,02376	0,01
S8	0,54	0,01	2	0,0054	0,0108	0,01
S9	0,01	0,1	4	0,001	0,004	0,1
				SUM	0,764	

Horizontal surfaces, face up

Surface	Length [m]	Width [m]	Number	Area for single surface [m^2]	Total area [m^2]	Characteristic length [m]
S1	1,188	0,09	2	0,10692	0,21384	0,041830986
S2	0,54	0,09	2	0,0486	0,0972	0,038571429
S3	1,388	0,01	2	0,01388	0,02776	0,004964235
S4	0,54	0,01	2	0,0054	0,0108	0,004909091
				SUM	0,3496	

Horizontal surfaces, face down

Surface	Length [m]	Width [m]	Number	Area for single surface [m^2]	Total area [m^2]	Characteristic length [m]
S1	1,388	0,1	2	0,1388	0,2776	0,046639785
S2	0,36	0,1	2	0,036	0,072	0,039130435
				SUM	0,3496	

Loop total area	1,4632	m^2
Degree of emssion	0,276	

Steel loop geometry for 45°

Loop angle 45 °

Vertical surfaces

Surface	Length [m]	Height [m]	Number	Area for single surface [m^2]	Total area [m^2]	Characteristic length [m]
S1	0,54	0,09	2	0,0486	0,0972	0,127279221
S2	0,36	0,1	2	0,036	0,072	0,141421356
S3	0,09	0,09	4	0,0081	0,0324	0,127279221
S4	0,1	0,01	4	0,001	0,004	0,014142136
S5	0,54	0,01	2	0,0054	0,0108	0,014142136
				SUM	0,2164	

Inclined surfaces, face up

Surface	Length [m]	Height [m]	Number	Area for single surface [m^2]	Total area [m^2]	Characteristic length [m]
S1	1,388	0,1	1	0,1388	0,1388	0,1
S2	1,188	0,09	1	0,10692	0,10692	0,09
S3	0,09	0,09	2	0,0081	0,0162	0,09
S4	1,188	0,09	2	0,10692	0,21384	0,09
S5	0,09	0,54	2	0,0486	0,0972	0,54
S6	1,388	0,01	2	0,01388	0,02776	0,01
S7	0,01	0,54	2	0,0054	0,0108	0,54
S8	1,188	0,01	1	0,01188	0,01188	0,01
				SUM	0,6234	

Inclined surfaces, face down

Surface	Length [m]	Height [m]	Number	Area for single surface [m^2]	Total area [m^2]	Characteristic length [m]
S1	1,388	0,1	2	0,1388	0,2776	0,1
S2	0,1	0,36	2	0,036	0,072	0,36
S3	1,188	0,09	1	0,10692	0,10692	0,09
S4	1,388	0,1	1	0,1388	0,1388	0,1
S5	0,09	0,09	2	0,0081	0,0162	0,09
S6	1,188	0,01	1	0,01188	0,01188	0,01
				SUM	0,6234	

Loop total area	1,4632	m^2
Degree of emssion	0,276	

Steel loop geometry for vertical orientation

Vertical surfaces

Surface	Length [m]	Height [m]	Number	Area for single surface [m^2]	Total area [m^2]	Characteristic length [m]
S1	1,388	0,1	2	0,1388	0,2776	0,1
S2	0,1	0,36	2	0,036	0,072	0,36
S3	1,188	0,09	2	0,10692	0,21384	0,09
S4	0,09	0,54	4	0,0486	0,1944	0,54
S5	0,1	0,36	2	0,036	0,072	0,36
S6	0,09	0,09	4	0,0081	0,0324	0,09
S7	1,388	0,01	2	0,01388	0,02776	0,01
S8	0,01	0,54	4	0,0054	0,0216	0,54
S9	0,1	0,01	4	0,001	0,004	0,01
				SUM	0,9156	

Horizontal surfaces, face up

Surface	Length [m]	Width [m]	Number	Area for single surface [m^2]	Total area [m^2]	Characteristic length [m]
S1	1,388	0,1	1	0,1388	0,1388	0,046639785
S2	1,188	0,09	1	0,10692	0,10692	0,041830986
S3	0,09	0,09	2	0,0081	0,0162	0,0225
S4	1,188	0,01	1	0,01188	0,01188	0,004958264
				SUM	0,2738	

Horizontal surfaces, face down

Surface	Length [m]	Width [m]	Number	Area for single surface [m^2]	Total area [m^2]	Characteristic length [m]
S1	1,388	0,1	1	0,1388	0,1388	0,046639785
S2	1,188	0,09	1	0,10692	0,10692	0,041830986
S3	0,09	0,09	2	0,0081	0,0162	0,0225
S4	1,188	0,01	1	0,01188	0,01188	0,004958264
				SUM	0,2738	

Loop total area	1,4632	m^2
Degree of emssion	0,276	

Aluminium loop geometry for horizontal orientation

Vertical surfaces

Surface	Length [m]	Height [m]	Number	Area for single surface [m^2]	Total area [m^2]	Characteristic length [m]
S1	1,03	0,05	2	0,0515	0,103	0,05
S2	0,9	0,05	2	0,045	0,09	0,05
S3	0,05	0,05	4	0,0025	0,01	0,05
S4	0,115	0,05	4	0,00575	0,023	0,05
S5	0,045	0,005	4	0,000225	0,0009	0,005
S6	1,22	0,005	4	0,0061	0,0244	0,005
S7	0,005	0,05	4	0,00025	0,001	0,05
S8	0,105	0,005	4	0,000525	0,0021	0,005
S9	0,495	0,045	4	0,022275	0,0891	0,045
S10	0,045	0,05	12	0,00225	0,027	0,05
S11	0,037	0,05	16	0,00185	0,0296	0,05
				SUM	0,4001	

Horizontal surfaces, face up

Surface	Length [m]	Width [m]	Number	Area for single surface [m^2]	Total area [m^2]	Characteristic length [m]
S1	1,03	0,05	2	0,0515	0,103	0,023842593
S2	0,9	0,05	2	0,045	0,09	0,023684211
S3	0,115	0,05	4	0,00575	0,023	0,017424242
S4	0,05	0,05	4	0,0025	0,01	0,0125
S5	0,045	0,005	4	0,000225	0,0009	0,00225
S6	0,495	0,045	2	0,022275	0,04455	0,020625
S7	1,22	0,005	2	0,0061	0,0122	0,002489796
S8	0,045	0,004	8	0,00018	0,00144	0,001836735
S9	0,037	0,004	8	0,000148	0,001184	0,001804878
S10	0,037	0,037	4	0,001369	0,005476	0,00925
				SUM	0,29175	

Horizontal surfaces, face down

Surface	Length [m]	Width [m]	Number	Area for single surface [m^2]	Total area [m^2]	Characteristic length [m]
S1	1,22	0,105	2	0,1281	0,2562	0,048339623
S2	0,395	0,045	2	0,017775	0,03555	0,020198864
				SUM	0,29175	

Loop total area	0,9836	m^2
Degree of emssion	0,18	

Aluminium loop geometry for 45°

Loop angle 45 °

Vertical surfaces

Surface	Length [m]	Height [m]	Number	Area for single surface [m^2]	Total area [m^2]	Characteristic length [m]
S1	0,495	0,045	4	0,022275	0,0891	0,06363961
S2	0,045	0,05	8	0,00225	0,018	0,070710678
S3	0,037	0,05	8	0,00185	0,0148	0,070710678
S4	0,105	0,005	4	0,000525	0,0021	0,007071068
S5	0,05	0,005	4	0,00025	0,001	0,007071068
				SUM	0,125	

Inclined surfaces, face up

Surface	Length [m]	Height [m]	Number	Area for single surface [m^2]	Total area [m^2]	Characteristic length [m]
S1	1,03	0,05	3	0,0515	0,1545	0,05
S2	0,9	0,05	3	0,045	0,135	0,05
S3	0,045	0,495	2	0,022275	0,04455	0,495
S4	0,045	0,05	2	0,00225	0,0045	0,05
S5	0,037	0,05	4	0,00185	0,0074	0,05
S6	0,037	0,037	4	0,001369	0,005476	0,037
S7	1,22	0,005	4	0,0061	0,0244	0,005
S8	0,004	0,045	8	0,00018	0,00144	0,045
S9	0,037	0,004	8	0,000148	0,001184	0,004
S10	0,045	0,005	6	0,000225	0,00135	0,005
S11	0,05	0,05	6	0,0025	0,015	0,05
S12	0,115	0,05	6	0,00575	0,0345	0,05
				SUM	0,4293	

Inclined surfaces, face down

Surface	Length [m]	Height [m]	Number	Area for single surface [m^2]	Total area [m^2]	Characteristic length [m]
S1	1,22	0,105	2	0,1281	0,2562	0,105
S2	0,045	0,395	2	0,017775	0,03555	0,395
S3	0,045	0,05	2	0,00225	0,0045	0,05
S4	0,037	0,05	4	0,00185	0,0074	0,05
S5	1,22	0,005	2	0,0061	0,0122	0,005
S6	0,9	0,05	1	0,045	0,045	0,05
S7	1,03	0,05	1	0,0515	0,0515	0,05
S8	0,045	0,005	2	0,000225	0,00045	0,005
S9	0,05	0,05	2	0,0025	0,005	0,05
S10	0,115	0,05	2	0,00575	0,0115	0,05
				SUM	0,4293	

Loop total area	0,9836	m^2
Degree of emssion	0,18	

Aluminium loop geometry for vertical orientation

Vertical surfaces

Surface	Length [m]	Height [m]	Number	Area for single surface [m^2]	Total area [m^2]	Characteristic length [m]
S1	1,22	0,105	2	0,1281	0,2562	0,105
S2	1,03	0,05	2	0,0515	0,103	0,05
S3	0,9	0,05	2	0,045	0,09	0,05
S4	0,115	0,05	4	0,00575	0,023	0,05
S5	0,05	0,05	4	0,0025	0,01	0,05
S6	0,045	0,005	4	0,000225	0,0009	0,005
S7	0,05	0,045	8	0,00225	0,018	0,045
S8	0,037	0,037	4	0,001369	0,005476	0,037
S9	0,045	0,495	6	0,022275	0,13365	0,495
S10	0,045	0,395	2	0,017775	0,03555	0,395
S11	1,22	0,005	2	0,0061	0,0122	0,005
S12	0,05	0,037	8	0,00185	0,0148	0,037
S13	0,004	0,045	8	0,00018	0,00144	0,045
S14	0,037	0,004	8	0,000148	0,001184	0,004
S15	0,005	0,105	4	0,000525	0,0021	0,105
S16	0,05	0,005	4	0,00025	0,001	0,005
				SUM	0,7085	

Horizontal surfaces, face up

Surface	Length [m]	Width [m]	Number	Area for single surface [m^2]	Total area [m^2]	Characteristic length [m]
S1	0,9	0,05	1	0,045	0,045	0,023684211
S2	1,03	0,05	1	0,0515	0,0515	0,023842593
S3	0,115	0,05	2	0,00575	0,0115	0,017424242
S4	0,05	0,05	2	0,0025	0,005	0,0125
S5	0,045	0,005	2	0,000225	0,00045	0,00225
S6	0,05	0,045	2	0,00225	0,0045	0,011842105
S7	0,05	0,037	4	0,00185	0,0074	0,010632184
S8	1,22	0,005	2	0,0061	0,0122	0,002489796
				SUM	0,13755	

Horizontal surfaces, face down

Surface	Length [m]	Width [m]	Number	Area for single surface [m^2]	Total area [m^2]	Characteristic length [m]
S1	0,9	0,05	1	0,045	0,045	0,023684211
S2	1,03	0,05	1	0,0515	0,0515	0,023842593
S3	0,115	0,05	2	0,00575	0,0115	0,017424242
S4	0,05	0,05	2	0,0025	0,005	0,0125
S5	0,045	0,005	2	0,000225	0,00045	0,00225
S6	0,05	0,045	2	0,00225	0,0045	0,011842105
S7	0,05	0,037	4	0,00185	0,0074	0,010632184
S8	1,22	0,005	2	0,0061	0,0122	0,002489796
				SUM	0,13755	

Loop total area	0,9836	m^2
Degree of	0,18	

Properties of air and critical Rayleigh numbers

Properties of dry air in different temperatures

T [°C]	ρ [kg/m^3]	ν [m^2/s]	κ [m^2/s]	β [1/K]	λ [W/(m*K)]
10	1.2306	0.0000144	0.00002029	0.0035428	0.025121
20	1.1885	0.00001532	0.00002163	0.0034209	0.025873
30	1.1492	0.00001626	0.00002301	0.0033071	0.026618
40	1.1124	0.00001723	0.00002442	0.0032007	0.027354
50	1.0779	0.00001822	0.00002585	0.003101	0.028082
60	1.0455	0.00001922	0.00002732	0.0030073	0.028804
70	1.015	0.00002025	0.00002882	0.0029192	0.029518
80	0.9862	0.0000213	0.00003035	0.0028361	0.030225
90	0.959	0.00002237	0.00003191	0.0027576	0.030925
100	0.9333	0.00002346	0.0000335	0.0026833	0.03162

Source: Stephan et al. VDI Heat Atlas 2010, page 173 (D2.2. table 1)

Critical Rayleigh numbers in terms of angle of inclination

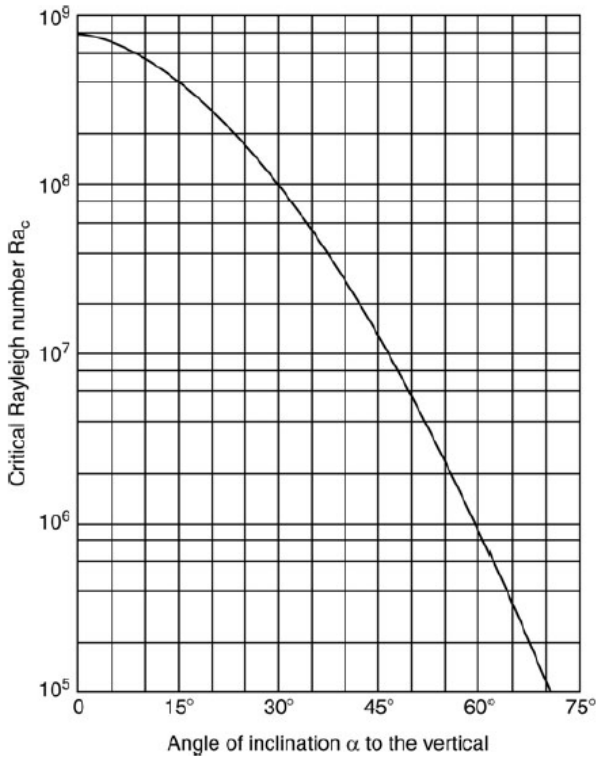

F2. Fig. 1. Upper limit Ra_c for the laminar range as a function of the angle of inclination α in free convection at heated upper surfaces or at cooled lower surfaces [a suitable approximation is given by $Ra_c = 10^{(8.9 - 0.00178\ \alpha\ 1.82)}$].

Source: Stephan et al. VDI Heat Atlas 2010, page 668 (F2. Fig. 1.)

Electrical conductivity determination for the loops

Simulation 1: Resistance calculation of steel loop using ANSYS EM DC conduction

Initial values		Calculations	
ΔU [V]	Conductivity, steel [S/m]	Loop current [A]	Loop resistance [Ω]
1	4400000	2509.57	0.000398475
1	4200000	2395.5	0.000417449
1	4000000	2281.43	0.000438322
1	3800000	2167.36	0.000461391
1	3600000	2053.29	0.000487023
1	3400000	1939.22	0.000515671
1	3200000	1825.14	0.000547903
1	3000000	1711.07	0.00058443
1	2800000	1597	0.000626174
1	2600000	1482.93	0.000674341

Simulation 2: Resistance calculation of aluminium loop using ANSYS EM DC conduction

Initial values		Calculations	
ΔU [V]	Conductivity, aluminium [S/m]	Loop current [A]	Loop resistance [Ω]
1	28000000	7461.39	0.000134023
1	26000000	6928.43	0.000144333
1	24000000	6395.48	0.00015636
1	22000000	5862.52	0.000170575
1	20000000	5329.56	0.000187633
1	18000000	4796.61	0.000208481
1	16000000	4263.65	0.000234541
1	14000000	3730.69	0.000268047
1	12000000	3197.74	0.000312721
1	10000000	2664.78	0.000375266

B-H curve points for the S355J0 steel

B-H curve points for the steel 1010 in the ANSYS material database

H [A/m]	B [T]
0	0
238.7	0.2003
318.3	0.3204
358.1	0.40045
437.7	0.50055
477.5	0.5606
636.6	0.7908
795.8	0.931
1114.1	1.1014
1273.2	1.2016
1591.5	1.302
2228.2	1.4028
3183.1	1.524
4774.6	1.626
6366.2	1.698
7957.7	1.73
15915.5	1.87
31831	1.99
47746.5	2.04
63662	2.07
79577.5	2.095
159155	2.2
318310	2.40000013

Source: ANSYS Electronics 19.2 material database (steel 1010)

Reduced B-H curve points for the S355J0 steel

B value reduction 30 %

Hysteresis curve points H [A/m]	Original hysteresis curve points B [T]	Reduced hysteresis curve points B [T]	
0	0	0	
238.7	0.2003	0.14021	
318.3	0.3204	0.22428	
358.1	0.40045	0.280315	
437.7	0.50055	0.350385	
477.5	0.5606	0.39242	
636.6	0.7908	0.55356	
795.8	0.931	0.6517	
1114.1	1.1014	0.77098	
1273.2	1.2016	0.84112	
1591.5	1.302	0.9114	
2228.2	1.4028	0.98196	
3183.1	1.524	1.0668	
4774.6	1.626	1.1382	
6366.2	1.698	1.1886	
7957.7	1.73	1.211	
15915.5	1.87	1.309	
31831	1.99	1.393	
47746,5	2.04	1.428	
63662	2.07	1.449	**Actually used in ANSYS**
79577.5	2.095	1.4665	1.48
159155	2.2	1.54	1.58
318310	2.40000013	1.680000091	1.78

Error message: The slope of BH curve may not be less than that of free space anywhere along the curve. The slope is less than that of free space between points (xxx, xxx) and (xxx, xxx)

Meshing of the problem domain in the ANSYS electromagnetic simulations

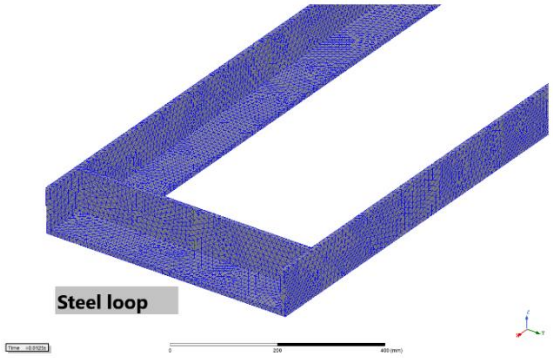

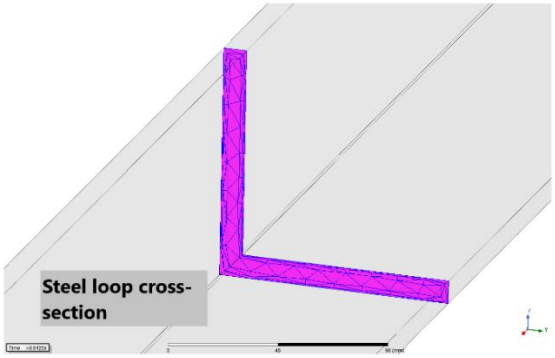

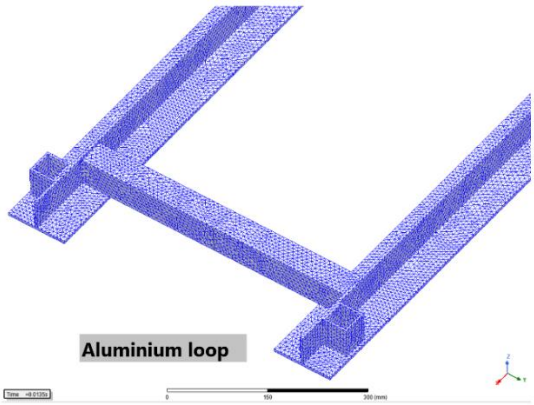

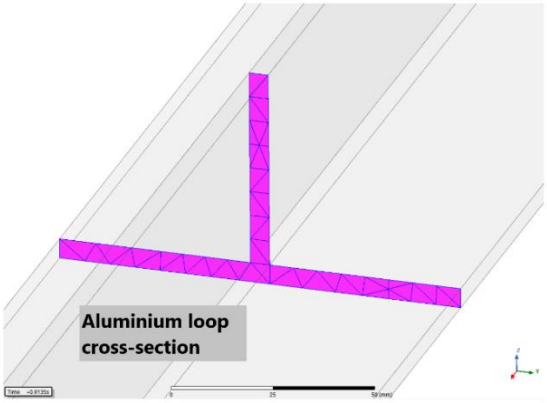

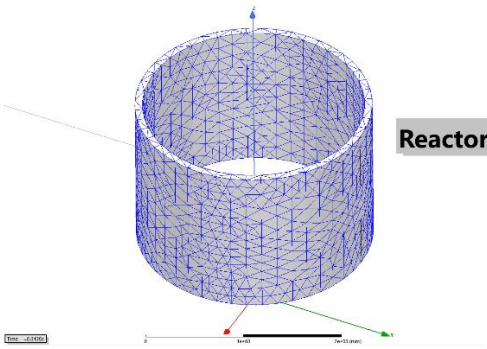

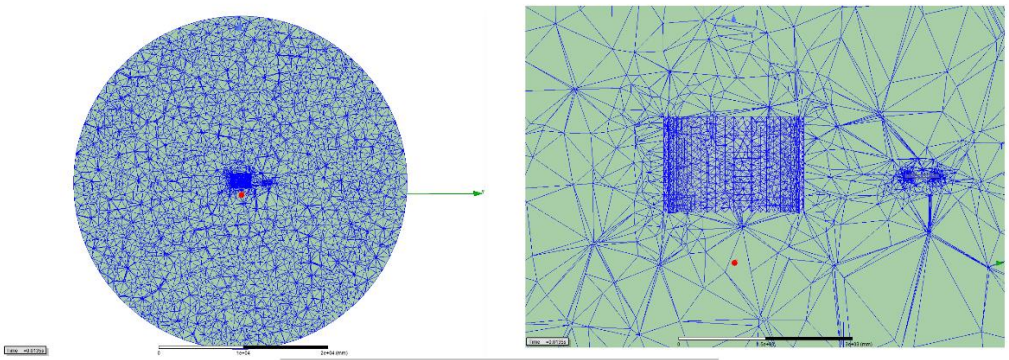

Meshing of the background volume

ANSYS Electronics fields calculator

Calculation of the total loss and current of the steel loop in horizontal orientation at 3.0 m distance, timestep 12.0 ms

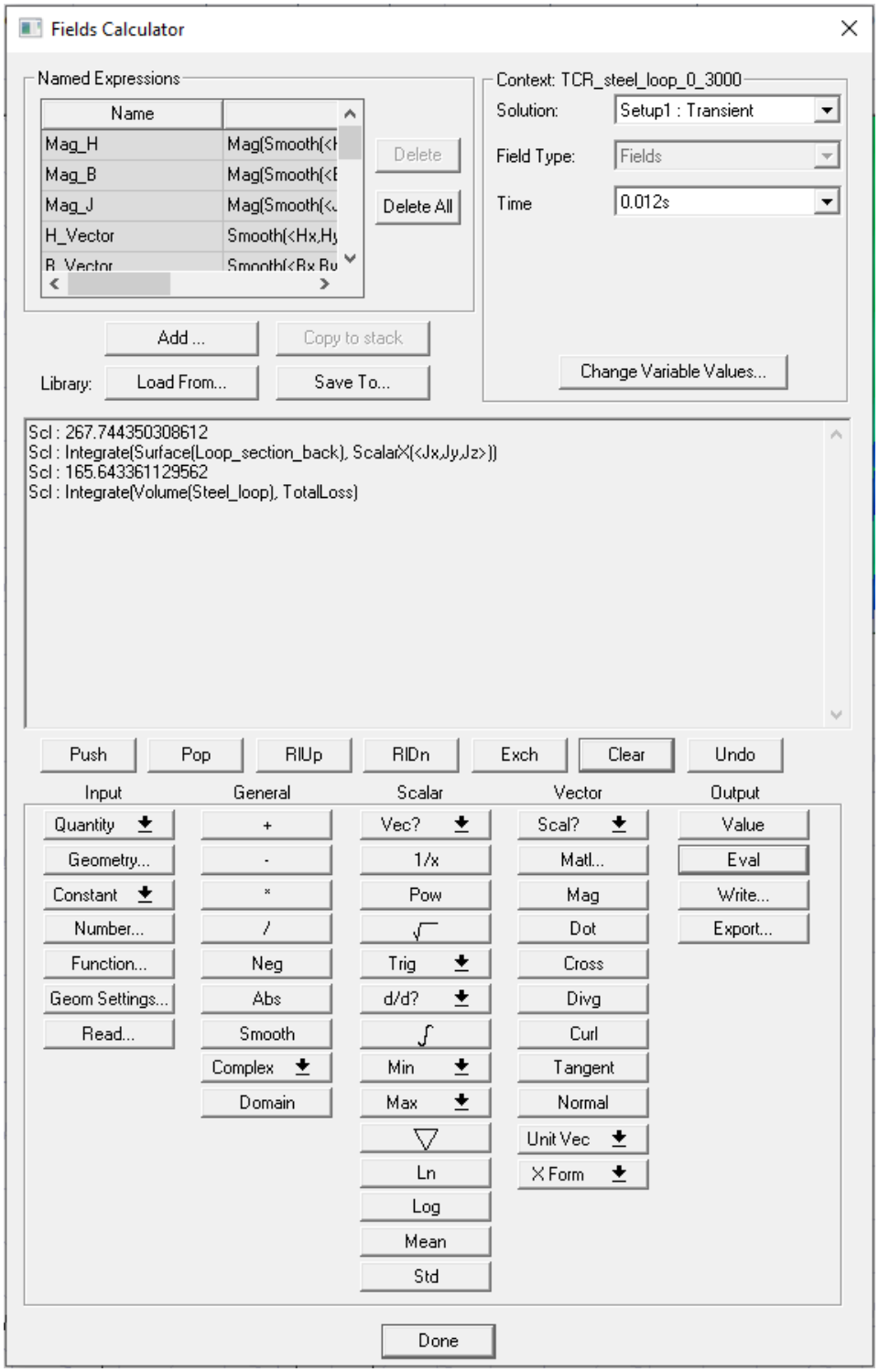

Simulation of the steel loop with reduced magnetic properties

Horizontal orientation, 3.0 m distance

	Lab test	**Simulation**	**Simulation, reduced magnetic properties**	
Loop RMS current [A]	262.9	176.4	206.5	
Difference [A]	-	86.5	56.4	Compared to the lab test value
Difference [%]	-	33 %	21 %	
Loop total loss [W]	119.3	93.3	108.7	
Difference [W]	-	26.0	10.6	Compared to the lab test value
Difference [%]	-	22 %	9 %	
Loop loss by circulating current [W]	60.2	27.1	37.1	
Difference [W]	-	33.1	23.1	Compared to the lab test value
Difference [%]	-	55 %	38 %	
Loop loss by eddy currents [W]	59.2	66.3	71.6	
P_{eddy} / P_{total} [%]	50 %	71 %	66 %	Fraction of eddy current losses from the total loss
Average ΔT [°C]	11.7	8.4	9.6	
Difference [°C]	-	3.3	2.1	Compared to the lab test value
Difference [%]	-	28 %	18 %	
Max ΔT [°C]	15.3	11.8	13.0	
Difference [°C]	-	3.4	2.3	Compared to the lab test value
Difference [%]	-	23 %	15 %	

Simulations of the geometrically identical steel and aluminium loops

Meshing of the loops

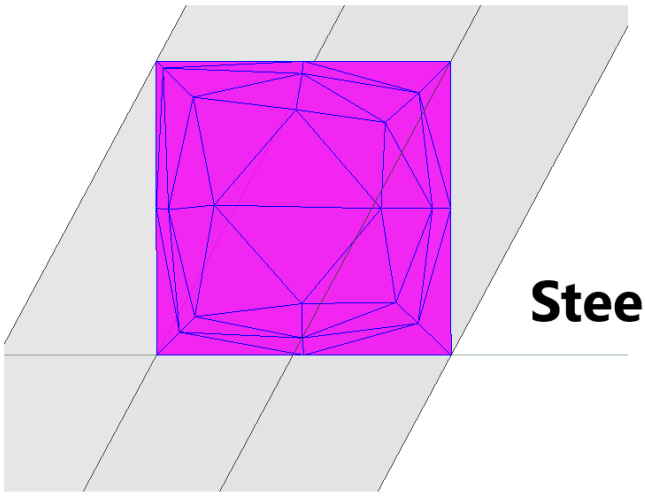

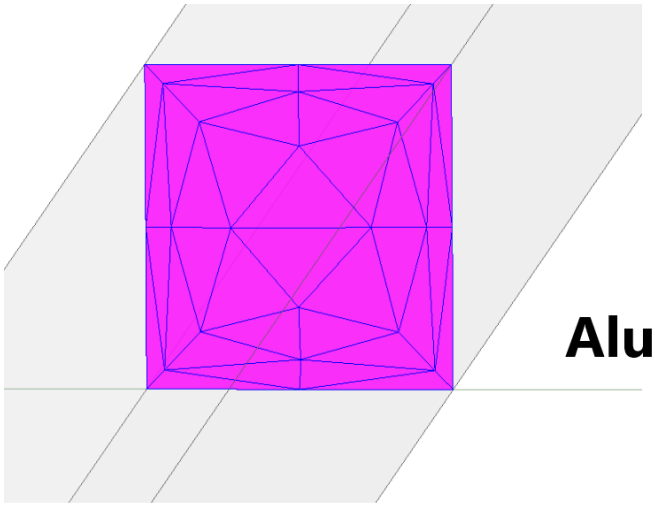

Simulation results

Loop size [m]	1x1	2x2	3x3	4x4	5x5	6x6	
Loop bulk conductivity [S/m]	4165978	4165978	4165978	4165978	4165978	4165978	Steel
	25323695	25323695	25323695	25323695	25323695	25323695	Aluminium
Loop circulating current, RMS [A]	19.0	26.5	28.4	31.5	33.0	33.0	Steel
	173.7	222.2	263.5	250.2	272.0	261.6	Aluminium
Loop total loss, RMS [W]	4.2	14.5	26.2	44.8	60.2	74.0	Steel
	16.6	54.9	116.6	138.9	207.2	228.6	Aluminium
Loop imported load [W]	3.9	13.7	23.3	41.5	55.6	68.3	Steel
	11.6	37.8	80.1	95.0	142.0	156.3	Aluminium
Loop temperature, min [°C]	21.7	22.9	23.5	24.5	24.7	25.4	Steel
	26.1	29.8	33.8	33.2	34.6	33.4	Aluminium
Loop temperature, max [°C]	22.1	23.6	24.0	25.6	26.1	26.8	Steel
	26.2	30.0	34.1	32.5	35.0	33.7	Aluminium
Loop temperature, avg [°C]	21.9	23.3	23.7	25.0	25.3	25.9	Steel
	26.1	29.9	33.9	32.4	34.8	33.6	Aluminium

Steel I-beam simulations

Meshing and profile of the simulated steel I-beam

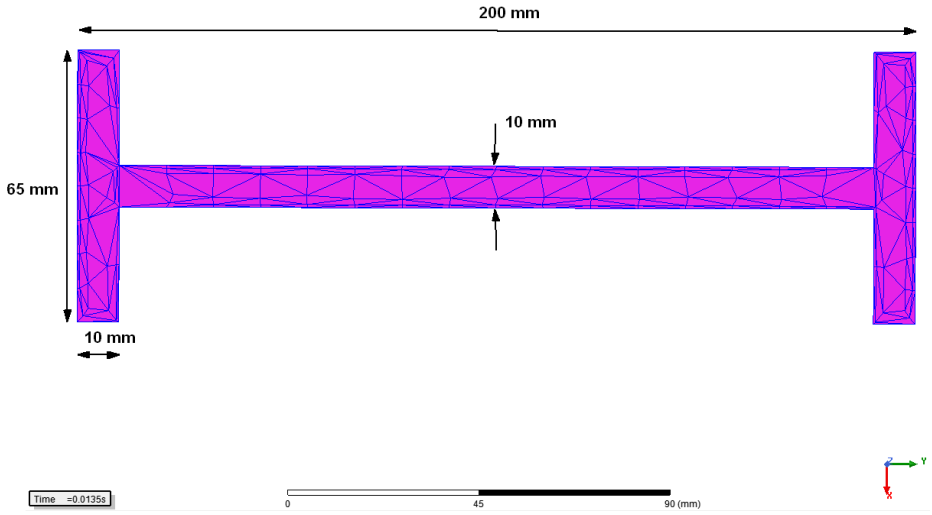

Simulation results

Beam distance [mm]	4000	5800
Beam bulk conductivity [S]	4165978	4165978
Beam total loss, RMS [W]	330.3	44.0
Beam imported load [W]	275.6	36.3
Beam temperature, min [°C]	23.0	20.7
Beam temperature, max [°C]	47.5	23.1
Beam temperature, avg [°C]	36.4	22.2
Average ΔT [°C]	16.4	2.2
Max ΔT [°C]	27.5	3.1